ELSEVIER

Physica E 5 (2000) 215–273

PHYSICA E

www.elsevier.nl/locate/physe

Material parameters of InGaAsP and InAlGaAs systems for use in quantum well structures at low and room temperatures

E. Herbert Li [1]

Division of Applied Sciences, Harvard University, Cambridge, MA 02138-2901, USA

Accepted 4 November 1999

Abstract

The set of material parameters for quantum well structures is of immense importance because of its usage in the development of theories, extraction of experimental data, and the proper design of devices. In particular, the (Al,In)GaAs/GaAs, InGaAs/InP and (In,Ga)AlAs/InGaAs quantum well systems have drawn a lot of attention. They form the center core of materials used for fundamental basic research and device applications. Despite the presence of some review articles and reference books, there is a lack of clear reference on the accurate determination of the material parameters for quantum wells. This review aims to provide a comprehensive and systematic set of material parameters for the above quantum well systems grown on (1 0 0) substrates at two different temperatures, below 10 K and at around 300 K. The parameters are compared against experimental data from various fabrication sources, measurement techniques, and quantum well structures. The values presented here serve as an accurate and up to date source of reference.

Keywords: InGaAsP; InAlGaAs; Quantum wells

1. Introduction

The quantum well (QW) structure is a useful material for high-speed digital, high-frequency microwave, and other optoelectronic device applications [1]. An accurate determination of the electronic and optical properties of the QW material systems, such as (Al,In)GaAs/GaAs, (In,Ga)AlAs/InGaAs, and InGaAs(P)/InP on GaAs and InP substrates, is very important. In particular, knowledge of the band-gap energy and optical absorption spectrum which varies in different QW structures (such as well width and alloy), is a subject that has been extensively studied [2]. This is because they hold the key to the operating wavelength and dynamic performance of optoelectronic devices, such as lasers, modulators, and detectors. In order to understand the material theories better, to extract data accurately from measurements, and to design devices properly, it is essential to use the correct material parameters (such as band gap,

[1] Permanent address: Department of Electrical and Electronic Engineering, University of Hong Kong, Pokfulam Road, Hong Kong.

1386-9477/00/$ - see front matter
PII: S1386-9477(99)00262-3

effective mass, and broadening factor) at appropriate temperatures in the QWs. However, this requires a detailed and precise knowledge of the material parameters at specific conditions, such as temperature, measurement method, and material quality. For instance, at room temperature (300 K), the band-gap energy of the GaAs system is 1.423 eV while at the low temperature (2 K), the band-gap energy is 1.519 eV. In the case of InGaAs/InP QW, optical and electronic measurements result in a large difference in the offset ratio (60 : 40 and 33 : 67, respectively) [3]. The direct band-gap quaternary system, InAlGaAs, covers the low loss and low dispersion wavelength region of 1.3–1.6 μm [4]. The presence of Stoke shift affects the peak resonance energy taken from photoluminescence (PL) data and the shift may vary up to 15 meV depending on the fabricated quality of the QW materials and temperature of measurements [5,6]. In addition, there is inconsistency in the parameters suggested by different authors even their experiments are performed with the same method, temperature, and QW structures. The success in obtaining a set of accurate materials data can produce a versatile simulator in which by varying any alloy composition and well width within a specific range, the electronic and optical properties of the QW structures can be obtained without relying on expensive and time-consuming experiments.

The currently available literature on the material parameters consists of the authoritative Landolt–Bornstein (LB) numerical data series [7], the EMIS Data review series [8], a few monographs [9–11], and several review articles [12–15]. The LB series on semiconductors (group III vol. 17) is dated 1981 and supplemented by an extension (group III vol. 22) dated 1986. It is the most comprehensive set, although it is 10 years backdated. The Adachi 1985 review [12] is perhaps the most widely referenced data for both theory and applications, especially for use at room temperature. However, some of the data (for binary alloy) for low temperature (below 10 K), such as electron and heavy hole mass, and the direct band gap formula, is only obtained using linear scheme. The EMIS series on the stiffness constant of InP at room temperature [13] actually uses a value which is for low temperature according to the Landolt–Bornstein (LB) series [7]. The AlGaAs parameters referenced in the EMIS series are given without considering the temperature. They are based on an averaged value over different experiments and temperatures [16]. The fact is they lack a clear reference on the two most commonly used temperatures, low temperature (below 10 K) and room temperature (300 K), and how well they represent the practical situation. Only a few reports have taken into account the experimental room-temperature band-gap equation of InGaAsP [19] and InAlGaAs [20]. No effort has been made on the low-temperature ones and other parameters of these two materials.

There are several calculation and modeling reports that are based on a mixture of both low and room temperatures. In one report calculating the band gap of InGaAs/GaAs QW, the author uses a low temperature electron mass while using a room temperature heavy hole mass [17]. In another report on the interfacial-band discontinuities, half of the material parameters in the table is of low temperature while the other half is of high temperature [18]. A few similar cases that can be found with their material tables also list out values of the two temperatures [19–21]. As a result, researchers are either confused when using the available data or being careless in extracting them. Some others simply ignore their differences [15]. Therefore, there is a genuine need to have an experimentally supported report that clearly provides this information.

This review offers and clarifies most of the commonly used material parameters of InGaAsP and InAlGaAs alloys from a systematic point of view. Several complete sets of oftenly used material parameters for both the low and room temperatures are considered. Their accuracy is justified by both theoretical calculations and experimental measurements from various sources and techniques. This review is conducted on several types of QW heterostructures, including AlGaAs/GaAs, InGaAs/GaAs, InGaAs/InP, InGaAs/AlGaAs, and InGaAs/InAlAs grown on (1 0 0) substrates. Both of the single and multiple QWs are under investigation. The band-gap energy and the higher state transitions energy of these QW structures are examined under the two different temperatures with zero electric field applied. From the available literature, we search for the experimentally measured band-gap energy of the three different QW structures. Different experimental

measuring methods of the QW samples, such as electronic and optical techniques, are under investigation.

The proposed sets of material parameters will be tested by putting them into a QW model to generate the band-gap energy and a higher state transitions energy. They are compared with the experimental, and in some cases, theoretical values with various well width and alloy concentration. Appropriate band offset ratios are taken for calculating the different QW structures. The effect of the Stoke shift is also taken into consideration in the comparisons. Our aim is to try out whether this set of parameters is in good agreement with the experimental values over a wide range of QW structures, thus, to give a scale of their reliability.

Although broadening factor is of great importance, its behavior has not been fully studied. In this review, different data is gathered. An empirical analysis is done to determine a coherent behavior representing the majority of the data set.

The rest of this review is arranged as follows: in Section 2, the theoretical calculation of the QW bandgap and absorption coefficient is shown. The hydrostatic and shear strain are taken into consideration in the strained QW models. In Section 3, four sets of parameters are presented. In Section 4, different experimental measuring methods, for example, photoluminescence (PL), photoconductance (PC), and photoreflectance (PR), are briefly discussed. In addition, an analysis on the distribution of the types of measured data is presented. In Section 5, a comprehensive analysis of several QW material systems between the experimental values and calculated values of the band-gap energy and high state transition energy are shown. Good agreement is obtained in general. In particular, excellent agreement is achieved in the AlGaAs/GaAs and InAlAs/InGaAs QW material systems. In addition, in each of the QW structure, our calculated results are also compared with other literature's calculated results. In Section 6, an analysis on the broadening factor of the three QW materials: AlGaAs/GaAs, InGaAs/GaAs, and InGaAs/InP with different well width, several alloy concentration fractions, and at different temperatures is made. The general trend is investigated.

In Section 7, conclusion is drawn. The proposed sets of material parameters for both the InGaAsP and InAlGaAs material systems are proven appropriate for practical calculations.

2. QW modeling

2.1. Eigenstate calculations

The state QW structure is modeled for both lattice matched and strained material, using the BenDaniel–Duke model [26] which employs the envelope function scheme [27]. The QW is assumed to be undoped, and the effect of unintentional impurities is ignored. The barrier is assumed to be infinitely thick. It should be noted that this model also applies for multi-QW with well width $L_b \geqslant 80$ Å.

The QW electron and hold subband edge at Γ (zone centre) can be solved by the Schrödinger equation which can be expressed in the self-adjoined form:

$$-\frac{\hbar^2}{2}\frac{\mathrm{d}}{\mathrm{d}z}\left[\frac{1}{m_r^*(z)}\frac{\mathrm{d}\psi_{rl}(z)}{\mathrm{d}z}\right]+U_r(z)\psi_{rl}(z)=E_{rl}\psi_{rl}(z), \tag{1}$$

where z is the growth direction, $\psi_{rl}(z)$ is the envelope wave function, E_{rl} is the quantized energy levels with the subband energy zero at the bottom of the QW, and $m_r^*(z)$ is the carrier mass in the z direction. The subscript r is either the electron in the conduction band (C) or the heavy and light holes in the valence band ($V = H$ or L). The quantized state (eigennumber) is denoted by l. l ($= p$ and q) refers to the quantized subband energy levels (E_{cp}, E_{vq}) and the envelope wavefunctions (ψ_{Cp}, ψ_{Vq}).

The above equation is solved numerically using the finite difference method to obtain E_{cp}, E_{vq}, and also ψ_{Cp}, ψ_{Vq}. Therefore the interband transitions energy $E_g + E_{Cp} + E_{Vq}$ between the pth conduction and the qth valence subband energy levels can be obtained. Their corresponding overlapping integral $\langle\psi_{Cp}|\psi_{Vq}\rangle$ is defined as

$$\langle\psi_{Cp}|\psi_{Vq}\rangle=\int_{-z_b}^{z_b}\psi_{Vq}^*(z)\psi_{Cp}(z)\,\mathrm{d}z, \tag{2}$$

with $-z_b$ and z_b taken to be the boundaries where $\psi_{rl}(z_b)\to 0$.

2.1.1. Unstrained confinement profile (AlGaAs/GaAs)

The $Al_wGa_{1-w}As/GaAs$ (where $w = w_o$ is the as-grown concentration of the aluminium alloy) QW confinement profile is $U_r(z)$, as shown in Fig. 1(a). It is defined as

$$U_r(z) = \Delta E_r \left[u\left(z - \frac{L_z}{2}\right) + u\left(-\frac{L_z}{2} - z\right)\right], \quad (3)$$

where $u(z)$ is the unit step function. In order to simplify the sign convention, the zero potential is defined to be at the bottom ($z = 0$) of the QW and positively up in both bands. The well-barrier discontinuity ΔE_g and well depth ΔE_r are given by

$$\Delta E_g = E_g(w = w_o) - E_g(w = 0), \quad (4)$$

$$\Delta E_r = Q_r \Delta E_g, \quad (5)$$

where E_g is the band-gap energy and Q_r is the band offset ratio.

Therefore, the eigenstate transition state energy of the lattice-method AlGaAs/GaAs QW is

$$E_{ij}^{QW} = E_g^{bulk} + E_{ci} + E_{vj} \quad (6)$$

and its band-gap energy is

$$E_g^{QW} = E_{11}^{QW}. \quad (7)$$

2.1.2. Strained confinement profile (InGaAs/ GaAs, InGaAs/ InP, InGaAs/ InAlAs, InGaAs/ AlGaAs)

The strained ternary III–V semiconductors to be analyzed are under the quaternary alloy groups $In_wGa_{1-w}As_vP_{1-v}$ (where w is the concentration of In and v is the concentration of As) and $In_wAl_vGa_{1-w-v}As$ (where w is the concentration of In and v is the concentration of Al). The QW material systems to be considered are InGaAs/GaAs (taking $v = 1$ for the well while $w = 0$ and $v = 1$ for the barrier in the InGaAsP system), InGaAs/InP (taking $v = 1$ for the well while $w = 1$ and $v = 0$ for the barrier in the InGaAsP system), and InGaAs/(In,Ga)AlAs (taking $w = 1$ and $v = 0$ for the well while $w + v \leqslant 1$ for barrier in the InAlGaAs). Lattice matched InGaAsP/InP only exists for the $In_{0.53}Ga_{0.47}As$ and $In_wGa_{1-w}As_vP_{1-v}$ materials with $v \approx 2.2(1-w)$ [28], while $In_wAl_vGa_{1-w-v}As$ can be grown lattice matched to InP for $w + v \approx 0.47$ [25]. The assumptions made are similar to those for the square AlGaAs/GaAs single QW. The material parameters are now functions of both $w(z)$ and $v(z)$.

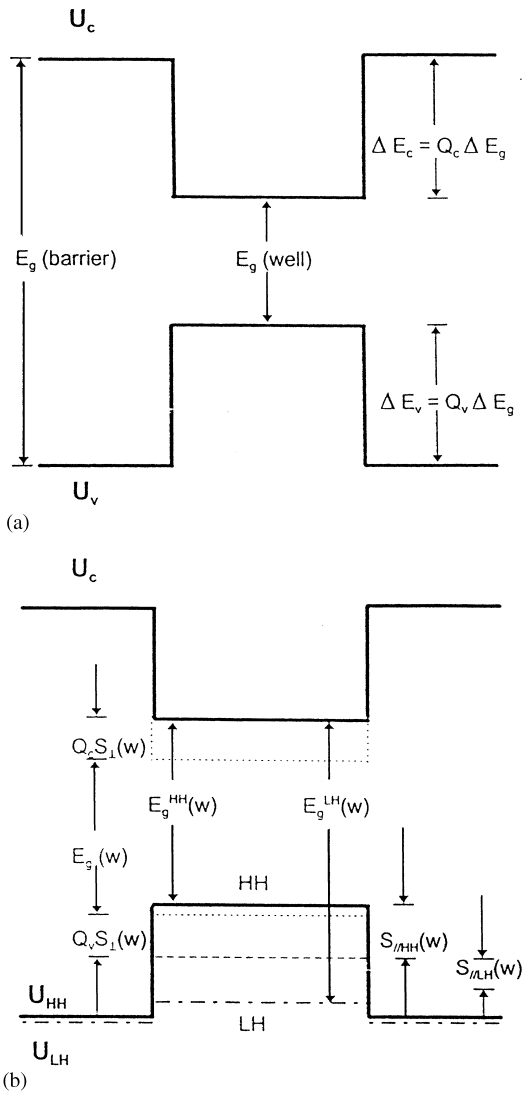

Fig. 1. (a) The lattice-matched QW confinement profile. $U_V = U_{HH} = U_{LH}$. (b) The compressive strained QW confinement profile. The HH profile is denoted by the solid line while LH by the dot-dash line. In the case for tensile strain, HH and LH components are swapped.

The QW confinement potential with the strain effect taken into consideration is given by

$$U_r(z) = Q_r[\Delta E_g(w, v) - S_{\|r}(w, v)] \pm S_{\|r}(w, v), \quad (8)$$

as shown in Fig. 1(b), where $\Delta E_g(w,v)$ is the unstrained band-gap offset taking from the two bulk heteromaterials; $S_{\perp r}(w,v)$ is the change in the bulk band gap due to biaxial component of strain and $\pm S_{\|r}(w,v)$ is the splitting energy between the heavy-hole and light-hole band edges, which is induced by the uniaxial component of shear strain with the positive and negative signs denoting the HH and LH cases, respectively, and for the electron $S_{\|c}(w,v)=0$. The well depth ΔE_r is the same as Eq. (5), and the well-barrier discontinuity ΔE_g is defined as follows:

$$\Delta E_g = E_g(w=0) - E_g(w_0) \quad \text{for } In_wGa_{1-w}As/GaAs, \tag{9}$$

$$\Delta E_g = E_g(w=1, v=0) - E_g(w_0, v=1) \quad \text{for } In_wGa_{1-w}As/InP, \tag{10}$$

$$\Delta E_g = E_g(0 \leqslant w+v \leqslant 1) - E_g(w_0, v=0) \quad \text{for } In_wAl_vGa_{1-w-v}As/InGaAs. \tag{11}$$

As the thickness of the QW layer is within the critical thickness regime, the QW structure is coherently strained, with a biaxial hydrostatic strain parallel to the interfacial plane and a uniaxial shear strain perpendicular to the interfacial plane. A compressive (tensile) hydrostatic strain causes an increase (decrease) in the band-gap energy. The shear strain disrupts the cubic symmetry of the semiconductor and lifts the degeneracy of the heavy-hole (HH) and light (LH) band edges at the Brillouin zone center Γ. The heavy-hole band shifts toward (away from) the conduction band and the light-hole band moves away from (toward) the conduction band. In addition, the shear strain causes the LH band to couple with the spin–orbit split-off band. In the InGaAs/GaAs material system, there is only compressive strain whereas in the InGaAs/InP and InGaAs/(In,Ga)AlAs material systems, both compressive and tensile strains are present.

The change in the bulk band gap due to the biaxial component of strain $S_{\|}(w,v)$, is given by:

$$S_{\perp}(w,v) = -2a(w,v)\varepsilon(w,v) \times [1 - c_{12}(w,v)/c_{11}(w,v)], \tag{12}$$

where $\varepsilon(w,v)$ is the in-plane strain in the well, $c_{ij}(w,v)$ is the elastic stiffness constants, and $a(w,v)$ is the hydrostatic deformation potential defined as

$$a(w,v) = -\tfrac{1}{3}E_p(w,v)[c_{11}(w,v) + 2c_{12}(w,v)], \tag{13}$$

where $E_p(w,v)$ is the hydrostatic pressure coefficient of the lowest direct energy gap E_g. The strain components for the in-plane biaxial hydrostatic stress parallel to the interface, assuming that the growth direction z is along $\langle 0\,0\,1\rangle$, are given by

$$\varepsilon_{xx} = \varepsilon_{yy} = \varepsilon(w,v),$$
$$\varepsilon_{zz} = -2[c_{12}(w,v)/c_{11}(w,v)]\varepsilon(w,v),$$
$$\varepsilon_{xy} = \varepsilon_{yz} = \varepsilon_{zx} = 0, \tag{14}$$

where $\varepsilon(w,v)$ is defined to be negative for compressive strain.

The splitting energy, $S_{\|}(w,v)$, between the HH and LH band edges induced by the uniaxial component of strain is given by

$$S_{\|}(w,v) = -b(w,v)[(1 + 2c_{12}(w,v)/c_{11}(w,v)]\varepsilon(w,v), \tag{15}$$

where $b(w,v)$ is the shear deformation potential. The coupling between the LH and split-off band gives rise to asymmetric heavy- to light-hole splitting, so that we have

$$S_{\|HH}(w,v) = S_{\|}(w,v), \tag{16}$$

$$S_{\|LH}(w,v) = -\tfrac{1}{2}[S_{\|}(w,v) + \Delta_0(w,v)] + \tfrac{1}{2}\{9[S_{\|}(w,v)]^2 + [\Delta_0(w,v)]^2 - 2S_{\|}(w,v)\Delta_0(w,v)\}^{1/2}, \tag{17}$$

where $\Delta_0(w,v)$ is the spin-orbit splitting. The parameters $a, b, c_{ij}, \Delta_0, \varepsilon$, and E_p in Eqs. (12)–(17) above are assumed to obey Vegard's law (sometimes with the effect of bowing included) so that their respective values depend directly on the compositional profiles across the QW. Therefore the eigenstate transition state energy for strained InGaAs/GaAs and InGaAs/InP QW band-gap energy is

$$E_{ij}^{QW} = E_g^V + E_{ci} + E_{vj}$$
$$E_g^{QW} = E_{11}. \tag{18}$$

With compressive strain,

$$E_g^{HH}(w) = E_g(w) + Q_c S_\perp(w) + Q_v S_\perp(w) - S_{\|HH}(w), \quad (19)$$

$$E_g^{LH}(w) = E_g(w) + Q_c S_\perp(w) + Q_v S_\perp(w) + S_{\|LH}(w). \quad (20)$$

With tensile strain,

$$E_g^{LH}(w) = E_g(w) + Q_c S_\perp(w) + Q_v S_\perp(w) - S_{\|LH}(w), \quad (21)$$

$$E_g^{LH}(w) = E_g(w) + Q_c S_\perp(w) + Q_v S_\perp(w) + S_{\|LH}(w). \quad (22)$$

2.2. Excitonic effects

The IS bound exciton wave function is determined here by the perturbation-variational method [29]. A variational parameter, β is obtained by minimizing the following equation:

$$\int\int \mathrm{d}z_e \mathrm{d}z_v |\psi_{c1}(z_e)|^2 |\psi_{v1}(z_v)|^2 \left\{ \tfrac{1}{4} a_B + Z - \tfrac{1}{2}\pi Z [H_1(4\beta Z/a_B) - N_1(4\beta Z/a_B)] \right\}, \quad (23)$$

where z_C and z_V represent the electron and holes positions, respectively. $Z = |z_C - z_V|$ is the distance between the electrons and holes. ψ_{C1}, ψ_{V1} are the electron and hole envelope wavefunctions, respectively. H_1 and N_1 are the Struve and Newmann functions of the first order, respectively, and $a_B = 4\hbar\pi\varepsilon^2/(\mu_\|^* e^2)$ is the exciton Bohr radius. The variation integral is evaluated by employing a four point finite difference scheme per dimension, with 1 Å between grid points.

The 1S exciton envelope wave function, $\psi_{1S}(\rho)$, and the binding energy, E_b, are given as

$$\psi_{1S}(\rho) = \frac{4\beta}{a_B\sqrt{2\pi}} \exp(-2\rho\beta/a_B), \quad (24)$$

$$E_b = -4\beta^2 R. \quad (25)$$

The exciton Rydberg energy, R, is defined as

$$R = \mu_\|^* e^4/32\pi\varepsilon_r^2\hbar^2. \quad (26)$$

ρ is the relative distance between the electrons and holes in the quantum well along the transverse direction, ε_r is the relative permittivity of the QW, and $\mu_\|^* = m_e m_\|/(m_e + m_\|)$ is the reduced mass in transverse direction.

The lattice matched and strained QW band-gap energy is

$$E_{ij}^{Exc} = E_g^{QW} + E_b. \quad (27)$$

2.3. Absorption coefficients

The unpolarized TE and TM polarization and absorption coefficient of the QW are calculated for the band edge Γ region of the Brillouin zone and includes 1S exciton, an upper-bound state (including the 2D enhancement Sommerfeld factor). The bound state absorption coefficient, $\alpha_{bd}(\omega)$, is shown as

$$\alpha_{bd}(\omega) = \frac{e^2\mu_\|^*\omega}{6\varepsilon_0 c_0 n_r m_e^* E_{CV}^2 L_z} M_0 \sum_{p,q} |\langle\psi_{Cp}|\psi_{Vq}\rangle|^2 I_{pq}(\hbar w), \quad (28)$$

where

$$M_0 = \frac{E_g(E_g + \Delta_0)}{E_g + \frac{2}{3}\Delta_0}, \quad (29)$$

$$I_{pq}(\hbar w) = \int_0^\infty \wp(E) S(E) \mathscr{L}(E)\, \mathrm{d}E, \quad (30)$$

$$S(E) = \frac{2}{1 + \exp(-2\pi\sqrt{R/E})} \quad (31)$$

and

$$\mathscr{L}(E) = \frac{\Gamma_b}{\pi\{[E_{cv} + E - \hbar w)^2 + \Gamma_b^2\}}, \quad (32)$$

where $S(E)$ is the Sommerfeld enhancement factor, $\mathscr{L}(E)$ is the Lorentzian broadening factor, Γ_b is the bound state line width (half-width half-maximum) broadening factor, $\wp(E)$ is the polarization factor, $E_{CV} = E_g^{bulk} + E_{C1} + E_{V1}, E_g$ is the band-gap at the zone center after the interdiffusion, c_0 is the velocity of light in free space, ε_0 is the permittivity in free space, and m_c^* is the effective electron

mass. Usual values are taken for the other physical constants.

For light passing through the quantum well layer perpendicularly, there is only one polarization (the electric field of light parallel to the plane of the quantum layer) and the polarization factor is given by $\wp = \frac{3}{2}$ (HH), $\frac{1}{2}$ (LH). On the other hand, for light propagating parallel to the quantum layer, the TE polarization (electric field of light parallel to the plane of the quantum well layer) and the orthogonal polarization (electric field of the light perpendicular to the quantum well layer), called TM polarization, occur. The polarization factor which accounts for both the TE and TM polarizations is given by

$$\wp^{\mathrm{TE}} = \begin{cases} \frac{3}{4}(1 + E_{\mathrm{R}}) & \text{for heavy hole,} \\ \frac{5}{4}(1 - \frac{3}{5}E_{\mathrm{R}}) & \text{for light hole,} \end{cases} \tag{33}$$

$$\wp^{\mathrm{TM}} = \begin{cases} \frac{3}{2}(1 - E_{\mathrm{R}}) & \text{for heavy hole,} \\ \frac{1}{2}(1 + 3E_{\mathrm{R}}) & \text{for light hole,} \end{cases} \tag{34}$$

where $E_{\mathrm{R}} = (E_{Cp} + E_{Vq})/(E_{Cp} + E_{Vq} + E)$.

The exciton absorption coefficient, $\alpha_{1\mathrm{S}}(w)$, is given by:

$$\alpha_{1\mathrm{S}}(w) = \frac{Aw}{c_0 n_r} |\psi(p = 0)|^2 \frac{\Gamma_{xb}}{\pi\{(E_{\mathrm{exc}} - \hbar w)^2 + \Gamma_{xb}^2\}}, \tag{35}$$

where

$$A = \frac{e^2\hbar^2}{3\varepsilon_0 m_{\mathrm{e}}^* E_{cv}^2 L_z} M_0 |\langle\psi_{c1}|\psi_{v1}\rangle|^2 \wp. \tag{36}$$

For the 1S exiton, only $\rho = 0$ is allowed and hence, the polarization factor $\wp$, $\wp^{\mathrm{TE}} = \frac{3}{2}$ (HH), $\frac{1}{2}$ (LH) and $\wp^{\mathrm{TM}} = 0$ (HH), 2 (LH).

3. Material parameters

The material parameters of the quaternary alloys InGaAsP and InAlGaAs are of great importance for the determination of the QW band-gap energy and other electronic and optical properties. The parameters should include band-gap energy, effective mass, spin-orbit energy, elastic stiffness parameter, lattice constant, hydrostatic pressure coefficient, permittivity, sheer deformation potential, heavy- and light-hole masses, and the luttinger parameters. However, for some parameters, there might not be sufficient data from the available literature. In this review, we aim to present comprehensive material parameters for InGaAsP and InAlGaAs. Those parameters that are not available directly will be interpolated using either linear or quadratic scheme with bowing as much as possible. Therefore, the parameters of the corresponding five binary alloys (GaAs, InAs, InP, GaP and AlAs), and two ternary compounds (AlGaAs and InAlAs) will also be discussed. The material parameter sets are divided into two different temperatures: room temperature (around 300 K) and low temperature (below 10 K). For the ternary and quaternary materials, some of the parameter equations are directly extracted from the major references such as data book, text, and review papers, while some are obtained by fitting using the different individual values of the binary alloy by the Vegard's law and by fitting using the different individual values of the binary alloy by the Vegard's law and various fitting methods. In some fittings, bowing effect is being added in order to deduce the parameter equations more accurately. All the material parameters discussed in this section are listed in Tables 1–5 for easy reference.

3.1. GaAs, InAs, GaP, InP, and AlAs

Since some of the parameters equations of the ternary and quaternary material systems are not available from literature and they have to be fitted by the interpolation scheme, it is important to make available a full set of binary parameters. In the available literature, however, there exists incoherence for some of these parameters. Some of the data extracted from different papers show large differences for the same material. In some cases, data which are obtained at low temperature originally may be quoted as room temperature. The definition of these temperatures varies without a clear indication. In addition, data are referred to a source based on other works. This often causes confusion. Therefore, careful considerations have to be taken when selecting the most accurate and reliable data in order to build a comprehensive and systemic set of parameters. In this review, five

Table 1
Parameters of the binary alloy systems (values used in this paper are bracketed)

	GaAs		Ref.	InAs		Ref.	GaP		Ref.	InP		Ref.	AlAs		Ref.
E_g	1.424	RT	[54]	(0.354)	295 K	[54,7]	(2.780)	300 K	[7]	(1.34)	RT	[7,54]	2.168	RT	[12]
(eV)	1.42	RT	[24,34]	0.355			2.74			1.35			2.95	RT	[34,24]
	1.423	RT	[72,167]	0.36									3.03	300 K	[7]
													3.14	300 K	[7]
													2.98	295 K	[7]
													(3.017)	RT	[161]
	1.5177	4.2 K	[7]	(0.418)	4.2 K	[7]	(2.895)	4.2 K	[7]	(1.4236)	2 K	[7]	(3.0994)	2 K	[72]
	1.5192	2 K	[7]	0.42	0 K	[33]	2.87	0 K	[33]	1.423	LT		3.13	4 K	[7]
	(1.5194)	2 K	[72]							1.42	0 K	[33]	3.06	0 K	[51]
m_e	0.068	RT	[54]	0.027	RT	[54]	0.33	RT	[54]	(0.077)	RT	[54]	(0.1719)	300 K	[72]
	0.063	RT	[7]	(0.0213)[a]	300 K										
(m^*/m_0)	(0.0632)	RT	[72,165]	0.0219	250 K	[7]	(0.158)	78 K	[55]						
				0.0231	150 K	[7]									
	(0.0665)	LT	[54,72]	0.023	LT	[54]	0.21	LT	[54]	0.0785	LT	[54]	0.15	LT	
	0.067	LT	[7,33]	(0.023)	15–	[33,7]	0.254	LT	[49]	(0.080)	LT	[33]	(0.1808)	2 K	[72]
			[165]		88 K		(0.17)	LT	[33]	0.0765	LT	[7]			
V_0(eV)	(0.34)	RT	[54,34]	(0.41)	300 K	[54,7]	(0.08)	RT	[54]	(0.11)	RT	[54]	0.3	RT	[12]
		300 K	[7,165]										0.28	RT	[34,7]
													(0.275)	300 K	[7]
	(0.341)	4.2 K	[7]	(0.38)	1.5 K	[7]	(0.082)	4.2 K	[7]	(0.108)	4.2 K	[7]	(0.275)[c]		
c_{11}	(11.9 ± 0.01)	RT	[7,165]	(8.329)	RT	[7]	(14.05)	300 K	[7]	(10.11)	RT	[7]	(12.02)	RT	[7]
	11.88	RT	[24,12]							10.22	RT	[7]	12.0	RT	[12,24]
	11.8	RT	[34]												
(10^{11}dyn/cm^2)	12.21 ± 0.03	77 K	[165]Exp	(8.33)	LT	[160]	(14.39)	LT	[160]	(10.22)	LT	[160]	(12.5)	LT	[160]
	12.15	77 K	[168]				14.12	LT	[163]						
	12.17	0 K	[165]Extr												
	11.26	0 K	[7,168]												
	(12.23)	LT	[160]												
c_{12}	(5.38)	RT	[24,12]	(4.526)	RT	[7]	(6.203)	300 K	[7]	(5.61)	RT	[7]	5.70	RT	[12,7]
			[7,167]												[24]
	5.4	RT	[34]										(5.30)	RT	[34]
	5.38 ± 0.01	300 K	[165]Exp												
(10^{11} dyn/cm^2)	(5.71)	0 K	[7,160]	(4.53)	LT	[160]	(6.52)	LT	[160]	(5.76)	LT	[160]	(5.34)		[160]
			[165]Ext.				6.25	LT	[163]						
	5.66 ± 0.01	77 K	[165]Ext.												
	5.56	77 K	[168]												
	5.58	0 K	[168]												
	5.48	0 K	[7]												

a_0(Å)	(5.6533)	RT	[12,7]	(6.0583)	RT	[7]	(5.4505)	RT	[7]	(5.8687)	RT	[7]	(5.6611)	RT	[12,24]
	5.6533	RT	[162,24] [167]	6.0584	RT	[162]	5.4512	RT	[162]	5.8686	RT	[7]			[24]
	(5.6525)	5 K	[7]	(6.0584)	4.2 K	[7]	(5.4512)	4.2 K	[7]	(5.8688)	4.2 K	[7]	(5.66)	291 K	[34,7]
dE_g/dP	(11.3)	RT	[167,7]	(10.2)	RT	[7]	(10.7)	RT	[7]	(8.4)	RT	[7]	(10.2)	RT	[12]
	12.6	300 K	[7]												
(10^{-9} eV/kbar)	11.5	RT	[12]												
		LT			LT			LT			LT				
$\varepsilon(0)$	(13.18)	RT	[33,12]	(14.55)	RT	[33]	(11.1)	RT	[33]	(12.35)	RT	[33]	(10.06)	RT	[12,7]
	12.91	300K	[7]												
	(12.4)	4 K	[33,165]	(14.55)	LT	[33]	(10.86)	4 K	[33]	(11.77)	4 K	[33]	(10.06)[c]	RT	
b (eV)				(−1.8)	300 K	[7]							(−1.5)	RT	[24,12] [34]
	−1.7	77 K	[7]				−1.8	4 K	[7]	−2.0	5 K	[7]			
$m_{LH\perp}$	0.068	RT	[54]	(0.024)	RT	[59]	(0.16)	77 K	[7]	(0.12)[e]			0.18	RT	[16]
(m^*/m_0)	(0.088)	RT	[72,165]	0.0281(100)[b]	RT								0.14	RT	[34]
	0.076	RT	[7]	0.0267(111)[b]	RT								0.145	300 K	
	0.0905(100)[b]	RT											(0.1415)	RT	[72]
	0.0791(111)[b]	RT													
	0.0802(100)[b]	LT		0.0275(100)[b]	LT		0.1623(100)[b]	LT		0.0958(100)[b]	LT		0.150	LT	[12,33]
	0.0704(111)[b]	LT		0.0261(111)[b]	LT		0.1330(111)[b]	LT		0.0847(111)[b]	LT		(0.1489)	LT	[72]
	0.074	LT	[33]	0.026	20 K	[7]	0.14	LT	[33]	0.089	LT	[33]			
	0.082	<100 K	[7,165]	(0.027)[d]	LT	[33]	0.17	1.6 K	[7]	0.12	4.2 K	[7]			
	(0.0951)	LT	[72]				(0.162)[d]	LT		(0.0958)[d]	LT				
$m_{HH\perp}$	(0.5)	RT	[54,7]	0.41	RT	[54]	(0.54)	77 K	[7]	0.56	110 K	[7]	0.44	RT	[34]
(m^*/m_0)	0.45	RT	[117]	0.4630(100)[b]	RT								(0.7)	RT	[57]
	0.3774(100)[b]	RT		3.1250(111)[b]	RT										
	0.9524(111)[b]	RT		(0.5172)[b]	RT										
	0.3534(100)[b]	LT		(0.3413(100))[d]	LT		(0.4464(100))[d]	LT		0.4717(100)[b]	LT		0.76	LT	[12,33]
	0.9174(111)[b]	LT		0.9174(111)[b]	LT		1.1364(111)[d]	LT		1.3158(111)[b]	LT	[7]	0.51	LT	[16]
	0.51	<100 K	[7]				0.67(111)	1.6 K	[7]	0.45	4.2 K		(0.50)	6 K	[7]
	0.62	LT	[33]							(0.472)[d]	LT				
	0.34	4 K	[51]												
	0.45	70 K	[7]												
	0.0475	50 K	[7]												
	0.33	LT	[166]												

Table 1 (*continued*)

	GaAs		Ref.	InAs		Ref.	GaP		Ref.	InP		Ref.	AlAs		Ref.
$m_{LH\|\|}$	(0.23)[d]	RT		0.082[d]	RT		(0.34)[d]	RT		0.29[d]	RT		0.36[d]	RT	
(m^*/m_0)				(0.084)[d]	RT					(0.2921)[d]	RT		(0.3523)[d]	RT	
	0.21[d]	LT		0.087[d]	LT		(0.32)[d]	LT		0.22[d]	LT		0.32[d]	LT	
	(0.2068)[d]	LT		(0.088)[d]	LT					(0.2381)[d]	LT		(0.3146)[d]	LT	
$m_{HH\|\|}$	(0.11)[d]	RT		0.031[d]	RT		(0.19)[d]	RT		0.15[d]	RT		0.13[d]	RT	
(m_*/m_0)				(0.0315)[d]	RT					(0.1493)[d]	RT		(0.1768)[d]	RT	
	0.12[d]	LT		0.035[d]	LT		(0.20)[d]	LT		0.11[d]	LT		0.18[d]	LT	
	(0.1160)[d]	LT		(0.036)[d]	LT					(0.1196)[d]	LT		(0.1806)[d]	LT	
	(6.68)[d]	RT		18.9	RT	[164]	(4.05)[d]			5.04	110 K	[7]	4.16	RT	
				(21.8)	RT	[59]				(5.060)[d]	RT		(4.2478)	RT	
	7.65	LT	[33]	(19.67)	LT	[33]	4.2	LT	[33]	(6.28)	LT	[33]	4.04	LT	[33]
	(6.7282)[d]	LT											(4.3580)[d]	LT	
γ_2	(2.34)[d]	RT		8.37	RT	[164]	(1.10)[d]	RT		1.56	110 K	[7]	1.37[d]	RT	
				(9.9333)[d]	RT					(1.637)[d]	RT		(1.4096)[d]	RT	
	2.41	LT	[33]	(8.37)	LT	[33]	(0.98)	LT	[33]	(2.08)	LT	[33]	0.78	LT	[33]
	(1.8935)[d]	LT			LT								(1.1790)[d]	LT	
γ_3				(9.29)	RT	[164]		RT		(1.73)	110 K	[7]		RT	
	(3.28)	LT	[33]	(9.29)	LT	[33]	(1.66)	LT	[33]	(2.76)	LT	[33]	(1.42)	LT	[33]

[a]Extrapolated by data from Ref. [53].

[b]Calculated by $m_{LH\perp} = (\gamma_1 + 2\gamma_2)^{-1}$, $m_{LH\|} = (\gamma_1 - 2\gamma_3)^{-1}$, $m_{HH\perp} = (\gamma_1 - 2\gamma_2)^{-1}$ and $m_{LH\|} = (\gamma_1 + 2\gamma_3)^{-1}$.

[c]Low-temperature data not available, hence, room-temperature values are used here.

[d]Calculated by $\perp$ effective mass ($m_{HH\perp}$ and $m_{LH\perp}$) chosen by $m_{LH\perp} = (\gamma_1 + 2\gamma_2)^{-1}$, $m_{LH\|} = (\gamma_1 - \gamma_2)^{-1}$, $m_{HH\perp} = (\gamma_1 - 2\gamma_2)^{-1}$ and $m_{HH\|} = (\gamma_1 + \gamma_2)^{-1}$.

[e]Calculated by γ chosen by $m_{LH\perp} = (\gamma_1 + 2\gamma_2)^{-1}$, $m_{HH\perp} = (\gamma_1 - 2\gamma_2)^{-1}$.

binary materials, GaAs, InAs, InP, GaP, and AlAs, are required in order to fit some of the parameters of AlGaAs, AlInAs, InGaAsP, and InAlGaAs,. The selected material parameters for these five binaries are shown in Table 1. Their band-gap energies, electron and hole masses will be discussed in detail.

3.1.1. Band-gap energy (E_g)

3.1.1.1. GaAs. GaAs is a direct band-gap material widely use in optoelectronics. A commonly referenced band-gap energy at room temperature is 1.424 eV, measured by Sell [29] using absorption and photoluminescence. However, a careful study of this paper leads to the realization that the room temperature defined by the author is 298 K, instead of the commonly used 300 K. Considering the equation of temperature (T) dependence of energy gap by Varshni [30]:

$$E_g(T) = E_g(0) - \frac{\alpha T^2}{T+\beta} = E_g(0) - \Delta E_g(T) \quad \text{eV}, \tag{37}$$

where different values of the parameters α and β can be found for different materials, and for GaAs [39], we get

$$E_g(T) = 1.519 - \frac{5.405 \times 10^{-4} T^2}{(T+204)} \quad \text{eV}. \tag{38}$$

In fact, it is found that E_g (298 K) = 1.424 eV. For this reason, many people are misled to use 1.424 eV as the band-gap at 300 K. To be more accurate, E_g (300 K) of GaAs is calculated to be 1.423 eV, using Eq. (38).

E_g at 2 K is 1.5192 eV in accordance to Sell [31] and the theoretical band gap from Lawaetz [32] is 1.52 eV. Apart from direct measurement, E_g of GaAs can be obtained by substituting $w = 0$ into the band-gap equation of $Al_wGa_{1-w}As$ (to be discussed in the next section), which yields 1.519 eV. In order to make this list consistent with the one of $Al_wGa_{1-w}As$, this more recent data is chosen as the low temperature band gap for GaAs in Table 1. It is also in good agreement with the other values mentioned above.

3.1.1.2. AlAs. A lot of data have been found for the room-temperature band-gap energy of AlAs [33–35] but they show a large variation ranging from 2.95 to 3.13 eV. In order to make the parameters consistent with the parameters concerning $Al_wGa_{1-w}As$, the band gap of AlAs at room temperature is calculated to be 3.017 eV by taking $w = 1$ in the band-gap equation of $Al_wGa_{1-w}As$. Similarly, for AlAs at low temperature, we get 3.0994 eV.

3.1.1.3. InP. InP is another direct-band-gap material usually used for substrate. A number of values of its band-gap energy found in different literatures agree with each other. An earlier electroreflectance measurement from Cadorna [36] listed in Landolt-Bornstein [7] is 1.34 eV at 297 K. Using the temperature dependence equation of InP [37],

$$E_g(T) = 1.421 - \frac{3.63 \times 10^{-4} T^2}{(T+162)} \quad \text{eV}, \tag{39}$$

the theoretical room-temperature band-gap energy is calculated to be 1.351 eV. More recently, Bennett's calculation [38] using effective-mass theory and absorption-curve fitting to estimate electrorefraction (ER) and electroabsorption (EA) in direct-gap III–V materials confirms that E_g (300 K) = 1.34 eV for InP. This value is selected in Table 1.

For InP at low temperature, the theoretical value is suggested to be around 1.42 eV from both literature [37] and Eq. (39). An experimental result by Rochon [39] at 4.2 K is 1.423 eV, which is obtained from the zero-field convergence point of the three upper curves of left and right polarizations. Another low temperature (2 K) value of 1.4236 eV from Ekardt [40] is listed in Landolt-Bornstein [7]. Since all the values found are very close to each other, the most recent value (1.4236 eV) is used.

3.1.1.4. InAs. InAs and GaP are not very commonly used for general purpose and so, not many data are widely published. For InAs, the temperature dependence equation [37] is

$$E_g(T) = 0.420 - \frac{2.5 \times 10^{-4} T^2}{(T+75)}. \tag{40}$$

Using Eq. (40), room-temperature band gap is estimated to be 0.36 eV. The only result found originates from Luke's electroreflectance measurement [43] in Bornstein is 0.354 eV at 295 K. The experimental and theoretical results show little difference. Thus, 0.354 eV is taken as our room temperature band gap of InAs, even our room temperature is defined as 300 K.

Table 2
The AlGaAs material parameter sets

	Unit	Temp.	$Al_wGa_{1-w}As$
E_g (eV)	eV	RT	$1.423 + 1.594w + w(1-w)(0.127 - 1.31w)$
		LT	$1.5194 + 1.36w + 0.22w^2$
Δ_0	eV	RT	$0.34 - 0.065w$
		LT	$0.341 - 0.066w$
m_c	m_0^a	RT	$0.0632 + 0.0856w + 0.0231w^2$
		LT	$0.0665 + 0.1006w + 0.0137w^2$
m_{HH}	m_0	RT	$0.50 + 0.2w$ $(w < 0.45)$
		LT	$0.34 + 0.16w$ $(w < 0.45)$
m_{LH}	m_0	RT	$0.088 + 0.0372w + 0.0163w^2$
		LT	$0.0951 + 0.0441w + 0.0097w^2$
c_{11}	$\times 10^{11}$ dyn/cm^2	RT	$11.90 + 0.12w$
		LT	$12.23 + 0.27w$
c_{12}	$\times 10^{11}$ dyn/cm^2	RT	$5.38 - 0.08w$
		LT	$5.71 - 0.37w$
a_o	Å	RT	$5.6533 + 0.0078w$
		LT	$5.6525 + 0.0075w$
dE_g/dP	eV/bar	RT	$11.5 - 1.3w$
		LT	
ε (static)	ε_0	RT	$13.18 - 3.12w$
		LT	$12.40 - 1.8w$
γ_1	—	RT	$6.68 - 2.4322w$
γ_2	—		$2.34 - 0.9304w$
γ_3	—		
		LT	$6.7282 - 2.3702w$
			$1.8935 - 0.7145w$
			$3.28 - 1.86w$
b	eV	RT	$-1.7 + 0.2w$
		LT	
$m_{LH\|\|}$	m_0	RT	$0.23 + 0.1223w$
		LT	$0.2068 + 0.1078w$
$m_{HH\|\|}$	m_0	RT	$0.11 + 0.0668w$
		LT	$0.1160 + 0.0646w^*$

*$m_0 = 9.11 \times 10^{-31}$ kg, $\varepsilon_o = 8.85$ pF/m.

In the same way, the theoretical value of low-temperature band gap of InAs is calculated to be 0.42 eV by Eq. (40), which is equal to the value listed in Lawaetz [32]. The value 0.418 eV [41], which is listed in the chapter of InAs in Landolt-Bornstein, is chosen to be our low-temperature band gap at 4.2 K due to the lack of available reference.

3.1.1.5. GaP. Controversy arises in determining the band gap of GaP, which is an indirect band-gap mate-

Table 3
The InAlAs material parameter set

	Unit	Temp.	$In_xAl_{1-x}As$
E_g (eV)	eV	RT	$3.017 - 3.363x + 0.7x^2$
		LT	$3.0994 - 3.3814x + 0.7x^2$
Δ_0	eV	RT	$0.275 - 0.015x + 0.15x^2$
		LT	$0.275 - 0.045 + 0.15x^2$
m_e	m_o	RT	$0.1719 - 0.1506x$
		LT	$0.1808 - 0.1578x$
m_{HH}	m_o	RT	$0.7 - 0.1828x$
		LT	$0.5 - 0.1587x$
m_{LH}	m_o	RT	$0.1415 - 0.1175x$
		LT	$0.1489 - 0.1219x$
c_{11}	$\times 10^{11}$ dyn/cm^2	RT	$12.02 - 3.691x$
		LT	$12.5 - 4.17x$
c_{12}	$\times 10^{11}$ dyn/cm^2	RT	$5.3 - 0.774x$
		LT	$5.34 - 0.81x$
a_o	Å	RT	$5.6611 + 0.3972x$
		LT	$5.66 + 0.3984x$
dE_g/dP	eV/bar	RT	10.2
		LT	
ε (static)	ε_0	RT	$10.06 + 4.49x$
		LT	$10.06 + 4.49$
γ_1	—	RT	$4.16 + 14.74x$
γ_2	—		$1.37 + 7x$
γ_3	—		
		LT	$3.76 + 15.91x$
			$0.68 + 7.69x$
			$1.42 + 7.87x$
b	eV	RT	$-1.5 - 0.3x$
		LT	
$m_{LH\|\|}$	m_o	RT	$0.3523 - 0.2683x$
		LT	$0.3146 - 0.2266x$
$m_{HH\|\|}$	m_o	RT	$0.1768 - 0.1453x$
		LT	$0.1806 - 0.1446x$*

*$m_0 = 9.11 \times 10^{-31}$ kg, $\varepsilon_0 = 8.85$ pF/m.

Table 4
The InGaAsP material parameters

	Unit	Temp.	$In_wGa_{1-w}AS_vP_{1-v}$
E_g	eV	RT	$1.35 - 1.17v + 0.668(1-w) + 0.069v(1-w) + 0.15v^2 + 0.03(1-w)v^2 + 0.785(1-w)^2 + 0.758(1-w)^2 - 0.322v(1-w)^2$
		LT	$0.418 + 1.10(1-w) + 1.005(1-v) - 0.493w(1-w) - 0.180v(1-v) - 0.265w(1-w)(1-v) - 0.030(1-w)(1-v)v + 0.347(1-w)(1-v) + 0.875wv(1-w)(1-v)$
SOS(Δ_0)	eV	RT	$0.34(1-w)v + 0.41wv + 0.08(1-w)(1-v) + 0.11w(1-v)$
		LT	$0.341(1-w)v + 0.38wv + 0.082(1-w)(1-v) + 0.108w(1-v)$
m_e	m_0	RT	$0.0632(1-w)v + 0.0213wv + 0.158(1-w)(1-v) + 0.077w(1-v)$
		LT	$0.0665(1-w)v + 0.023wv + 0.17(1-w)(1-v) + 0.08w(1-v)$
m_{LH}	m_0	RT	$0.088(1-w)v + 0.024wv + 0.16(1-w)(1-v) + 0.12w(1-v)$
		LT	$0.0951(1-w)v + 0.027wv + 0.162(1-w)(1-v) + 0.0958w(1-v)$
m_{HH}	m_0	RT	$0.5(1-w)v + 0.5172wv + 0.54(1-w)(1-v) + 0.56w(1-v)$
		LT	$0.34(1-w)v + 0.3413wv + 0.4464(1-w)(1-v) + 0.472w(1-v)$
c_{11}	$\times 10^{11}$ dyn/cm^2	RT	$11.9(1-w)v + 8.329wv + 14.05(1-w)(1-v) + 10.11w(1-v)$
		LT	$12.23(1-w)v + 8.33wv + 14.39(1-w)(1-v) + 10.22w(1-v)$
c_{12}	$\times 10^{11}$ dyn/cm^2	RT	$5.38(1-w)v + 4.526wv + 6.203(1-w)(1-v) + 5.61w(1-v)$
		LT	$5.71(1-w)v + 4.53wv + 6.52(1-w)(1-v) + 5.76w(1-v)$
a_0	Å	RT	$5.6533(1-w)v + 6.0583wv + 5.4505(1-w)(1-v) + 5.8687w(1-v)$
		LT	$5.6525(1-w)v + 6.0584wv + 5.4512(1-w)(1-v) + 5.8688w(1-v)$
dE_g/dP	eV/bar	RT	$11.3(1-w)v + 10.2wv + 10.7(1-w)(1-v) + 8.4w(1-v)$
		LT	
ε	ε_0	RT	$13.18(1-w)v + 14.55wv + 11.1(1-w)(1-v) + 12.35w(1-v)$
(static)		LT	$12.4(1-w)v + 14.55wv + 10.86(1-w)(1-v) + 11.77w(1-v)$
γ_1	—	RT	$6.68(1-w)v + 21.8wv + 4.05(1-w)(1-v) + 5.060w(1-v)$
		LT	$6.7282(1-w)v + 19.67wv + 4.2(1-w)(1-v) + 6.28w(1-v)$
γ_2	—	RT	$2.34(1-w)v + 9.9333wv + 1.10(1-w)(1-v) + 1.637w(1-v)$
		LT	$1.8935(1-w)v + 8.37wv + 0.98(1-w)(1-v) + 2.08w(1-v)$
γ_3	—	RT	
		LT	$3.28(1-w)v + 9.29wv + 1.66(1-w)(1-v) + 2.76w(1-v)$
b	eV		$-1.7(1-w)v + (-1.8)wv + (-1.8)(1-w)(1-v) + (-2.0)w(1-v)$
$m_{LH\|\|}$	m_0	RT	$0.23(1-w)v + 0.084wv + 0.34(1-w)(1-v) + 0.2921w(1-v)$
		LT	$0.2068(1-w)v + 0.088wv + 0.32(1-w)(1-v) + 0.2381w(1-v)$
$m_{LH\|\|}$	m_0	RT	$0.11(1-w)v + 0.0315wv + 0.19(1-w)(1-v) + 0.1493w(1-v)$
		LT	$0.1160(1-w)v + 0.036wv + 0.20(1-w)(1-v) + 0.1196w(1-v)$*

*RT = 300 K, LT ⩽ 10 K; $m_0 = 9.11 \times 10^{-31}$ kg, $\varepsilon_0 = 8.85$ pF/m.

rial. Both indirect and direct band gaps are available and they differ largely in magnitude. As observed, most of the fitting work applications use the direct band-gap energy instead of indirect band gap, though quite a number of publications has emphasized its importance. Since not many publications are concerned with this material, data are simply extracted from Landolt-Bornstein – the direct band gap is measured to be 2.780 eV at 300 K [42] and extrapolated to be 2.894 eV at 0 K [46]. The extrapolated value agrees with the one mentioned in Lawaetz [32].

3.1.2. Electron effective mass (m_c)

3.1.2.1. GaAs. Stillman [45] suggests $0.0665m_0$ to be the low temperature m_e for GaAs, while Lawaetz's [32] calculations indicate $0.067m_0$. With the theoretical calculation from the m_e of $Al_wGa_{1-w}As$ at low temperature (to be discussed later), $0.0665m_0$ is further confirmed to be the low temperature m_e of GaAs. It is listed in Table 1.

For room temperature m_e of GaAs, measurement of Cadorna [46] AT 296 k SUGGESTS $0.067m_0$, which

Table 5
The InGaAsP material parameters

	Unit	Temp.	$In_wAl_vGa_{1-w-v}AS$
E_g(eV)	eV	RT	$\frac{WVT_{InAlAs}+v(1-w-v)T_{AlGaAs}+w(1-w-v)T_{InGaAs}}{wv+v(1-w-v)+w(1-w-v)}$
			$E_g(In_wAl_vAs) = 0.354w + 3.017v - 0.7wv$
			$E_g(Al_vGa_{1-w-v}As) = 1.423 + 0.594v + v(1-w-v)(0.127 - 1.313v)$
		LT	$E_g(In_wGa_{1-w-v}As) = 1.425 - 1.501w + 0.436w^2$
			$E_g(In_wAl_vAs) = 0.418w - 3.0994v - 0.7wv$
			$E_g(Al_vGa_{1-w-v}As) = 1.5194 + 1.36v + 0.22v^2$
			$E_g(In_wGa_{1-w-v}As) = 1.5194(1-w-v) + 0.418w - 0.51w(1-w-v)$
Δ_0	eV	RT	$0.41w + 0.275v + 0.34(1-w-v)$
		LT	$0.38w + 0.275v + 0.341(1-w-v)$
m_e	m_0*	RT	$0.0213w + 0.1719v + 0.0632(1-w-v)$
		LT	$0.023w + 0.1808v + 0.0665(1-w-v)$
m_{HH}	m_0	RT	$0.5172w + 0.7v + 0.5(1-w-v)$
		LT	$0.3413w + 0.5v + 0.34(1-w-v)$
m_{LH}	m_0	RT	$0.024w + 0.1415v + 0.088(1-w-v)$
		LT	$0.027w + 0.1489v + 0.0951(1-w-v)$
c_{11}	$w10^{11}$ dyn/cm^2	RT	$11.90 - 3.571w + 0.12v$
		LT	$12.23 - 3.9w + 0.27v$
c_{12}	$w10^{11}$ dyn/cm^2	RT	$5.38 - 0.854w - 0.08v$
		LT	$5.71 - 1.18w - 0.37v$
a_0	Å	RT	$5.653325 + 0.404975w + 0.007775v$
		LT	$5.6525 + 0.4059w + 0.0075v$
dE_g/dP	eV/bar	RT	$11.3 - 1.1w - 1.1v$
		LT	
ε (static)	ε_0	RT	$13.18 + 1.37w - 3.12v$
		LT	$12.40 + 2.15w - 2.34v$
γ_1	—	RT	$6.68 + 12.22w - 2.52v$
γ_2	—		$2.34 + 6.03w - 0.97v$
γ_3	—		
		LT	$7.65 + 12.02w - 3.89v$
			$2.41 + 5.96w - 1.73v$
			$3.28 + 6.01w - 1.86v$
b	eV	RT	
		LT	$-1.7 - 0.1w + 0.2v$
$m_{LH\|\|}$	m_0	RT	$0.23 - 0.148w + 0.13v$
		LT	$0.21 - 0.123w + 0.11v$
$m_{HH\|\|}$	m_0	RT	$0.11 - 0.079w + 0.02v$
		LT	$0.12 - 0.085w + 0.06v$

*$m_0 = 9.11 \times 10^{-31}$ kg, $\varepsilon_0 = 8.85$ pF/m.

is very different from those suggested in Bornstein [7] and Blakemore [14]. As a rule of thumb, effective mass will increase with decreasing temperature. $0.067m_0$ will seem quite unreasonable since it is larger than our pre-assumed low temperature m_e of GaAs ($0.0665m_0$). As the aim is to make the table agree with the parameters of $Al_wGa_{1-w}As$, the theoretical low temperature m_e of GaAs of $0.0632m_0$ calculated from $Al_wGa_{1-w}As$ is selected, which is in good agreement with the data listed in Bornstein [7] and does not contradict the rule.

3.1.2.2. AlAs. Due to experimental difficulties, not much research has been done for effective mass, especially for room temperature. For AlAs, not many publications are available. Therefore, $0.1719m_0$ is simply chosen as the room temperature m_e of AlAs, which is calculated from the parameters of $Al_wGa_{1-w}As$ with

$w = 1$. The value of $0.15m_0$ is used by Adachi [47] as low temperature m_e of AlAs. Since it is smaller than our calculated room temperature m_e of $0.1719m_0$, it is considered to be inappropriate. Lawaetz [37] has published a calculated low temperature m_e of $0.22m_0$, which, however, is much larger than our room temperature m_e. Thus, a more reasonable low temperature m_e, $0.1808m_0$, which is again utilized from the parameters of $Al_wGa_{1-w}As$, is chosen in Table 1.

3.1.2.3. InAs. $0.023m_0$ is the only low temperature m_e for InAs found in literatures [7,32]. Although its lowest applicable temperature is 15 K, it is applied in our list due to the lack of available data. Landolt-Bornstein has used an m_e of $0.027m_0$ [49] for room temperature m_e of InAs, which again does not make sense. Hence, an interpolated value [50] of $0.0213m_0$ at 300 K is chosen instead.

3.1.2.4. InP. Only a few papers are concerned with InP, and even fewer for GaP. Therefore, results are mainly quoted from Landolt-Bornstein [7] for room temperature data and Lawaetz for low temperature ones. For InP, $0.077m_0$ [51] and $0.080m_0$ [52] are chosen for room and low temperature m_e, respectively.

3.1.2.5. GaP. For GaP, low-temperature effective mass was found to be around $0.21m_0$ [53] and $0.254m_0$ in some publications [48] while as pointed out by Lawaetz [32], it is $0.17m_0$. These values show large discrepancies. Without further confirmation from other papers, it is difficult to judge which one is more appropriate. Lawaetz's review [7] is believed to be popular and is widely used. Hence, $0.17m_0$ is chosen for the low-temperature m_e of GaP. A room-temperature effective mass of $0.33m_0$ is quoted by Fiedler [53], which is much larger than the low-temperature one listed in its own paper and does not satisfy our assumption. The highest temperature effective mass found from other publications is $0.158m_0$ at 78 K [54]. Although 78 K is rather low compared to our proposed room temperature of 300 K, $0.158m_0$ is more reasonable and appropriate than $0.33m_0$. Thus, $0.158m_0$ is chosen in Table 1.

3.1.3. Heavy hole and light hole masses (m_{LH}, m_{HH})

It is well known that heavy- and light-hole masses (both perpendicular and parallel) are related to the Luttinger parameter by the following equations:

$$m_{LH\perp} = (\gamma_1 + 2\gamma_2)^{-1}, \quad m_{HH\perp} = (\gamma_1 - 2\gamma_2)^{-1},$$
$$m_{LH\parallel} = (\gamma_1 - \gamma_2)^{-1}, \quad m_{HH\parallel} = (\gamma_1 + \gamma_2)^{-1}. \qquad (41)$$

Difficulties are encountered in constructing Table 1 since there is not much interest in parameters, especially the parallel masses and the Luttingers parameters. Some of the data found are not coherent with each other and do not satisfy the above four equations. Therefore, some of them are calculated theoretically by these four equations based on other parameters found.

3.1.3.1. GaAs. The calculated $m_{LH\perp}$ of GaAs from $Al_wGa_{1-w}As$ if $0.088m_0$ at room temperature and $0.0951m_0$ at low temperature. Some other data are also available from Landolt Bornstein and Lawaetz, but they are very different from what we have interpolated. In order to make the tables agree with each other, 0.088 and $0.0951m_0$ are taken to be the room and low temperature $m_{LH\perp}$ in the list, respectively.

Without any other available data for comparison, $0.5m_0$ [55] listed in Bornstein is selected to be our room temperature $m_{HH\perp}$, while Miller's measurement [50] of $0.34m_0$ at 4 K is the low temperature $m_{HH\perp}$.

With the above perpendicular hole masses at both temperatures found, the Lutinger parameters and the parallel hole masses at different temperatures can be calculated by the four equations. Refer to Table 1 for results.

3.1.3.2. AlAs. Not many reports have commented particularly on the hole masses of AlAs. Therefore, values for $m_{LH\perp}$ at room and low temperature are obtained from the parameters of $Al_wGa_{1-w}As$. They are $0.1415m_0$ and $0.1489m_0$, respectively. For $m_{HH\perp}$, we refer to the 6 K temperature of $0.50m_0$ from Bornstein [7], and $0.7m_0$ at room temperature by Perlin [56]. Using the same method for GaAs, the rest of the parameters are calculated by Eq. (41).

3.1.3.3. InAs. For InAs at room temperature, the $m_{HH\perp}$ found in the text of Fiedler [53], which is claimed to be room temperature, actually applies to 0 K in the notation of the paper of Kane [57]. From

another publication, a 298 K experimental $m_{LH\perp}$ of $0.024m_0$ and γ_1 of 0.351 are found [58]. With $m_{LH\perp}$ and γ_1 found, the corresponding γ_2 and $m_{HH\perp}$ are then to be 9.9333 and $0.5172m_0$ by Eq. (41). The corresponding parallel masses can be deduced.

For low-temperature InAs, parameters including $m_{LH\perp}, \gamma_1$, and γ_2 are listed in Lawaetz. Cross-checking these values with Eq. (41) proves coherence among them and they are listed in our table. Using the same method, the remaining $m_{HH\perp}$, and the two parallel hole masses can be calculated.

3.1.3.4. GaP. For GaP, the 77 K cyclotron measurements of 0.16 and $0.54m_0$ listed in Landolt-Bornstein [59] are the only available reference for both the $m_{LH\perp}$ and $m_{HH\perp}$, respectively. They are chosen as the room-temperature data in the table although 77 K is much lower than our defined room temperature. Since no other significant work has been done for the Luttinger parameters as well as the parallel masses for GaP at room temperature, they are simply obtained by calculation using Eq. (41).

Not much data are available for low temperature $m_{HH\perp}$ and a large discrepancy is shown in the $m_{LH\perp}$ obtained from Lanbolt-Bornstein [7] and Lawaetz [32]. For this reason, low temperature γ_1 (4.21) and γ_2 (0.98) from Lawaetz are used to deduce all the other parameters.

3.1.3.5. InP. The only found room temperature $m_{HH\perp}$ of $0.56m_0$ is measured at 110 K and the only room temperature $m_{LH\perp}$ is interpolated to be $0.12m_0$ [7]. Due to the lack of available reference, the rest of the room-temperature parameters of InP will be obtained by calculations. As for the low-temperature parameters, they will be calculated based on the Luttinger parameters quoted by Lawaetz [32], which are $\gamma_1(6.28)$ and $\gamma_2(2.08)$.

3.1.4. Other parameters

For the rest of the parameters which are concerned in Table 1, the room-temperature ones are quoted mainly from Landolt Bornstein [7], and the low-temperature ones are referenced from Lawaetz [32].

3.2. $Al_wGa_{1-w}As$ and $In_wAl_{1-w}As$

The ternary alloy AlGaAs and InAlAs are of considerable interest since they cover a wide range of device applications such as light emitting diodes, solar cells and lasers. They are also the basis for the interpolation of the quaternary material InAlGaAs. It is therefore essential to make a complete set of parameters for these two material systems.

3.2.1. $Al_wGa_{1-w}As$

Many publications report about the band structure of this material and comment on the dependencies on alloy composition w of its band-gap energy [60–66]. However, there are discrepancies among the published data. Dingle [62] has put a lot of effort working on them and has solved the problem. However, his work is 10 years backdated. In fact, no other attempts are made to verify his results. Therefore, a transmission measurement at 2 K is performed on $Al_wGa_{1-w}As$ with low aluminium concentration by Bosio [67]. This put the work of Dingle into question. Using polynomial functions to fit the experimental data, the most recent band-gap equation of $Al_wGa_{1-w}As$ at low temperature is obtained:

$$E_g(w) = 1.5194 + 1.36w + 0.22w^2 \quad \text{eV}. \tag{42}$$

Due to the lack of data points, the cubic dependence term in the equations is ignored, which reduces the accuracy of the equation. However, since no other recent band-gap equations are found for $Al_wGa_{1-w}As$ Eq. (42) is selected, as listed in Table 2.

In the same literature from Bosio [67], band-gap energy at room temperature is evaluated:

$$E_g(w) = 1.423 + 1.36w + 0.22w^2 \quad \text{eV}. \tag{43}$$

However, a simple quadratic function cannot describe the characteristics of the band-gap energy over the entire range. Therefore, work from Aspnes [68], in which a cubic equation describing its band gap at room temperature is presented, is more reliable:

$$E_g(w) = 1.424 + 1.519w + w(1-w)(0.127 - 1.310w) \quad \text{eV}. \tag{44}$$

Since it is confirmed that the band gap for GaAs is 1.423 eV at 300 K, a minor modification has to be

made by changing the constant term in the equation. Therefore, the equation becomes

$$E_g(w) = 1.423 + 1.519w + w(1-w)(0.127 - 1.310w) \quad \text{eV}. \tag{45}$$

It is used as the room-temperature band-gap equation for $Al_wGa_{1-w}As$ in Table 2.

Only a few reports have commented on the m_e of $Al_wGa_{1-w}As$, which include the Camras's equation [69] at low temperature, approximated from other data [70] and numerical results [71]:

$$m_e(w) = 0.0665 + 0.0835w \quad m_0. \tag{46}$$

Another low-temperature effective mass function of $Al_wGa_{1-w}As$ is also fitted from experimental results by Jani [72].

$$m_e(w) = 0.0657 + 0.0174w + 0.145w^2 \quad m_0. \tag{47}$$

From a more recent report, Hrivnak [73] has demonstrated the determination of electron effective masses in $Al_wGa_{1-w}As$ compounds using the experimental data of energy gaps, band offsets, and energy levels in $Al_wGa_{1-w}As/GaAs$ quantum wells. The Al concentration dependence equation of $Al_wGa_{1-w}As$ at low temperature is obtained as follows:

$$m_e(w) = 0.0665 + 0.1006w + 0.0137w^2 \quad m_0. \tag{48}$$

The room-temperature effective mass relationship is utilized in the same literature:

$$m_e(w) = 0.0632 + 0.0856w + 0.0231w^2 \quad m_0. \tag{49}$$

It is believed that the report from Hrivnak is more suitable for the modeling purpose of $Al_wGa_{1-w}As$ in this report since it gives the latest calculation of $Al_wGa_{1-w}As$ effective mass at both room and low temperatures. Furthermore, this is a complete review which not only includes effective masses, but also the light-hole effective mass relations at both temperatures (to be discussed later). Therefore, the m_e at both room and low temperatures from Hrivnak is chosen in Table 2.

Only one report [73] is concerned with the equation of $m_{LH\perp}$ for $Al_wGa_{1-w}As$, which suggest the room and low temperatures to be

$$m_{LH\perp}(w) = 0.088 + 0.0372w + 0.0162w^2, \tag{50}$$

$$m_{LH\perp}(w) = 0.0951 + 0.0441w + 0.0097w^2, \tag{51}$$

respectively. Hence, these two equations are chosen in the parameter list.

Since information about $m_{HH\perp}, m_{LH\parallel}$ and $m_{HH\parallel}$ of $Al_wGa_{1-w}As$ is not available in literature, they are fitted theoretically using an interpolation scheme which can efficiently approximate the ternary relationship by using the equation

$$T_{ABC}(w) = wB_{AC} + (1-w)B_{BC} + w(w-1)C_{AB}, \tag{52}$$

where T is the ternary parameter, B is the binary parameter, and C is the bowing parameter. However, in this review, the bowing parameter is ignored due to the lack of reference and data. The corresponding missing $m_{HH\perp}, m_{LH\parallel}$ and $m_{HH\parallel}$ (refer to Table 2) can then be fitted using the relevant binary parameters, as listed in Table 1.

Since no available literature is found for other parameters, they are all interpolated using Eq. (52) and are listed in Table 2.

3.2.2. $In_wAl_{1-w}As$

As the literature reveals, only room-temperature alloy dependence of band-gap energy of $In_wAl_{1-w}As$ is available [37]:

$$E_g(w) = 3.07 - 3.408w + 0.698w^2 \quad \text{eV}. \tag{53}$$

However, the literature does not provide the corresponding low-temperature equation. Hence, the band-gap equations of InAlAs for both room (Eq. (54)) and low temperatures (Eq. (55)) are determined by the interpolation method shown in Eq. (52):

$$E_g(w) = 3.017 - 3.363w + 0.7w^2 \quad \text{eV}, \tag{54}$$

$$E_q(w) = 3.0994 - 3.3814w + 0.7w^2 \quad \text{eV}, \tag{55}$$

where the bowing factor is referenced from Krijn [33]. In addition to band gap, this report mentions the bowing factor for interpolating the spin-orbit energy of $In_wAl_{1-w}As$. As a result,

$$\Lambda_0(w) = 0.275 - 0.015w + 0.15w^2 \quad \text{eV}, \tag{56}$$

$$\Lambda_0(w) = 0.275 - 0.045w + 0.15w^2 \quad \text{eV}, \tag{57}$$

for room and low temperatures, respectively.

The electron effective mass and other parameters of $In_wAl_{1-w}As$ are all interpolated using Eq. (52) with the bowing factor omitted due to the lack of reference. Results are listed in Table 3.

3.3. $In_wGa_{1-w}As_vP_{1-v}$

InGaAsP is a very attractive material for optoelectronic applications, and hence, a lot of work has been done concerning its room-temperature alloy composition dependence of direct band-gap. One simple band-gap equation of $In_wGa_{1-w}As_vP_{1-v}$ at room temperature has been deduced [22] as

$$E_g(w,v) = 1.35 + 0.668(1-w) - 1.17v + 0.758(1-w)^2 + 0.18v^2 - 0.069(1-w)v - 0.322(1-w)^2v + 0.03(1-w)v^2 \quad \text{eV}. \tag{58}$$

An equivalent analysis by Moon using earlier ternary data is also reported [72]:

$$E_g(w,v) = 1.42 + (0.36v - 1.36)v + [0.76(1-w) + 0.67](1-w) + [0.09 - 0.15v + 0.28(1-w)](1-w)v \quad \text{eV}. \tag{59}$$

In addition to direct reference, equation for $In_wGa_{1-w}As_vP_{1-v}$ can be fitted using interpolation scheme. For this quaternary system $In_wGa_{1-w}As_vP_{1-v}$, the simplest relation is derived from four binary parameters as shown:

$$Q(w,v) = w(1-v)B_{InP} + wvB_{InAs} + (1-w)(1-v)B_{GaP} + (1-w)vB_{GaAs}, \tag{60}$$

where B is the binary parameter.

With the finalized band-gap energies of the corresponding four binary alloys listed in Table 1, a very simple equation describing the band-gap energy of $In_wGa_{1-w}As_vP_{1-v}$ is obtained:

$$E_g(w,v) = 1.34w(1-v) + 0.354wv + 2.78(1-w)(1-v) + 1.423(1-w)v \ \text{eV}. \tag{61}$$

However, band-gap energy does not vary linearly with concentration. The above linear fitting method obviously cannot describe the band-gap energy appropriately.

If relationships for the ternary material parameters are available, the quaternary parameter can be expressed as [23]

$$Q(x,y) = \frac{w(1-w)[(1-v)T_{InGaP} + yT_{InGaAs}] + v(1-v)[(1-w)T_{GaAsP} + xT_{InAsP}]}{w(1-w) + v(1-v)}, \tag{62}$$

where the ternary parameters may include a quadratic dependence term and make a fairly reliable quadratic equation for the quaternary alloy. The compositional dependence data of E_g in the relevant ternary systems used are as follows [37]:

$$E(In_wGa_{1-w}P) = 1.35 + 0.643(1-w) + 0.786(1-w)^2 \quad \text{eV}, \tag{63}$$

$$E(In_wGa_{1-w}As) = 0.36 + 0.505(1-w) + 0.555(1-w)^2 \quad \text{eV}, \tag{64}$$

$$E(InAs_vP_{1-v}) = 1.35 - 1.083v + 0.091v^2 \quad \text{eV}, \tag{65}$$

$$E(GaAs_vP_{1-v}) = 2.74 - 1.473v + 0.146v^2 \quad \text{eV}. \tag{66}$$

By substitution into Eq. (62), the alloy composition dependence of the direct band-gap energy of $In_wGa_{1-w}As_vP_{1-v}$ is obtained.

Another way to approximate the band-gap energy of $In_wGa_{1-w}As_vP_{1-v}$ is referenced as follows [24]:

$$\begin{aligned} E_g(w,v) = {} & wvE_g(GaAs) + (1-w)vE_g(InAs) \\ & + w(1-v)E_g(GaP) \\ & + (1-w)(1-v)E_g(InP) \\ & + w(w-1)[vC_{In\text{-}Ga}(InGaAs) \\ & + (1-v)_{C_{In\text{-}Ga}}(InGaP)] \\ & + v(v-1)[wC_{As\text{-}P}(GaAsP) \\ & + (1-w)C_{As\text{-}P}(InAsP)], \end{aligned} \tag{67}$$

where, for example, $C_{In\text{-}Ga}(InGaAs)$ is the band-gap nonlinearity factor (bowing factor) of InGaAs.

With our previously determined binary parameters of GaAs, InAs, GaP and InP, together with the band nonlinearity provided in Ref. [24], the band-gap equation is deduced to be

$$\begin{aligned} E_g(w,v) = {} & 1.423(1-w)v + 0.354wv \\ & + 2.78(1-w)(1-v) + 1.34w(1-v) \\ & + w(w-1)[0.51v + 0.7(1-v)] \\ & + v(v-1)[0.3(1-w) + 0.23w] \quad \text{eV}. \end{aligned} \tag{68}$$

An alloy dependence equation on band-gap energy $In_wGa_{1-w}As_vP_{1-v}$ is published [73]:

$$\begin{aligned}E_g(w,v) = {} & 0.418 + 1.10(1-w) + 1.005(1-v) \\ & - 0.493w(1-w) - 0.180v(1-v) \\ & - 0.265w(1-w) - 0.030v(1-w)(1-v) \\ & + 0.347(1-w)(1-v) \\ & + 0.875wv(1-w)(1-v) \quad \text{eV}. \end{aligned} \tag{69}$$

Interpolating the band-gap equation for $In_wGa_{1-w}As_vP_{1-v}$ at low temperature using Eq. (62) is not possible since the low-temperature relations for the corresponding four ternary systems are not available. Therefore, the only theoretical way to implement the low-temperature band-gap relation of $In_wGa_{1-w}As_vP_{1-v}$ is using Eq. (67). This results as

$$\begin{aligned}E_g(w,v) = {} & 1.5194(1-w)v + 0.418wv \\ & + 2.895(1-w)(1-v) \\ & + 1.4236w(1-v) + w(w-1) \\ & \times[0.51v + 0.7(1-v)] \\ & + v(v-1)[0.3(1-w) + 0.23w] \quad \text{eV}. \end{aligned} \tag{70}$$

For the six available room-temperature relations of $In_wGa_{1-w}As_vP_{1-v}$, Eq. (58) is chosen while Eq. (69) is used as the low-temperature band-gap equation in Table 4, since these two equations give the best result in our calculations.

For the rest of the parameters, they are all fitted using the simplest fitting method as stated in Eq. (61), which is mentioned at the beginning of this section.

3.4. $In_wAl_vGa_{1-w-v}As$

Very little has been done on the quaternary system InAlGaAs as compared to that of InGaAsP because of the difficulty in preparing this crystal by liquid phase epitaxy. This is due to the large distribution coefficient for Al [25]. As far as the available literature reveals, only two equations for the dependence of band-gap energy on alloy composition of $In_wAl_vGa_{1-w-v}As$ at room temperature are obtained experimentally. The first one [74], which is frequently referenced in other papers [7,75], is fitted using measured PL compositional dependence of the band-gap energies with an interpolated bowing factor:

$$\begin{aligned}E_g(w,v) = {} & 0.36 + 2.093v + 0.629(1-w-v) \\ & + 0.577v^2 + 0.436(1-w-v)^2 \\ & + 1.013v(1-w-v) - 2wv(1-w-v) \ \text{eV}. \end{aligned} \tag{71}$$

Another alloy dependence band-gap equation obtained experimentally at room temperature [76] is

$$\begin{aligned}E_g(w,v) = {} & 1.424 + 1.455v + 0.191v^2 \\ & - 1.614w + 0.55w^2 + 0.043wv \quad \text{eV}. \end{aligned} \tag{72}$$

This equation gives a reasonable agreement with the published expression of AlGaAs, InGaAs, and AlInAs.

Material parameters of $In_wAl_vGa_{1-w-v}As$ can also be estimated by the same method used for $In_wGa_{1-w}As_vP_{1-v}$ [24] in Eq. (67) in the last section. As a result,

$$\begin{aligned}E_g(w,v) = {} & wE_g(\text{InAs}) \\ & + vE_g(\text{AlAs}) + (1-w-v)E_g(\text{GaAs}) \\ & - v(1-w-v)C_{\text{Al-Ga}}(\text{AlGaAs}) \\ & - wvC_{\text{In-Al}}(\text{InAlAs}) \\ & - w(1-w-v)C_{\text{In-Ga}}(\text{InGaAs}). \end{aligned} \tag{73}$$

Therefore, using this method, the band-gap parameter at room temperature is

$$\begin{aligned}E_g(w,v) = {} & 0.354w + 3.017v + 1.423(1-w-v) \\ & - 0.99wv - 0.51w(1-w-v) \\ & + 0.04v(1-w-v) \quad \text{eV}. \end{aligned} \tag{74}$$

The one at low temperature can be obtained as follows:

$$\begin{aligned}E_g(w,v) = {} & 0.418w + 3.0994v + 1.5194(1-w-v) \\ & - 0.99wv - 0.51w(1-w-v) \\ & + 0.04v(1-w-v) \quad \text{eV}. \end{aligned} \tag{75}$$

Adachi [77] introduces one more method to interpolate quaternary materials with this kind of alloy composition $A_wB_vC_{1-w-v}D$, which is

$$Q(x,y) = \frac{xyT_{\text{ABD}}(u) + yzT_{\text{BCD}}(v) + zxT_{\text{ACD}}(w)}{xy + yz + zx}, \tag{76}$$

where

$$u = \frac{1+x-y}{2},$$
$$v = \frac{1+y-z}{2},$$
$$w = \frac{1+x-z}{2}.$$

Therefore, for $In_wAl_vGa_{1-w-v}As$, its equation of alloy composition dependence of band-gap energy at both room and low temperatures can be approximated with the substitution of band-gaps from InGaAs (refer to Table 4), AlGaAs (refer to Table 2), and InAlAs (to be discussed).

By using Vegard's law, the band gap for $In_wAl_vGa_{1-w-v}As$ is deduced:

$$E_g(w,v) = \frac{wvT_{InAlAs} + v(1-w-v)T_{AlGaAs} + w(1-w-v)T_{InGaAs}}{wv + v(1-w-v) + w(1-w-v)} \quad (77)$$

and the corresponding ternary parameters at room temperature are

$$E(In_wAl_vAs) = 0.354w + 3.017v - 0.7wv \quad \text{eV}, \quad (78)$$

$$E(Al_vGa_{1-w-v}As) = 1.423 + 1.594v + v(1-w-v)(0.127-1.313v) \quad \text{eV}, \quad (79)$$

$$E(In_wGa_{1-w-v}As) = 1.425 - 1.501w + 0.436w^2 \quad \text{eV}. \quad (80)$$

The band-gap equation for $In_wAl_vGa_{1-w-v}As$ at low temperature is also fitted using the same principle as with the ternary parameters at low temperature:

$$E(In_wAl_vAs) = 0.418w + 3.0994v - 0.7wv \quad \text{eV}, \quad (81)$$

$$E(Al_vGa_{1-w-v}As) = 1.5194 + 1.36v + 0.22v^2 \quad \text{eV}, \quad (82)$$

$$E(In_wGa_{1-w-v}As) = 1.5194(1-w-v) + 0.418w - 0.51w(1-w-v) \quad \text{eV}. \quad (83)$$

All the band-gap parameters available are tested against programs using the available experimental data, and their accuracy and availability are judged.

The remaining parameters are fitted linearly, as shown in Table 5.

4. Experimental data

In this review, both single and multiple QW material systems of AlGaAs/GaAs, InGaAs/GaAs, InGaAs/InP, InGaAs/InAlAs, and InGaAs/AlGaAs are considered. The band-gap energy of these material systems are examined under low temperature (below 10 K) and room temperature (around 300 K), both with zero field applied. All the calculated band-gap energies are compared with the experimental values which are obtained by different optical and electrical measuring techniques. These techniques include photoluminescence (PL), photoluminescence excitation (PLE), photoreflectance (PR), absorption (Ab), photoconductance (PC), electroreflectance (ER), and transmission (TR). As mentioned before, different measurement techniques have different significant effects on the band-gap energy of different QW structures. Therefore, a brief discussion on the major measuring methods (PL, PC, and PR), which most data are collected from, is presented.

4.1. Measuring techniques

PL has been extensively used for the assessment of quantum well structures such as thin GaAs layers embedded in an AlGaAs medium. This is a non-destructive technique and does not require any contact with the materials under investigation. Under normal excitation conditions, the main photoluminescence peak corresponds to an excitonic transition which is close to the band-to-band transition energy in the QW.

From the shift in energy of this peak with respect to the band gap of bulk GaAs, one can get direct evidence of the quantum localization energy due to the existence of an energy well in the thin GaAs layer. Under luminescence excitation conditions, additional peaks appear, which correspond to higher-order transitions in the well. Although it is the most well-developed measurement technique, it does have its limitations: it only yields information about the ground-state

absorption peak energy and gives no detail for the higher state transition energy.

PLE is also a commonly used method in measuring band-gap energy of QW structures. It is analogous to absorption spectroscopy and provides information about the higher-lying energy levels.

PC is an effective technique in determining the band-gap energy of the QW structures as the PC spectra in QW is proportional to the absorption spectra for the intrinsic optical transitions. In addition, PC measurements do not require the substrate etching process (which is required for absorption measurements) that may cause strain in QW. However, PC measurements do not have an application of an electric field which changes the intrinsic energy (Stark shift), the transition strength, and the transition lifetime.

PR is a measuring technique which requires no special mounting of the sample and can be performed in a variety of conditions. Since PR measurement is a contactless technique, it tends to be used in studies of external parameters such as temperature, pressure, and stress. Furthermore, important information can be gained by varying the properties of the pump beam such as wavelength, frequency, and amplitude.

4.2. Distribution of measuring technique analysis

In this section, a comprehensive analysis of the distribution of data collected from different QW material systems at specific temperatures is presented. The statistics of the room and low temperatures of the AlGaAs/GaAs QW material system are shown in Figs. 2 and 3, respectively. Fig. 2 shows that at room temperature, PR and PC are the most popular measuring techniques. Nearly 160 sets of data are obtained from them. For low temperature, as shown in Fig. 3, the measurements are mainly taken from Ab, PL, and PLE. More than 90% of the total data are measured by these three techniques. The room- and low-temperature statistics for the InGaAs/GaAs QW material system are shown in Figs. 4 and 5, respectively. It is observed that the phenomenon is quite similar to that of the AlGaAs/GaAs QW material system. Again, the PR and PC dominate the distribution of measurements at room temperature while Ab, PL, and PLE dominate at low temperature. However, in this QW material system, there are also about 17% of measurements taken from PC at low temperature.

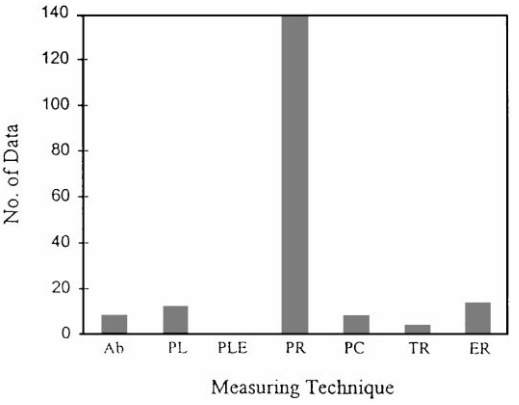

Fig. 2. Distribution of the measurement technique of AlGaAs/GaAs QW structures at 300 K.

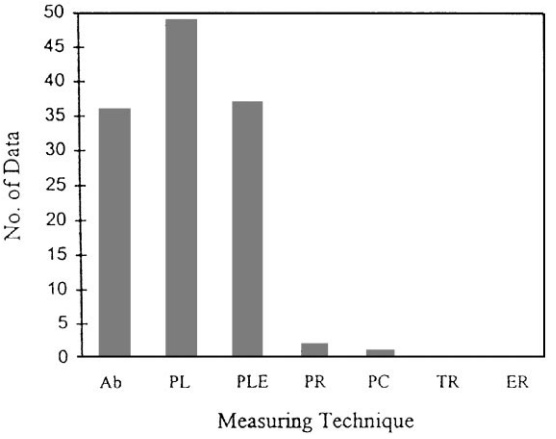

Fig. 3. Distribution of the measurement technique of AlGaAs/GaAs QW structures at low temperature.

The statistics for InGaAs/InP QW material system at room- and low-temperatures are shown in Figs. 6 and 7, respectively. For low-temperature measurements, the majority is taken from Ab, PL, and PLE, as in the above two cases. For the room temperature case, data is mostly obtained using the Ab technique. There are also a few sets measured by PL, PC, and TR. However, they only make up a small amount when compared to Ab. In addition, observing the six figures reveals that a large amount of experimental data of the AlGaAs/GaAs and InGaAs/GaAs QW structures are available in literature while there is a lack of the InGaAs/InP QW data. This also creates

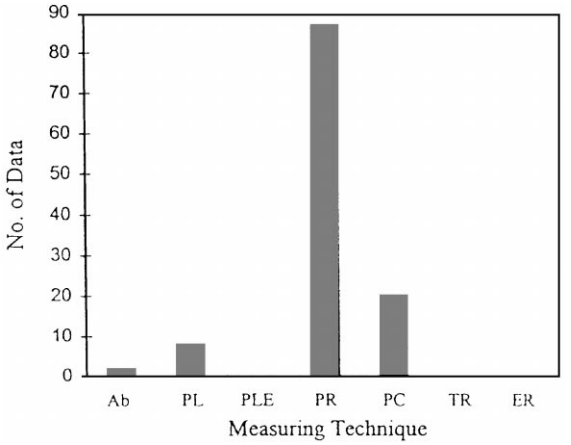

Fig. 4. Distribution of the measurement technique of InGaAs/GaAs QW structures at 300 K.

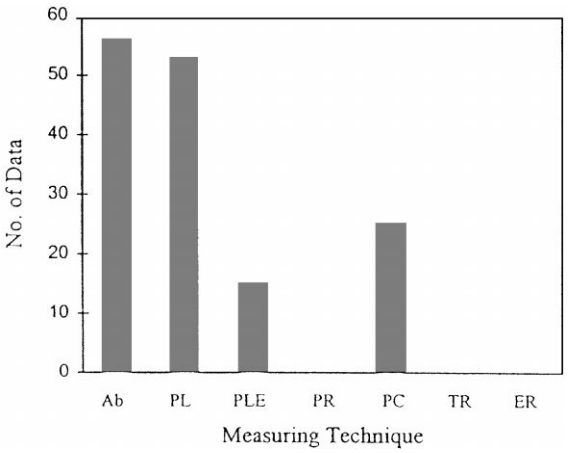

Fig. 5. Distribution of the measurement technique of InGaAs/GaAs QW structures at low temperature.

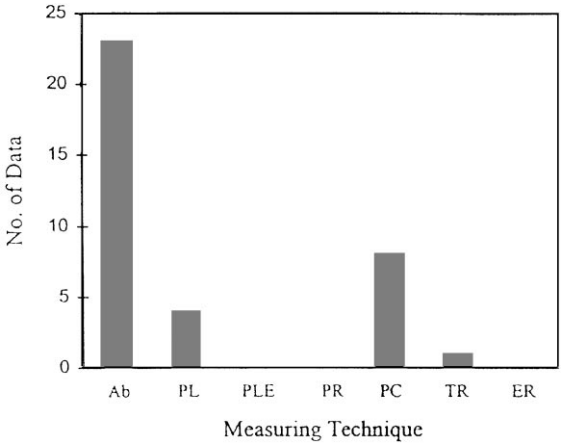

Fig. 6. Distribution of the measurement technique of InGaAs/InP QW structures at 300 K.

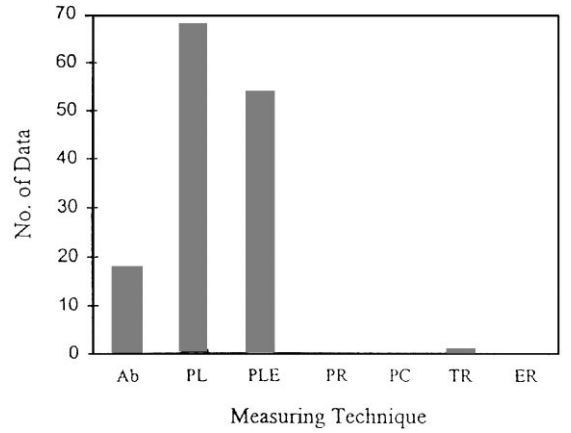

Fig. 7. Distribution of the measurement technique of InGaAs/InP QW structures at low temperature.

some difficulties in preparing the review paper as only little InGaAs/InP data can be used to compare with the experimental data.

The available literatures show that the measured band-gap energy of these systems varies with different temperatures, well widths, and alloy concentration of QW material systems. For a constant well width, each QW exhibits different behavior with a change in the concentration of alloy. This will be discussed in the later sections. In addition, the energy varies as the temperature changes from low temperature to room temperature. For all the QW material systems, the band-gap values obtained from low temperature are higher than that obtained from room temperature. At temperature below 30 K, Stokes shift, which results from spectral diffusion of excitons towards the low-energy localized states in the inhomogeneous line, affects the band-gap energy in fair quality QW samples. This shift mainly affects the measured data which is obtained from PL and PR measurement techniques in which a maximum deviation of 15 meV may be introduced. Comparing with the measurement by PLE or Ab, Stoke shift only shows little effect on them.

Moreover, it is claimed that Stoke shift does not affect much on high-quality QW samples with smooth and abrupt interfaces.

Disagreements are also observed between experimental values obtained from QWs of the same material system (even with same well width and same concentration) but different measuring methods. In addition, there are some experimental results from different reports showing largely deviated values with the same measuring method for QWs of exactly the same structure. This clearly demonstrates the inconsistency in the measurement of QW data and we cannot depend only on the experimental results obtained. Therefore, it is necessary to use the appropriate parameters in the theoretical calculation to accurately and consistently determine the band-gap energy in order to predict the behavior of the QWs of different structures.

Using the parameters listed in Tables 1–5, a theoretical model is set up to calculate the band-gap energy at any alloy composition and QW dimension. With different band offset ratio chosen appropriately for each of the systems as suggested by recent studies, the band-gap energy of different QW structures are calculated and compared with the respective experimental results. Generally, most of the calculated results are in good agreement with the representative experimental results obtained by different measuring methods at different temperatures except a few cases.

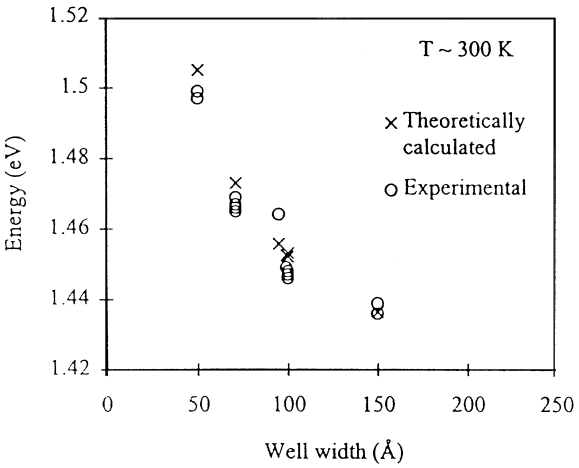

Fig. 8. Band-gap energy of AlGaAs/GaAs QW with Al alloy concentration around 0.18 (0.15–0.2) and varying well width at room temperature.

5. Band-gap analysis

5.1. AlGaAs/GaAs

In the AlGaAs/GaAs QW system, QW structures with well width varying from 4 to 20 nm and alloy concentration of Al from 0.1 to 0.6 are investigated. The band offset ratio for this system is chosen to be 70 : 30 at both low and room temperatures [3]. The band-gap energy of QW structure varies for different temperatures. In this QW system, the values obtained from low temperature are higher than that obtained from room temperature. With constant well width, it is found that the band-gap energy of AlGaAs/GaAs QW increases with alloy concentration.

At room temperature, the calculated results all agree with the results obtained from different experimental measuring techniques. The average absolute error for the total fifteen sets of room temperature data is only 2 meV. The smallest differences between our calculated values and some PL experimental values [80,85] are only 0.3 and 0.7 meV while our best theoretical results for the PR and ER experimental values listed [78,79] only differ by 0.2 and 2 meV. In addition, comparisons are made between calculated results and the ones obtained from other literatures. The difference between our result and one PR theoretical value [78] is only 2 meV. For some theoretical results from other literatures [83,86,87], the error is as small as 4 meV. All other results are listed in Table 6. The room-temperature experimental values and the calculated values of the band-gap energies from QWs with similar alloy concentrations (± 0.05) are grouped and plotted against the well width, as shown in Figs. 8–10. As observed from the results in Table 6, little variation in the concentration of alloy has an insignificant effect on the band-gap energy. From Fig. 8, it is shown that for room temperature, theoretically calculated results lie fairly close to the experimental ones with an alloy concentration around 0.18. Excellent agreement is obtained when alloy concentration is around 0.26, as shown in Fig. 9. Even with an alloy concentration as high as 0.55 (Fig. 10), a generally good agreement is achieved. From all the figures, it is clear that as well width of the QW increases, the band-gap energy of the

Table 6
Summary of the comparison of the experimental band-gap energy from different authors and our calculated values of the AlGaAs/GaAs QW structures on both room and low temperatures

Temp. (K)	Tech.	Ref.	Conc.	Well width (Å)	Barrier width (Å)	MQW/ SQW	Theory (eV)	Experiment (eV)	Error (meV)
Room temperature									
300	PR	[2]	0.26	42	200	MQW	1.5331	1.535	−1.9
300	PR	[78]	0.26	54	100	MQW	1.5037	1.506	−2.3
297	ER	[79]	0.54	70	—	SQW	1.4872	1.485	2.2
295	PL	[80]	0.26	80	80	MQW	1.4687	1.469	−0.3
300	TR	[81]	0.3	80	—	MQW	1.4700	1.473	−2.6
300	PC	[82]	0.3	95	65	MQW	1.4585	1.454	3.9
300	PR	[83]	0.17	99.1	150	MQW	1.4525	1.499[a]	3.5
300	ER	[84]	0.3	100	200	MQW	1.4547	1.459	−4.6
300	PL	[85]	0.3	101	145	MQW	1.4549	1.468	−13.1
300	PR	[78]	0.26	102	100	MQW	1.4536	1.456	−2.3
300	PL	[85]	0.5	120	80	MQW	1.4479	1.454	−0.7
300	PR	[86]	0.3	144	—	MQW	1.4393	1.443[a]	3.7
300	PR	[78]	0.15	150	100	MQW	1.4364	1.436	0.5
300	PR	[78]	0.26	190	100	MQW	1.4317	1.432	−0.2
300	PR	[78]	0.26	190	100	MQW	1.4317	1.434[a]	−2.2
300	PR	[87]	0.24	210	150	MQW	1.4297	1.426[a]	3.8
Low temperature									
2	PL	[88]	0.25	60	70	MQW	1.5881	1.587	1.1
5	PLE	[89]	0.27	64	—	SQW	1.5836	1.5833	0.3
4	PL	[79]	0.54	70	—	SQW	1.5856	1.5873	−1.7
4	Ab	[90]	0.18	75	105	MQW	1.5638	1.562[a]	1.8
8	PLE	[91]	0.35	75	—	MQW	1.5733	1.5726	0.7
2	PLE	[92]	0.3	79	—	SQW	1.5669	1.5671	−0.1
4	Ab	[90]	0.26	81	—	SQW	1.5634	1.563[a]	0.5
6	PLE	[93]	0.26	90	175	MQW	1.5562	1.5556	0.7
6	PLE	[93]	0.26	90	175	MQW	1.5562	1.556[a]	0.7
4	PLE	[94]	0.335	101	—	SQW	1.5512	1.5498	1.4
5	PL	[95]	0.27	102	207	MQW	1.5492	1.5485	0.7
2	PL	[96]	0.207	120	—	SQW	1.5399	1.5397	0.3
8	PL	[97]	0.3	120	—	SQW	1.5476	1.5382	3.6
10	PL	[98]	0.21	140	—	SQW	1.5345	1.5440	4.1
6	PL	[99]	0.5	142	—	SQW	1.5363	1.5319	4.5
3	Ab	[100]	0.25	150	25	MQW	1.5328	1.5302	2.8
1.8	PLE	[101]	0.3	188	19	MQW	1.5273	1.5263	1
2	PC	[102]	0.25	245	100	MQW	1.5225	1.5209	1.7

[a]Calculated results.

QW decreases. The drop in band-gap energy becomes less significant when the well width is beyond 100 Å.

At low temperature, even better results are obtained. The deviations between most of the calculated and experimental results are insignificant, with an average absolute error of 2 meV for 18 sets of low-temperature data. The smallest error obtained for some experimental results [89,91,95,96] are only 0.3 and 0.7 meV. Comparisons are also made between our calcualated values and those from other authors. Our calculations only differ from the values of Chu et al. and Gershoni et al. [90,93] by less than 1 meV. Some other comparisons are shown in Table 6. For QWs with similar alloy concentrations (± 0.06), their theoretical and experimental band-gap energies are divided into groups and plotted against varying well width for discussion

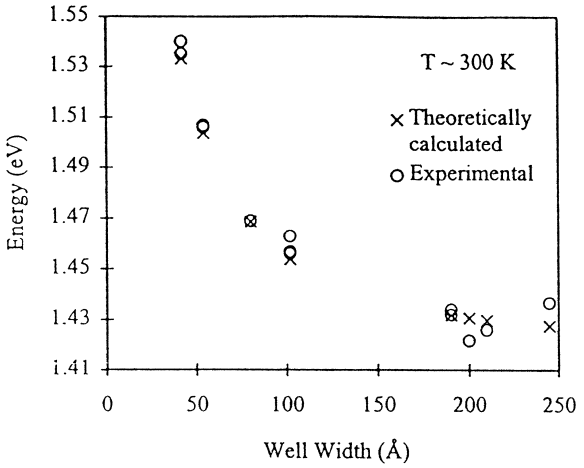

Fig. 9. Band-gap energy of AlGaAs/GaAs QW with Al alloy concentration around 0.26 (0.24–0.28) and varying well width at room temperature.

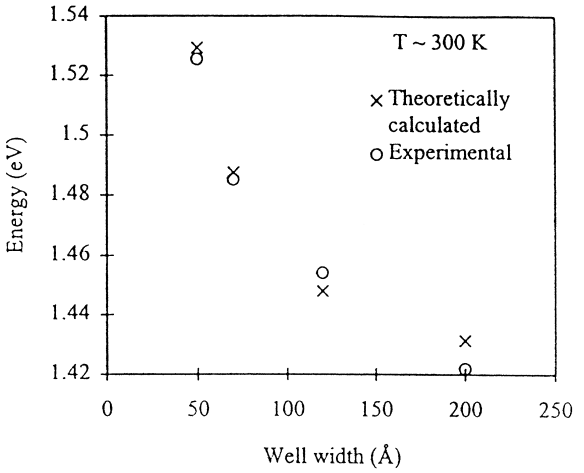

Fig. 10. Band-gap energy of AlGaAs/GaAs QW with Al alloy concentration around 0.55 (0.5–0.6) and varying well width at room temperature.

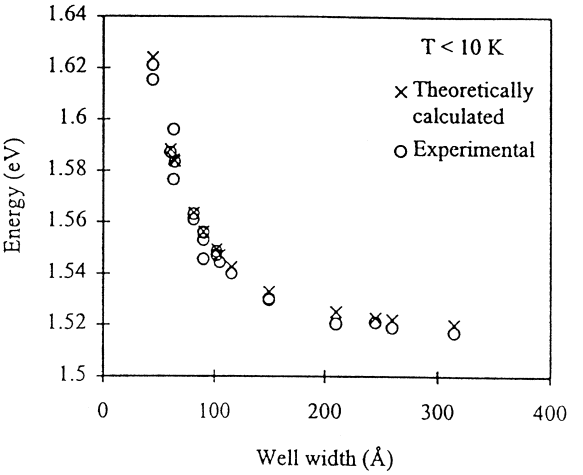

Fig. 11. Band-gap energy of AlGaAs/GaAs QW with Al alloy concentration around 0.26 (0.24–0.28) and varying well width at low temperature.

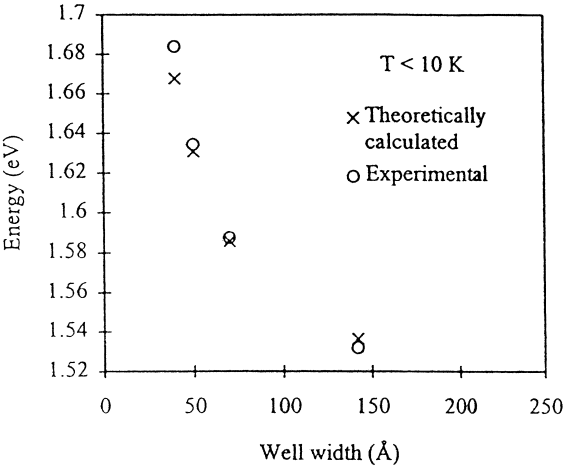

Fig. 12. Band-gap energy of AlGaAs/GaAs QW with Al alloy concentration around 0.52 (0.5–0.54) and varying well width at low temperature.

as shown in Figs. 11 and 12. From these two graphs, it is observed that both theoretical and experimental results lie very close to each other over a wide range of alloy concentration (from 0.26 to 0.52). It is also observed that the decrease in band-gap energy is slowed down when well width is larger than 10 nm.

Apart from the above, there are a few sets of data which do not agree well with us. Among them, one presented a data 13 meV away from our expected value [85]. However, there are two other sets of data [78,84], with nearly the same well width and concentration, showing good agreement with our calculated values. Their average absolute deviation from ours is only 4 meV. This value is neglected.

From Table 6, it is observed that the experimental data measured by different techniques: PL, PLE, Ab, ER, PC, and PR, are all consistent with our calculated values. The most accurate results are obtained from

PR at room temperature and PLE at low temperature. The experimental results which are obtained by the PLE method stay very close to the theoretical results. It is mainly due to the fact that Stoke shift effect is completely eliminated in the PLE spectrum while we have to take that into account in the PL and PR spectra. However, we find that the Stoke shift effect is very small in the AlGaAs/GaAs system. It is stated that Stokes shift between emission and 11H is as small as 0.6 meV [99]. Miller [106] also demonstrates that the Stokes shift of the photoluminescence peak is only up to 1 to 2 meV. Therefore, in this system, effect caused by the Stoke shift is neglected.

For both room temperature and low temperature, the comparisons of the experimental and calculated higher state transition energy are presented in Table 7. At room temperature, the differences between them are mostly within ±3 meV. For the 11L transition energy, our best results only deviate from Reddy et al. [78] and Fritz et al. [84] by 1 meV. For the 22H transition energy, the differences between our calculated values and the published data [84,102] are only 1 meV. In addition, comparisons are made between our calculated results and those from other literatures. Calculated 11L and 22H transition energy values are given in the report by Reddy et al. [78], which deviate from our calculation by 3 and 1 meV, respectively. In general, the experimental and calculated data are in agreement over a wide range of concentration and well width. For low temperature, the differences between them are mostly within ±3 meV. For the 11L transition energy, the differences between our theoretical calculated values and some experimental values [89,105] are 0.2 meV only. For the 22H transition energy, differences are found to be 0.1 and 2 meV only [100]. Comparisons are also available between our results and those obtained from other literatures, as listed in Table 7.

The agreement between the calculated and experimental values for a wide range of concentration of alloy and well width confirms the reliability of our assignment of the set of parameters for the QW model of the AlGaAs system.

5.2. *InGaAs/GaAs*

In the InGaAs/GaAs QW system, QW structure with well width from 1.4 to 25 nm and concentration

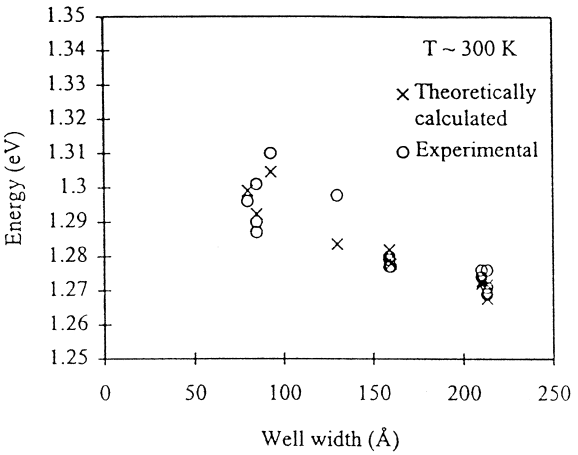

Fig. 13. Band-gap energy of InGaAs/GaAs QW with In alloy concentration around 0.15 (0.14–0.155) and varying well width at room temperature.

of In from 0.1 to 0.28 are investigated. The band offset ratio chosen in this system is 60 : 40 [3] for both low and room temperatures. In this QW system, it is observed that the band-gap energy decreases with an increase in the alloy concentration, which is opposite to the behavior of the AlGaAs/GaAs QW.

At room temperature, almost all the calculated results are in good agreement with the results obtained from different measuring methods experimentally except a few. The average absolute error for the nineteen sets of data is 3 meV. Our best calculated values deviate from the experimental values of Reddy et al. [108] and Arent et al. [109] by 1 and 2 meV only. These are both measured by PR. In addition, some calculations from other authors are available. The differences between the values of ours and Arent et al. [109] and Ji et al. [110] are 0.3 and 0.8 meV, respectively. All the other comparisons are shown in Table 8. In addition, the room-temperature experimental values and the calculated values of the band-gap energy are again plotted against well width, as shown in Figs. 13 and 14, with different alloy concentrations. It is observed that the band-gap energy of the InGaA/GaAs QW structure is quite sensitive to the change in alloy concentration compared with the AlGaAs/GaAs QW. From the figures, it can be clearly observed that as the well width of the QW increases, the band-gap energy of the QW decreases, as discussed in the last section.

Table 7
Summary of the comparison of the experimental higher state transition energy from different authors and our calculated values of the AlGaAs/GaAs QW structures on both room and low temperatures.

Temp. (K)	Tech.	Ref.	Conc.	Well width (Å)	Barrier width (Å)	MQW/ SQW	Theory (eV)	Experiment (eV)	Error (meV)
Room temperature									
300	PR	[78]	0.26 1L	54	100	MQW	1.5327	1.532	0.7
295	ER	[79]	0.54 1L	70	—	SQW	1.5178	1.5141	3.7
300	PR	[103]	0.18 2H	71	99	MQW	1.6218	1.618	3.8
300	TR	[104]	0.3 1L	80	—	MQW	1.4906	1.4933	−2.7
300	PR	[84]	0.3 1L	100	200	MQW	1.4710	1.4721	−1.1
300	PR	[84]	0.3 2H	100	200	MQW	1.5703	1.5672	3.1
300	PR	[86]	0.3 1L	144	—	MQW	1.4485	1.450	−1.5
300	PR	[86]	0.3 1L	144	—	MQW	1.4485	1.452[a]	−3.5
300	PR	[86]	0.3 2L	144	—	MQW	1.5422	1.545[a]	−2.4
300	PR	[86]	0.3 3H	144	—	MQW	1.6109	1.614[a]	−3.1
300	PR	[78]	0.15 1L	150	100	MQW	1.4438	1.443	0.8
300	PR	[78]	0.15 1L	150	100	MQW	1.4438	1.446[a]	−2.2
300	PR	[78]	0.26 1L	190	190	MQW	1.4375	1.437	0.5
300	PR	[78]	0.26 1L	190	190	MQW	1.4375	1.440[a]	−2.5
300	PR	[78]	0.26 2H	190	190	MQW	1.4728	1.474[a]	−1.2
300	PR	[78]	0.26 2L	190	190	MQW	1.4968	1.496	0.8
300	PR	[78]	0.26 3H	190	190	MQW	1.5393	1.541	−1.7
300	PR	[78]	0.26 3H	190	190	MQW	1.5393	1.537[a]	2.3
300	PR	[87]	0.24 1L	210	150	MQW	1.4345	1.431	3.5
296	PC	[102]	0.25 2H	245	100	MQW	1.4541	1.4555	−1.4
Low temperature									
4	Ab	[90]	0.23 1L	52	140	MQW	1.6215	1.620[a]	1.5
5	PLE	[89]	0.27 1L	64	—	SQW	1.6031	1.6029	0.2
2	PLE	[92]	0.3 1L	79	—	SQW	1.5833	1.5838	−0.5
5	PL	[95]	0.27 1L	81	205	MQW	1.5791	1.5771	2.0
3	Ab	[100]	0.25 1L	90	100	MQW	1.5689	1.5664	2.5
4	PLE	[94]	0.34 1L	100	—	SQW	1.5644	1.5657	−1.3
5	PL	[95]	0.27 1L	102	207	MQW	1.5607	1.5611	−0.4
5	PL	[105]	0.24 1L	105	—	MQW	1.5574	1.5576	−0.2
3	Ab	[100]	0.25 1L	116	100	MQW	1.5517	1.5514	0.3
3	Ab	[100]	0.25 1L	150	100	MQW	1.5392	1.5374	1.8
3	Ab	[100]	0.25 1L	150	25	MQW	1.5392	1.5372	2.0
3	Ab	[100]	0.25 1L	210	100	MQW	1.5286	1.5250	3.6
3	Ab	[100]	0.25 2H	210	100	MQW	1.5599	1.5600	−0.1
7	PL	[106]	0.28 1L	260	260	MQW	1.2971	1.5238	0.6
3	Ab	[100]	0.25 1L	315	100	MQW	1.5217	1.5200	1.7
3	Ab	[100]	0.25 2H	315	100	MQW	1.5375	1.5355	2.0
3	Ab	[100]	0.25 2L	315	100	MQW	1.5457	1.5477	−2.0
3	Ab	[100]	0.25 3H	315	100	MQW	1.5654	1.5694	−4.0

[a]Calculated results.

Fig. 13 indicates the behavior of the band-gap energy over a wide range of well width, with alloy concentration around 0.15. Results show that most of our calculated results agree with the experimental ones. When alloy concentration continues to increase to 0.24, good agreement is still achieved, as shown in Fig. 14. There is, however, some disagreement in a little part of the range: when the concentration of the alloy is around 0.3, the experimental data seems to be smaller than our calculated ones. However, as the errors are within

Table 8
Summary of the comparison of the experimental band-gap energy from different authors and our calculated values of the InGaAs/GaAs QW structure on both room and low temperatures

Temp. (K)	Tech.	Ref.	Conc.	Well width (Å)	Barrier width (Å)	MQW/ SQW	Theory (eV)	Experiment (eV)	Error (meV)
Room temperature									
300	PR	[106]	0.12	32 ± 3	95 ± 5	MQW	1.3660	1.372	−5.2
300	PR	[106]	0.12	32 ± 3	95 ± 5	MQW	1.3660	1.376[a]	−1.6
300	PR	[107]	0.11	40	70	MQW	1.3628	1.357	5.9
300	PR	[108]	0.15	80	200	MQW	1.2990	1.296[a]	3.1
300	PR	[109]	0.236	81	200	MQW	1.2187	1.222	−3.3
300	PR	[109]	0.236	81	200	MQW	1.2187	1.219[a]	−0.3
300	PR	[110]	0.155	85	200	MQW	1.2922	1.290[a]	2.3
300	PR	[108]	0.193	85	200	MQW	1.2566	1.252	4.6
300	PC	[111]	0.1	93	200	MQW	1.3419	1.347	−5.1
300	PC	[111]	0.2	93	200	MQW	1.2476	1.245	2.6
300	Ab	[112]	0.13	100	150	MQW	1.3103	1.3055	4.8
300	PR	[110]	0.146	159	200	MQW	1.2819	1.277	4.9
300	PR	[110]	0.146	159	200	MQW	1.2819	1.279[a]	2.9
300	PR	[108]	0.149	159	200	MQW	1.2788	1.280[a]	1.9
300	PR	[108]	0.15	160	200	MQW	1.2776	1.277	−2.3
300	PR	[108]	0.15	210	200	MQW	1.2729	1.276	3.9
300	PR	[109]	0.151	210	200	MQW	1.2729	1.274	−1.1
300	PR	[110]	0.151	213	200	MQW	1.2717	1.276	−4.2
300	PR	[110]	0.155	213	200	MQW	1.2717	1.271[a]	0.8
Low temperature									
4	PL	[113]	0.12	14	100	MQW	1.4946	1.4989	−4.3
6	PL	[109]	0.13	40	—	SQW	1.4401	1.455	4.1
7	PL	[114]	0.09	52	200	MQW	1.4613	1.4636	−2.3
10	Ab	[115]	0.2	80	150	MQW	1.3363	1.3330	3.3
4	Ab	[116]	0.193	85	200	MQW	1.3402	1.337[a]	3.2
7	PL	[114]	0.24	96	200	MQW	1.2862	1.2864	−0.2
2	Ab	[117]	0.136	100	—	MQW	1.3891	1.3907	−2.6
10	PL	[118]	0.21	100	—	SQW	1.3139	1.3120	2.7
4	Ab	[116]	0.13	106	200	MQW	1.3942	1.3917	2.5
4	Ab	[116]	0.13	106	200	MQW	1.3942	1.393[a]	0.9
2	Ab	[117]	0.073	150	—	MQW	1.4441	1.4465	−2.4
4	Ab	[116]	0.15	159	200	MQW	1.3558	1.3604	−3.5
15	PL	[119]	0.28	171	—	SQW	1.2209	1.2253	−4.4
4	Ab	[116]	0.15	213	200	MQW	1.3550	1.3500	5.0
4	Ab	[116]	0.15	213	200	MQW	1.3550	1.351[a]	−4.0
4	Ab	[109]	0.155	213	200	MQW	1.3550	1.358[a]	−3.0

[a]Calculated results.

± 5 meV and the comparisons show good agreement generally in the whole range, we still have confidence in our chosen sets of material parameters.

At low temperature, as expected, only small deviations are found between the calculated results and the experimental results. The average absolute error for the sixteen sets is only 3 meV. Differences as small as 0.2 and 2 meV are obtained between the theoretically calculated values and the experimental values suggested by some publications [114,117]. Comparisons are also made between our calculated values for low temperature and those from other authors [116], in which the deviations are only 0.4 to 4 meV. The rest of the comparisons are shown in Table 8. Again, graphs

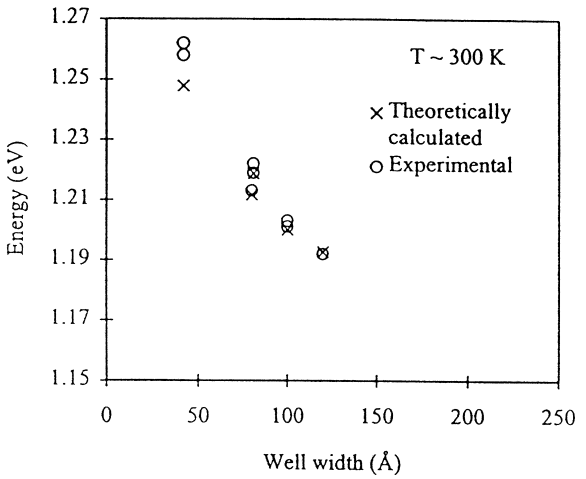

Fig. 14. Band-gap energy of InGaAs/GaAs QW with In alloy concentration around 0.24 (0.23–0.256) and varying well width at room temperature.

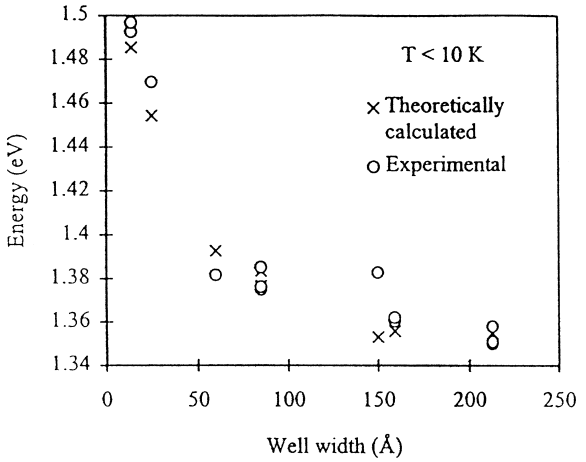

Fig. 15. Band-gap energy of InGaAs/GaAs QW with In alloy concentration around 0.155 (0.15–0.16) and varying well width at low temperature.

of the experimental values and the calculated values of the band-gap energy from similar QWs at low temperature are plotted against the well width as shown in Figs. 15 and 16. As observed, a small change in alloy concentration will lead to a great change in band-gap energy. Both Figs. 15 and 16 show clearly that as well width of the QW increases, the band-gap energy of the QW decreases. In Fig. 15, results are generally in fair agreement with a few whose differences are rather

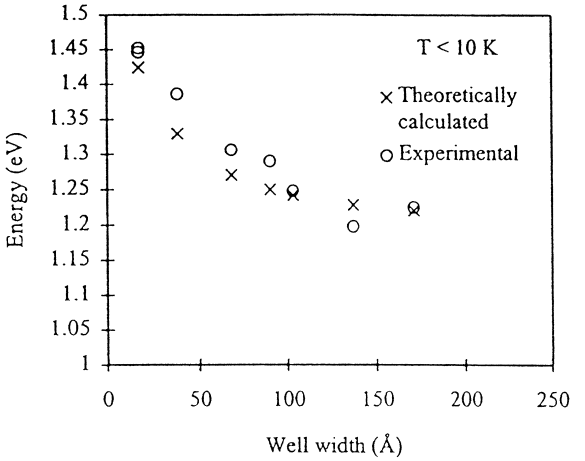

Fig. 16. Band-gap energy of InGaAs/GaAs QW with In alloy concentration 0.28 and varying well width at low temperature.

large. With lower concentration around 0.16, the drop in band-gap energy against increasing well width is rapid until the well width is around 6 nm. On the other hand, experimental results are less satisfactory with alloy concentration around 0.28, as shown in Fig. 16. The drop in band-gap energy slows down when well width is around 6 nm and the drop in values slows down when the well width is over 100 Å.

It is found that the average absolute error at both temperatures is a bit larger than that of the AlGaAs/GaAs system. However, the mean value of the error is only 0.77 and −0.31 for room and low temperatures, respectively. This means that our values always lie in the middle of the error range. As observed from the figures, the number of positive and negative errors are equally distributed over the whole range of alloy concentration and well width. The large fluctuation in the error can be explained by the fact that there is compressive strain in all compositions of indium in the InGaAS/GaAs QW structure. It is very difficult to achieve good quality InGaAs/GaAs materials fabricated under strain. Therefore, a comparatively larger fluctuation in error is expected.

From Table 8, it can be observed that the experimental data measured by different techniques, PL, Ab, PC, and PR, are all consistent with our calculated values. It is clearly shown that our calculated values for room temperature are in good agreement with those results obtained from PR. For low temperature, the

measurements from PL and Ab give reliable results. Stoke shift is also noted in the low temperature measurements. However, as the effect is so small in the good quality QW structure, it can be ignored. One significant point is the energy position of the 11H transition is very sensitive to the conduction-band offset because the 11H position scarcely depends on it as it stays close to the GaAs valence-band extremum. As a result, the conduction-band offset ratio has to be carefully selected in the calculation. Recently study suggests the value 66 : 40 [1].

For both room temperature and low temperature, the comparisons between the experimental and calculated higher state transition energy are discussed. For room temperature, the differences between them are mostly within ±8 meV. Only a few sets of data show a comparatively larger error. For the 11L transition energy, the difference between our calculated value and the experimental value of Tang [107] is 4 meV. For the 22H transition energy, our best results only indicate errors of 1 and 2 meV [108]. Comparisons are also made between our calculated results and those obtained from other literatures. Differences of 1.9 and 4.1 meV for two sets of calculated 22H transition energy are obtained [108]. For low temperature, the differences between them are found to be smaller than that obtained at room temperature. Most of them are within ±4 meV. For the 11L transition energy, the differences between our calculated values and the experimental values [116,117] are 1 and 4 meV. For the 22H transition energy, differences of 0.1 and 1.1 meV are resulted [106,114]. In addition, comparisons are made between our calculated results and those obtained from other literatures. Some other comparisons are shown in Table 9. In general, the experimental and calculated data for a wide range of concentration and well width agree with each other.

As the calculated results generally agree well with the experimental values for a wide range of concentration of alloy and well width, it is believed that our assignment of the set of parameters for the InGaAsP system is correct.

5.3. *InGaAs/InP*

In the InGaAs/InP QW system, QW structures with well width from 0.9 to 50 nm and concentration of In from 0.53 to 0.74 are investigated. The band offset ratio chosen at this system is 60 : 40 for measurements using optical techniques and 33 : 67 for measurements using electronic techniques at both low and room temperatures [1]. Observing the results listed in Table 10, it is found that the band-gap energy of this QW system decreases with an increase in the alloy concentration at both temperatures.

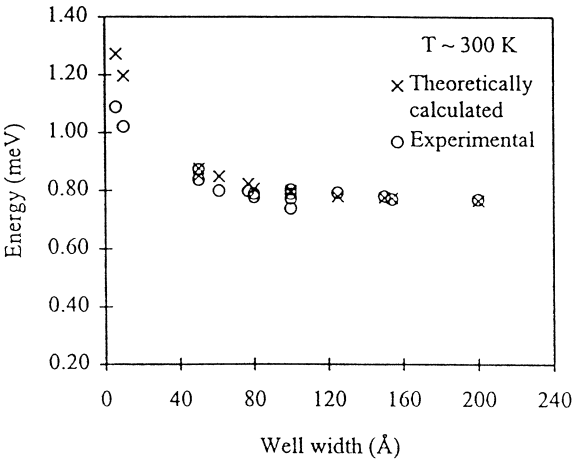

Fig. 17. Band-gap energy of InGaAs/InP QW with In alloy concentration 0.53 and varying well width at room temperature.

At room temperature, the calculated results generally have a fair agreement with the measured ones. From Table 10, the average difference between 14 sets of room temperature data is calculated to be 10 meV. Some of the differences between our theoretical calculated values and the experimental values [114,120] are only about 3 meV. For this QW structure, no theoretical calculations from other publications are available. The room temperature experimental values and the calculated values of the band-gap energy from similar QWs are plotted against well width as shown in Fig. 17 with an alloy concentration of 0.53. In this figure, it can be observed that the experimental values and the calculated values are generally in good agreement, and the effect of a decrease in band-gap energy becomes insignificant with well width larger than 5 nm. Also, comparisons with band-gap energy and varying alloy concentration at a fixed well width of 50 and 77 Å are shown in Figs. 18 and 19, respectively. It is observed in both figures that as concentration increases, the band-gap energy decreases. The agree-

Table 9
Summary of the comparison of the experimental higher state transition energy from different authors and our calculated values of the InGaAs/GaAs QW structure on both room and low temperatures

Temp. (K)	Tech.	Ref.	Conc.	Well width (Å)	Barrier width (Å)	MQW/ SQW	Theory (eV)	Experiment (eV)	Error (meV)
Room temperature									
300	PR	[106]	0.12 1L	32 ± 3	95 ± 5	MQW	1.4079	1.397[a]	10.9
300	PR	[107]	0.11 1L	40	70	MQW	1.4055	1.409	−3.5
300	PR	[107]	0.11 1L	40	70	MQW	1.4055	1.410[a]	−4.5
300	PR	[107]	0.12 1L	50	100	MQW	1.3969	1.386[a]	10.9
300	PR	[106]	0.11 1L	52 ± 3	105 ± 5	MQW	1.3988	1.388[a]	10.8
300	PC	[111]	0.1 1L	93	200	MQW	1.3860	1.376	10
300	PL	[118]	0.21 2H	100	—	SQW	1.3168	1.329	−12.2
300	PR	[108]	0.149 1L	159	200	MQW	1.3448	1.331[a]	13.8
300	PR	[108]	0.149 2H	159	200	MQW	1.3216	1.326[a]	−4.4
300	PR	[108]	0.15 2H	160	200	MQW	1.3203	1.318	2.3
300	PR	[108]	0.15 1L	210	200	MQW	1.3386	1.330	8.6
300	PR	[108]	0.15 2H	210	200	MQW	1.3023	1.302	0.6
300	PR	[108]	0.155 2H	210	200	MQW	1.2981	1.305[a]	−1.9
300	PR	[108]	0.15 3H	210	200	MQW	1.3416	1.348	−6.4
300	PR	[108]	0.155 3H	210	200	MQW	1.3416	1.350[a]	−8.4
300	PR	[108]	0.155 2H	213	200	MQW	1.2969	1.301[a]	−4.1
300	PR	[108]	0.155 3H	213	200	MQW	1.3403	1.347[a]	−6.7
Low temperature									
4K	PC	[xxx]	0.244 1L	80	200	SQW	1.3959	1.391	4.9
4K	Ab	[116]	0.193 2H	85	200	MQW	1.4381	1.4393	−1.1
4K	Ab	[116]	0.193 2H	85	200	MQW	1.4381	1.4342[a]	3.9
4K	Ab	[116]	0.193 1L	85	200	MQW	1.4239	1.4115	−3.8
7K	PLE	[114]	0.24 2H	96	200	MQW	1.3928	1.3929	−0.1
7K	PLE	[114]	0.24 2H	96	200	MQW	1.3928	1.3955[a]	−2.7
2K	Ab	[117]	0.136 1L	100	—	MQW	1.4517	1.4430	−3.9
4K	Ab	[117]	0.136 2H	100	—	MQW	1.4606	1.4662	−5.6
4K	PC	[117]	0.184 1L	100	200	SQW	1.4212	1.415	6.2
4K	PC	[117]	0.184 1L	100	200	SQW	1.4212	1.417[a]	4.2
4K	PC	[117]	0.184 2H	100	200	SQW	1.4281	1.433[a]	−4.9
2k	Ab	[117]	0.206 1L	100	—	MQW	1.4069	1.4025	4.3
2K	Ab	[117]	0.253 1L	100	—	MQW	1.3752	1.379	−3.8
4K	Ab	[116]	0.13 2H	106	200	MQW	1.4605	1.4683	−7.8
4K	Ab	[116]	0.13 2H	106	200	MQW	1.4605	1.4613[a]	−0.8
4K	PC	[xxx]	0.244 1L	120	200	SQW	1.3719	1.371	0.9
4K	PC	[xxx]	0.244 1L	120	200	SQW	1.3719	1.318[a]	3.9
4K	PC	[xxx]	0.244 2H	120	200	SQW	1.3559	1.359	−3.1
4K	PC	[xxx]	0.244 2H	120	200	SQW	1.3559	1.355[a]	0.9
4K	Ab	[116]	0.15 2H	159	200	MQW	1.4086	1.4058[a]	2.8
4K	Ab	[116]	0.15 2H	213	200	MQW	1.3856	1.3785	−4.5
4K	Ab	[116]	0.15 2H	213	200	MQW	1.3856	1.3811[a]	4.5
4K	Ab	[116]	0.15 1L	213	200	MQW	1.4065	1.4110[a]	−4.5

[a]Calculated results.

ment of the experimental data collected from different literatures and calculated data for different alloy concentrations in both figures proves that our calculation is reliable, both in the case of lattice matched, and in the presence of tensile and compressive strain in the InGaAs/Inp QW structures.

At low temperature, results are more satisfactory compared with those obtained at room temperature.

Table 10
Summary of the comparison of the experimental band-gap energy from different authors and our calculated values of the InGaAs/InP QW structures on both room and low temperature

Temp. (K)	Tech.	Ref.	Conc.	Well width (Å)	Barrier width (Å)	MQW/ SQW	Theory (meV)	Experiment (meV)	Error (meV)
Room temperature									
300	Ab	[120]	0.53	50	500	MQW	0.8736	0.8706	3.0
300	PC	[121]	0.53	50	75	MQW	0.8487	0.8360	13.0
300	PCE	[114]	0.53	77	—	MQW	0.8206	0.7958	24.8
300	PCE	[114]	0.64	79	—	MQW	0.7260	0.7181	7.9
300	PC	[122]	0.53	80	400	MQW	0.8053	0.7885	16.8
300	PCE	[114]	0.73	93	—	MQW	0.6502	0.6535	−3.3
300	PC	[122]	0.74	97	400	MQW	0.6403	0.6367	3.6
300	Ab	[124]	0.53	100	100	MQW	0.7983	0.772	26.3
300	Ab	[120]	0.53	100	500	MQW	0.7983	0.7882	10.1
300	PC	[123]	0.53	100	100	MQW	0.7907	0.8008	−10.2
300	TR	[125]	0.53	125	—	MQW	0.7791	0.7909	−11.8
300	Ab	[120]	0.53	150	200	MQW	0.7750	0.7794	−4.4
300	Ab	[126]	0.532	154	160	MQW	0.7725	0.769	3.5
300	Ab	[120]	0.53	200	200	MQW	0.7650	0.7686	−3.7
Low temperature									
20	Ab	[120]	0.53	50	500	MQW	0.9522	0.9306	11.2
2	PL	[127]	0.53	50	—	SQW	0.9522	0.9426	−0.8
2	PL	[128]	0.53	60	700	MQW	0.9260	0.8925	23.5
2	PL	[129]	0.53	60	—	MQW	0.9260	0.902[a]	14.0
10	PL	[130]	0.53	79	—	SQW	0.8936	0.873[a]	11.0
7	PL	[114]	0.64	79	—	MQW	0.8115	0.7708	32.1
2	PL	[131]	0.53	80	600	MQW	0.8923	0.8619	20.8
2	PL	[128]	0.53	80	700	MQW	0.8923	0.8702	12.5
2	PL	[129]	0.53	80	—	MQW	0.8923	0.875[a]	7.7
20	Ab	[120]	0.53	100	500	MQW	0.8721	0.8537	9.2
2	PL	[127]	0.53	100	—	SQW	0.8721	0.8651	−3.2
2	PL	[129]	0.53	100	—	MQW	0.8721	0.859[a]	3.9
10	PL	[130]	0.53	104	—	SQW	0.8690	0.848	11.8
2	PL	[129]	0.53	120	—	MQW	0.8590	0.847[a]	2.8
2	PL	[131]	0.53	130	600	MQW	0.8537	0.820	25.5
2	PL	[129]	0.53	140	—	MQW	0.8494	0.840[a]	1.4
20	Ab	[120]	0.53	150	200	MQW	0.8461	0.8413	−3.4
2	PL	[128]	0.53	150	700	MQW	0.8461	0.8267	11.2
2	PL	[127]	0.53	150	—	SQW	0.8461	0.822	15.9
2	PLE	[106]	0.56	150	—	SQW	0.8226	0.8164	−2.0
4	Ab	[126]	0.53	154	160	MQW	0.8448	0.8394	−2.8
2	PL	[129]	0.53	160	—	MQW	0.8428	0.835[a]	0.2
2	PL	[129]	0.53	180	—	MQW	0.8379	0.830[a]	0.5
20	Ab	[120]	0.53	200	200	MQW	0.8341	0.8353	−8.4
2	PL	[127]	0.53	200	—	SQW	0.8341	0.8141	12.8
2	PL	[131]	0.53	200	500	MQW	0.8313	0.7950	31.9
4	PL	[132]	0.53	500	—	SQW	0.8178	0.7954	16

[a]Calculated results.

Most of the differences between theoretical results and the experimental ones are within ±8 meV. In some cases [104,127], errors obtained are only 1 and 2 meV. Comparisons are also made for our calculated values and those from other papers. Hrivnak [129] has presented three sets of theoretical data, with

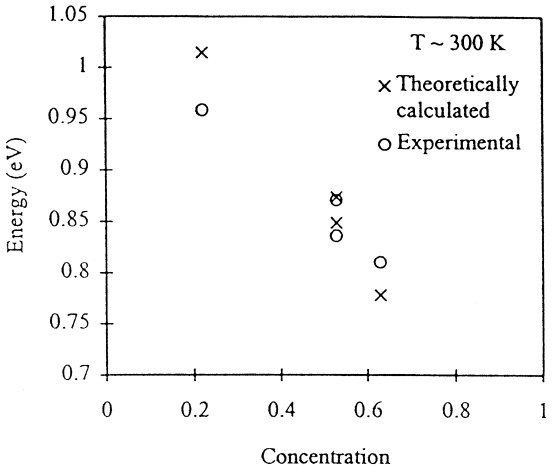

Fig. 18. Band-gap energy of the InGaAs/InP QW with fixed well width ($L_z = 50$ Å) and varying concentration 0.22, 0.55, and 0.63 at room temperature.

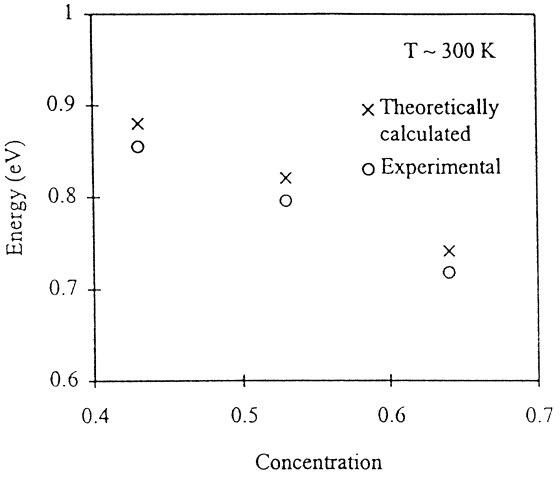

Fig. 19. Band-gap energy of the InGaAs/InP QW with fixed well width ($L_z = 77$ Å) and varying concentration 0.43, 0.53, and 0.64 at room temperature.

different well width 100, 120, 140, 160, and 189 Å, and the same alloy concentration 0.53, which agree very well with our calculated results. Differences are around 1–4 meV only. For the purpose of making a comparison, the low temperature experimental values and the calculated values of the band-gap energy against well width are plotted, as shown in Fig. 20, with concentration of the alloy equals 0.53. From this figure, it is

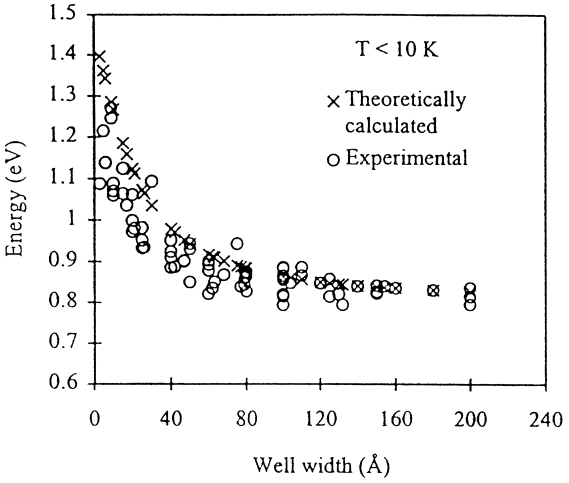

Fig. 20. Band-gap energy of the InGaAs/InP QW with In alloy concentration 0.53 and varying well width at low temperature.

found that the experimental values and the calculated values are generally in good agreement except when the well width of the QW structures is approximately below 30 Å. In this case, errors can be as large as 30 meV. It is because envelope function approach is used in this calculation and this method is only applicable when the well width of the QW structures is above the minimum requirement of 30 Å. In addition, comparisons with varying alloy concentration at fixed well width of 26 and 104 Å are shown in Figs. 21 and 22, respectively. All the three figures result in the same conclusion that as the concentration increases, the band-gap energy decreases. In these figures, it is clearly shown that when well width increases from 26 to 104 Å, the deviations between the experimental and theoretical results are greatly reduced. When the well width reaches 104 Å, good agreements are achieved. This observation can also be explained by the limitation of the envelope function application.

The average absolute error for the fourteen sets of data at room temperature is 10 meV, which is much larger than the average errors of AlGaAS/GaAs and InGaAS/GaAs QW structures. However, the accuracy of some data is being suspected. Firstly, one set of data with well width 100 Å and alloy concentration 0.53 shows an error of 26 meV [124]. Another set of data [120] with the same QW structure except the barrier width only deviates from our result by 10 meV. Both the mentioned QW structures are multi-QWs but

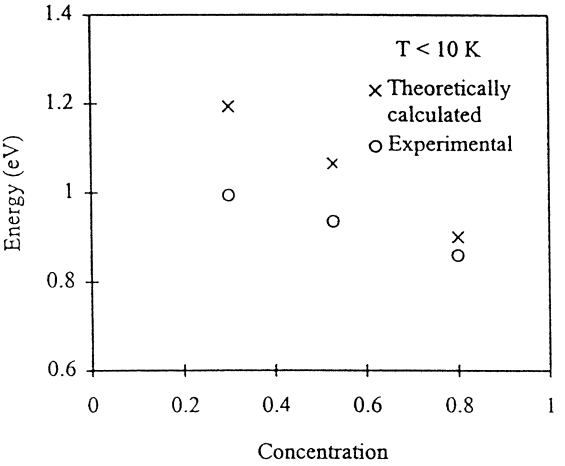

Fig. 21. Band-gap energy of the InGaAs/InP QW with fixed well width ($L_z = 26$ Å) and varying concentration 0.3, 0.53, and 0.9 at low temperature.

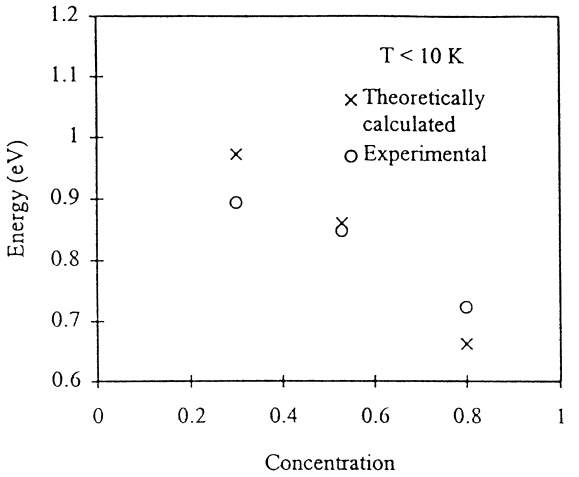

Fig. 22. Band-gap energy of the InGaAs/InP QW with fixed well width ($L_z = 104$ Å) and varying concentration 0.3, 0.53, and 0.8 at low temperature.

the latter one has a larger barrier 500 Å while the former one has only 100 Å in which tunneling effect may happen and affect the accuracy of measurement. Secondly, the data with well width 50 Å, alloy concentration 0.53, and barrier width 75 Å is put into question [121]. It deviates from our calculation by 13 meV. There is another set of data with well width 50 Å, concentration of alloy 0.53 and a larger barrier width 500 Å which deviates from our value by 3 meV only [120]. For the same reason as the above discussion, it is believed that the result with a larger barrier is more reasonable. On the whole, if these two suspected sets of data is discarded from our studies, a smaller average absolute error of 8.6 will be obtained, which is more acceptable.

For low temperature, the average absolute error for the twenty-five sets of data is 11 meV. Again, this error would seem large when compared to the case in AlGaAS/GaAs and InGaAS/GaAs QW structures. However, for low temperature, effect of the Stoke shift has to be taken into account. As stated from other literature [5,6], the Stoke shift can affect the measurements of the band-gap energy of QW structures up to 15 meV. Therefore, the unexpected shift of the value of the error to a positive value may be due to the Stoke shift effect. The Stoke shift will affect the results from measurements by PL method only. Therefore, for the three sets of data [131], their deviations of 21, 26 and 32 meV are corrected by subtracting 15 meV from each one, which will become 6, 11 and 17 meV. Data showing large deviations of 32 and 16 meV are also found [114,132]. If 15 meV is taken into account again from the two values, the deviations will then be 17 and 1 meV. For the three sets of data showing deviations of 24, 13 and 11 meV [128], 15 meV is also subtracted from each of them and three smaller deviations of 9, 2, and 4 meV are resulted, respectively. By eliminating the Stoke shift effect in various cases, a better average absolute error of 6 meV and a better mean value of total error 6 meV are obtained.

For both room temperature and low temperature, the comparisons between the experimental and calculated higher state transition energies are also discussed. For the room temperature, the differences between them are mostly within ± 15 meV and only a few sets of data exceed this limit and deviates up to 25 meV. For the 11L transition energy, the difference between the two experimental values [120] and our calculated values are 1 and 3 meV. For the 22H transition energy, differences of 3.2 and 6.4 meV are found [120]. All other results are listed in Table 11. At low temperature, smaller differences are observed. Most of them lie within ± 13 meV, but there is still some data which lies beyond this bound. For the 11L transition energy, the differences between our calculated values and the experimental values of Skolnick et al. [120] and Dalfors et al. [104] are 1.3 and 2.3 meV. For other higher

Table 11
Summary of the comparison of the experimental higher state transition energy from different authors and our calculated values of the InGaAs/InP QW structures on both room and low temperatures

Temp. (K)	Tech.	Ref.	Conc.	Well width (Å)	Barrier width (Å)	MQW/ SQW	Theory (eV)	Experiment (eV)	Error (meV)
Room temperature									
294	Ab	[121]	0.53 1L	50	75	MQW	0.9228	0.8976	25.3
300	Ab	[120]	0.53 1L	50	500	MQW	0.9228	0.9356	0.9
300	PC	[122]	0.64 1L	77	400	MQW	0.8203	0.7979	22.4
300	PC	[122]	0.53 1L	80	400	MQW	0.8425	0.8214	21.2
300	PC	[122]	0.74 1L	97	400	MQW	0.7631	0.7750	3.3
300	Ab	[120]	0.53 1L	100	500	MQW	0.8205	0.8098	10.8
300	Ab	[120]	0.53 1L	150	200	MQW	0.7871	0.7843	2.9
300	Ab	[120]	0.53 2L	150	200	MQW	0.8573	0.8510	6.4
300	Ab	[126]	0.53 2H	154	160	MQW	0.8544	0.8402	14.2
300	Ab	[120]	0.53 2H	200	200	MQW	0.8169	0.8137	3.2
300	Ab	[120]	0.53 3H	200	200	MQW	0.9042	0.8863	18.0
Low temperature									
10	PLE	[114]	0.53 1L	47	120	MQW	0.9984	1.0204	−22.0
20	Ab	[120]	0.53 1L	50	500	MQW	0.9861	0.9924	−6.3
6	PLE	[133]	0.53 1L	68	365	MQW	0.9326	0.918	14.6
10	PLE	[114]	0.53 1L	79	461	MQW	0.9109	0.9060	−5.1
20	Ab	[120]	0.53 1L	100	500	MQW	0.8827	0.8717	11.0
6	PLE	[134]	0.53 1L	100	—	SQW	0.8827	0.9311	−9.7
20	PLE	[104]	0.56 1L	100	—	SQW	0.8744	0.8575	16.9
20	Ab	[120]	0.53 1L	150	200	MQW	0.8483	0.8470	1.3
20	PLE	[104]	0.43 1L	150	—	SQW	0.8759	0.8630	12.9
20	PLE	[104]	0.43 2H	150	—	SQW	1.0055	0.9824	23.1
20	PLE	[104]	0.56 1L	150	—	SQW	0.8395	0.8372	2.3
20	PLE	[104]	0.56 2L	150	—	SQW	0.9790	0.9771	1.9
20	PLE	[104]	0.56 3L	150	—	SQW	1.2148	1.1028	7.6
4	Ab	[126]	0.53 3H	154	160	MQW	1.0863	1.0672	−2.5
20	Ab	[120]	0.53 2H	200	200	MQW	0.8864	0.8778	8.6
20	Ab	[120]	0.53 4H	200	200	MQW	1.1340	1.0399	−5.9
20	PLE	[104]	0.56 1L	250	—	SQW	0.8144	0.8274	−13
20	PLE	[104]	0.56 2H	250	—	SQW	0.8388	0.8327	−6.1
20	PLE	[104]	0.56 2L	250	—	SQW	0.8752	0.8558	19.4

state transition energies, a deviation of 2.5 meV for 3HH measurement [120] and a deviation of 5.9 meV for 4HH transition measurement [120] are obtained. In addition, comparisons are made between our calculated results and those obtained from other literatures. There are also some other comparisons shown in Table 11. As there is a lack of relevant reference from the available literature, comparison between our calculated results and those obtained from others cannot be made. In general, the experimental and calculated data of the higher state transition energy are also in good agreement with a wide range of alloy concentration and well width.

As the calculated results generally agree well with the experimental values for a wide range of concentration of alloy and well width, it is believed that our assignment of the set of parameters for the InGaAsP system is indeed correct.

5.4. InGaAs/InAlAs

In the InGaAs/InAlAs QW system, QW structures with well width ranging from 3 to 25 nm, aluminium concentration in barrier varying from 0.52 to 0.57, and aluminium concentration in well from 0.4 to 0.6, are analyzed. The band offset ratio is chosen as 78 : 22 for

this material system at both room and low temperatures [155]. Since this QW system is not as mature as the InGaAs/GaAs or the AlGaAs/GaAs, not many experimental results of QW band-gap analysis are available. In fact, over half of the experimental data we get are gathered from those devices' reports in which their operating information, such as operating wavelength, is available.

For the InGaAs/InAlAs QW, there are five band-gap equations available for theoretical calculation, as listed in Section 3. Each of them is tested and compared with the experimental results. It is found that they all give similar results. Eq. (77) is finally chosen in our model for the InGaAs/InAlAs QW structure since it gives the least error among others. For all the theoretically calculated band gaps, excitonic effect is taken into account. An average of 5 meV is taken as the exciton binding energy and subtracted from the calculated band-gap energies. All the calculated results are listed in Table 12.

At room temperature, the calculated results are in fair agreement with the experimental ones obtained from different measuring methods. The differences between theoretical and the experimental results are mostly within ± 10 meV. The theoretical model approximates the band-gap energies fairly well. Differences as small as 4 and 5 meV are obtained for two sets of experimental results [143]. Theoretical calculations are also compared with the band-gap energies of some optical devices. Excellent agreement is observed in which they differ from each other by 0.5, 0.7 and 0.3 meV only [138]. For the purpose of further analysis, both the experimental and theoretical results from different QWs, with indium concentration in barrier equals 0.52 and indium concentration in well equals 0.53 ± 0.07, are grouped and plotted against different well widths, as shown in Fig. 23. It is observed that the band-gap energy is quite sensitive to the change in well width. Band-gap energy drops rapidly with an increase in well width until the well width reaches 12 nm. An insignificant decrease in band-gap energy is observed both experimentally and theoretically, when the well width increases from 12 to 20 nm. However, the change in band-gap energy becomes obviously large again when the well width is larger than 20 nm.

For some room-temperature data, a rather great error between the calculated and the experimental results is shown. In the most serious case [140], an error as large as 21 meV is observed. There is also an error of 12 meV. Since the majority of all the other errors observed lies within 10 meV, the theoretical model of InGaAs/InAlAs for room-temperature band-gap calculation is still considered valid.

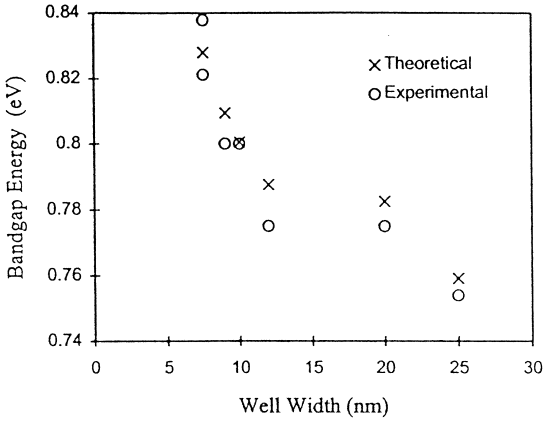

Fig. 23. Band-gap energy of $In_{0.52}Al_{0.48}As/In_{0.53}Ga_{0.47}As$ QW at room temperature versus varying well width.

At low temperature, the calculated results are in agreement with the experimental ones, except for one set of data [144] which shows an abnormally large error of 11 meV. Since this is the only experimental result which disagrees with our theoretical model, it is neglected. For the rest of the data at low temperature, differences also vary within 10 meV only. The theoretical model predicts the band-gap energy very accurately. The smallest differences between the calculated values and the experimental data [145] are only about 1 and 3 meV. The rest of the calculated values are all very close to the expected experimental data. To investigate the change in band-gap energy with a change in well width at low temperature, experimental results and theoretical results from QWs, with indium content in barrier equals to 0.52 and indium content in well equals to 0.53, are plotted in Fig. 24. Results show that the band-gap energy decreases exponentially with increasing well width. It is observed that theoretical results lie very closely with the experimental ones, especially with well width in the range 3–8 nm. As observed, band gap changes slow down with well width larger than 80 Å.

The average absolute error for the twelve sets of data at room temperature is 8 and 6 meV for the

Table 12
Summary of the comparison of the experimental higher state transition energy from different authors and our calculated values of the $In_xGa_{1-x}As/In_yAl_{1-y}As$ QW structures on both room and low temperature (x= indium concentration in barrier, y= indium concentration in well)

Temp. (K)	Tech.	Ref.	Conc. x, y	Well width (Å)	Barrier width (Å)	MQW/ SQW	Theory (eV)	Experiment (eV)	Error (meV)
Room temperature									
300	PC	[135]	0.52, 0.53	75	50	MQW	0.8279	0.8212[a]	11.7
300	TR	[136]	0.52, 0.53	75	75	MQW	0.8279	0.8378[a]	−9.9
300	PC	[137]	0.52, 0.53	90	30	MQW	0.8095	0.8[a]	9.5
300	Ab	[139]	0.52, 0.53	90	70	MQW	0.8095	0.8	9.5
300	Em	[138]	0.52, 0.4	100	60	SQW	0.8576	0.8583[a]	−0.7
300	Em	[138]	0.52, 0.53	100	60	SQW	0.8005	0.8[a]	0.5
300	Em	[138]	0.52, 0.66	100	60	SQW	0.7056	0.7026[a]	3.0
300	ER	[140]	0.57, 0.49	107	—	MQW	0.7892	0.81	−20.8
300	Ab	[141]	0.52, 0.53	120	55	MQW	0.7876	0.775[a]	12.6
300		[142]	0.52, 0.5	200	—	MQW	0.7825	0.775[b]	7.5
300	PR	[143]	0.52, 0.53	250	3000	SQW	0.7592	0.754	5.2
300	PR	[143]	0.52, 0.6	250	3000	SQW	0.7057	0.710	−4.3
Low temperature									
4	PL	[144]	0.52, 0.53	29	2500	SQW	1.0615	1.072	−10.5
5	Ab	[145]	0.52, 0.53	34	—	MQW	0.0227	1.02	2.7
LT	PL	[146]	0.52, 0.53	40	75	MQW	0.9868	0.983	3.8
5	Ab	[145]	0.52, 0.53	80	—	MQW	0.8788	0.88	−1.2
4	PL	[144]	0.52, 0.53	103	2500	SQW	0.8606	0.87	−9.4
4	PL	[144]	0.52, 0.53	132	2500	SQW	0.8440	0.847	−3.0
5	Ab	[145]	0.52, 0.53	138	—	MQW	0.8416	0.85	−8.4

[a]Experimental band-gap energy obtained from device measurement.
[b]Calculated value.

seven sets of low-temperature data. Although this error is much larger compared to those obtained in the InGaAs/GaAs and AlGaAs/GaAs systems, it is within 10 meV, which is acceptable for general application. In fact, the difference between the experimental and the theoretical results is greatly influenced by the growth quality of the QW material under investigation. It is suspected that the large error is due to the low growth quality. It is also believed that the large error is resulted from the broadening effect during measurement at room temperature.

Almost over 90% of the QW structures concerned in this analysis are the unstrained $In_{0.52}Al_{0.48}As/In_{0.53}Ga_{0.47}As$. For all QW structures listed in Table 12, the indium content in the barriers only varies from 0.52 to 0.57 while the indium content in the wells varies from 0.4 to 0.66. By theoretical calculations of band-gap energies with different concentrations in both well and barrier, it is found that the unstrained condition remains unchanged by varying the alloy concentration in the barrier alone. On the other hand, it is observed that while varying the alloy content in the well, both strained and unstrained conditions can be achieved. With indium concentration ranging approximately from 0.44 to 0.7, the QW is still free of strain. However, once the concentration of indium drops below 43%, the strained QW is obtained. It is also observed that the band-gap energy of InGaAs/InAlAs is quite sensitive to the variation of the alloy concentration in either the well or the barrier, and the well width. From the three sets of data at room temperature [138], it is seen that increasing the indium concentration in well will introduce a significant decrease in band-gap energy.

Experimental data from Table 12 are measured by different techniques, which includes PL, Ab, PC, PR,

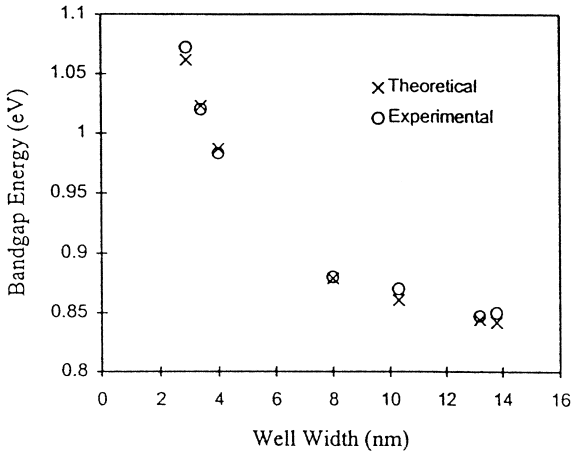

Fig. 24. Band-gap energy of $In_{0.52}Al_{0.48}As/In_{0.53}Ga_{0.47}As$ QW at low temperature with varying well width.

TR, EM (emission), and ER, and with one case by calculation. It has been observed that at room temperature, the emission method measures the band-gap energy of the InGaAs/InAlAs QWs most accurately. For the other measuring methods employed at room temperature, their performances are only fair. For the low-temperature experimental data, they are all measured by PL and Ab, and they determine band-gap energies which are very close to what we expect.

The excellent agreement between the calculated and the experimental results for a wide range of concentration of alloy and well width confirms the reliability of the sets of parameters assigned for the QW model of InAlGaAs system.

5.5. *InGaAs/GaAs*

In the InGaAs/AlGaAs QW system, QW structures with well width 6–100 nm, indium concentration in well varying from 5% to 25%, and aluminium concentration in barrier varying from 10% to 40% will be considered. The band offset ratio is chosen to be 70 : 30 for both room and low temperature for this system [154]. For all the calculated band-gap energies, excitonic effect is considered. All the excitonic binding energies are assumed to be 5 meV for both room and low temperatures. All the results are listed in Table 13.

For the InAlAs/InGaAs QW system, Eq. (77) is chosen as the band-gap equation. Since the InAlAs/InGaAs is still not a very mature QW structure, not many reports concerning its band-gap analysis are available. This is the most difficult problem encountered in this research.

At room temperature, it is observed that all the calculated results are shifted away from the experimental results. All the theoretical band gaps are much smaller than the experimental ones. The average absolute error for a total of nine sets of room-temperature data is 24 meV. All the experimental data are tested against every band-gap equation available for both well and barrier. It is found that they all give similar results, which is very different from the corresponding experimental data. Therefore, it is believed that errors are introduced by the broadening effect during experimental measurement.

At low temperature, the calculated results are in excellent agreement with the experimental data. The differences between the calculated and the experimental results are all within 10 meV. The average absolute error for 17 sets of data is only 4 meV, which is very small compared to the room-temperature results. The smallest difference between the experimental and the theoretical calculations obtained is only 0.3 meV [154]. It implies that this theoretical QW model can predict the band-gap energy very well at low temperature.

The band-gap energy is found to be quite sensitive to well width by analyzing Table 13. Experimental and theoretical band gaps from $In_{0.28}Ga_{0.72}As/Al_{0.1}Ga_{0.9}As$ are plotted against different well widths, as shown in Fig. 25. It is observed that increasing the well width will introduce a decrease in the direct band-gap energy. Band-gap energy decrease faster before well width reaches 200 Å. Among all the data we have searched, the indium concentration in well only varies slightly from 0.05 to 0.25 for the room temperature data, and from 0.1 to 0.16 for the low temperature data. It is observed from all the theoretical results that increasing the indium concentration in the well will decrease the band-gap energy. The aluminium concentration in barrier among our experimental data varies from 0.1 to 0.4 at room temperature and from 0.28 to 0.29 at low temperature. It is also observed that band-gap energy decreases with increasing aluminium concentration. From the set of data suggested by Buydens [153], our theoretical results show that band-gap

Table 13
Summary of the comparison of the experimental band-gap energy from different authors and our calculated values of the $In_xGa_{1-x}As/Al_yGa_{1-y}As$ QW structures on both room and low tempertures (x= concentration of indium in well, y= concentration of aluminium in barrier)

Temp. (K)	Tech.	Ref.	Conc. x, y	Well width (Å)	Barrier width (Å)	MQW/ SQW	Theory (eV)	Experiment (eV)	Error (meV)
Room temperature									
300	PL	[147]	0.2, 0.4	60	160	MQW	1.3028	1.3420	−39.2
300	PR	[148]	0.25, 0.1	65	—	MQW	1.2347	1.2675	−32.8
300	TR	[149]	0.05, 0.2	80	80	MQW	1.4171	1.451	−33.9
300	Ab	[150]	0.15, 0.2	80	80	MQW	1.3176	1.329	−11.4
300	PC	[151]	0.1, 0.15	100	250	MQW	1.3512	1.3702	−19
300	PC	[152]	0.15, 0.2	100	100	MQW	1.3019	1.3207	−18.8
300	PC	[152]	0.15, 0.1	100	100	MQW	1.2996	1.3152	−15.6
300	PC	[152]	0.15, 0.4	100	100	MQW	1.3030	1.3252	−22.2
300	PR	[148]	0.2, 0.1	110	—	MQW	1.2448	1.2689	−24.1
Low temperature									
LT	PL	[153]	0.16, 0.29	20	300	SQW	1.634	1.6402	1.2
LT	PL	[153]	0.16, 0.29	50	300	SQW	1.4471	1.453	−5.9
4	PL	[154]	0.1, 0.28	100	600	SQW	1.4391	1.442	−2.9
4	PL	[154]	0.15, 0.28	100	600	SQW	1.3843	1.395	−10.7
LT	PL	[153]	0.16, 0.29	100	300	SQW	1.3735	1.382	−8.5
LT	PL	[153]	0.16, 0.29	130	300	SQW	1.3585	1.366	−7.5
LT	PL	[153]	0.16, 0.29	160	300	SQW	1.3501	1.358	−7.9
4	PL	[154]	0.1, 0.28	200	600	SQW	1.4106	1.411	−0.4
4	PL	[154]	0.15, 0.28	200	600	SQW	1.3843	1.355	−0.3
4	PL	[154]	0.1, 0.28	300	600	SQW	1.4037	1.404	−0.3
4	PL	[154]	0.15, 0.28	300	600	SQW	1.3475	1.351	−3.5
4	PL	[154]	0.1, 0.28	400	600	SQW	1.4060	1.4042	−3.2
4	PL	[154]	0.15, 0.28	400	600	SQW	1.3439	1.347	−2.2
4	PL	[154]	0.1, 0.28	500	600	SQW	1.3997	1.4044	−4.7
4	PL	[154]	0.1, 0.28	700	600	SQW	1.3985	1.400	−1.5
4	PL	[154]	0.15, 0.28	700	600	SQW	1.3472	1.346	−3.8
4	PL	[154]	0.1, 0.28	1000	600	SQW	1.4028	1.4005	−2.7

energy increases only slightly with an increase in alloy concentration in the well.

It is once again shown that most of the band-gap measurement at low temperature is done by photoluminscence, which gives quite accurate results. For our analysis here, all the low-temperature data are obtained by photoluminiscence. However, the room-temperature data are obtained by various methods.

The excellent agreement between the calculated and experimental values at low temperature for a wide range of concentration of alloy and well width confirms the reliability of the sets of parameters for the QW model of the InAlGaAs system.

6. Broadening factor analysis

The dependence of the spectral line width of QW materials and structural dimensions is of considerable importance. The characteristics of the optical spectra and the absorption peaks, which provide information on the structural nature of the interfaces between the well and barrier materials, are strongly determined by the exciton line width. From a photonic device application point of view, such as a modulator, the peak of absorption determines the ON/OFF ratios of the switching. Although a great effort has been put on the AlGaAs/GaAs system [156–158], there is no clear and systematic data of the exciton line width in other QW

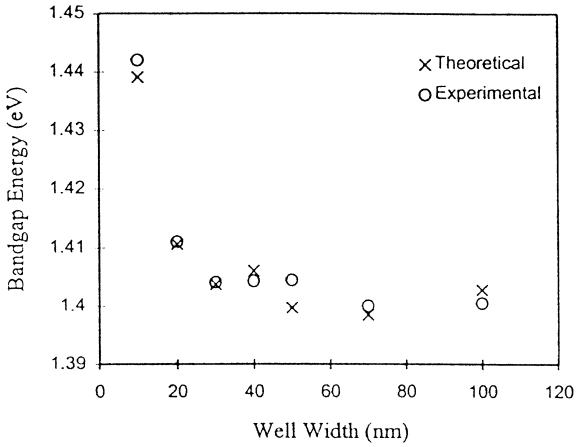

Fig. 25. Band-gap energy of $In_{0.28}Ga_{0.72}As/Al_{0.1}Ga_{0.9}As$ QW at low temperature versus varying well width.

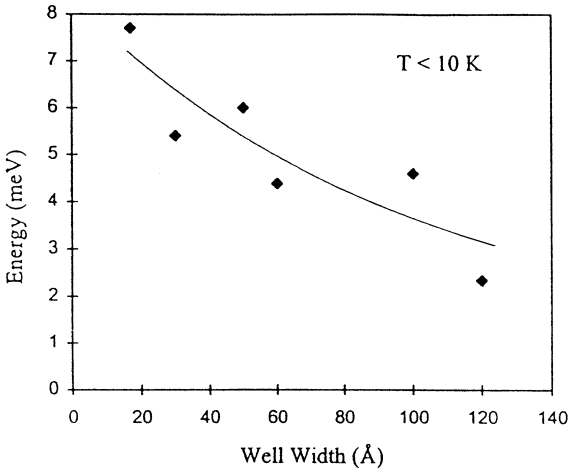

Fig. 26. Broadening line width full-width half-maximum (FWHM) energy of the AlGaAs/GaAs QW with Al concentration 0.2 at low temperature.

material systems. The reason for this scattered set of data may due to the lack of sharp excitonic features in the QW structures because of inhomogeneous line broadening, presumably arising from the alloy and interface quality in the strained QWs. The analysis in this section attempts to give a more comprehensive report on the broadening factor of the three QW materials: AlGaAs/GaAs, InGaAs/GaAs, and InGaAs/InP with different well width, several alloy concentration fractions, and at different temperatures.

For each of the three QW material systems, experimental data is extracted from various literatures. The collected data is sorted according to the structures, temperature of measurements, and experimental measuring techniques. The data are sorted out for the full-width half-maximum (FWHM) energy of the broadening line width with varying well width and alloy concentrations of the QW structures. Statistical method (least squares) is used in giving a somewhat trendwise fitting of the experimental data. A line of best fit is drawn on each graph. It is found that the data generally agrees with the empirical equation as given by

$$\Gamma_{\mathrm{FHWM}} = P_1 \mathrm{e}^{P_2 w + P_3 w^2} \tag{84}$$

where P_1, P_2, and P_3 are parameters to be determined on different QW material system and structures at different temperatures, Γ_{FWHM} is the FWHM energy (meV), and w is the well width of the QW material system.

The parameters P_1, P_2, and P_3 which vary over different QW material systems, structures, temperatures, and alloy concentrations are summarized in Table 14.

In general, two trends are found. In one case, FWHM energy of broadening line width decreases as well width increases. In the other case, FWHM energy increases initially as well width decreases until a maximum point is reached. After that, FWHM energy falls as well width continues to decrease further. The latter trend is more popular amongst various sets of data.

6.1. AlGaAs/GaAs

Data for the AlGaAs/GaAs QW structure is shown in Table 15.

It is grouped according to their alloy concentration and temperature, as shown in Figs. 26–35. For low temperature (from 1.8 to 10 K), data have well width ranging from 5 to 260 Å and Al alloy concentration ranging from 0.207 to 0.54. The data are largely obtained by the PL types of measurement. Data for 77 K has a well width ranging from 5 to 136 Å. The technique used is basically PL. For low temperature and 77 K, both single and multi-quantum well structures are considered. For room temperature, most of the data is obtained by the PR technique. The range of the well width varies from 42 to 214 Å and the alloy

Table 14
The parameters P_1, P_2 and P_3 of the general equation for different QW structures with different well width and different concentration at temperature 4, 80 and 300 K

QW structure	Temperature (K)	Alloy concentration (w)	Parameter 1 (P_1)	Parameter 2 (P_2)	Parameter 3 (P_3)	Figure no.
$Al_wGa_{1-w}As/GaAs$	4	0.2	8.36081	−0.00928	0.00001	26
	4	0.25	5.68477	−0.00729	0	27
	4	0.3	9.91081	−0.01531	0	28
	4	0.38	7.47753	0.02838	−0.00057	29
	4	0.4	15.98120	−0.01486	0	30
	80	0.17	6.64531	0.00983	−0.00014	31
	80	0.3	6.21255	0.00550	−0.00019	32
	80	0.4	17.57018	−0.01378	0	33
	300	0.26	6.64531	0.00983	−0.00014	34
	300	0.3	8.85263	−0.00277	0	35
$In_wGa_{1-w}As/GaAs$	4	0.12	0.15989	0.20242	−0.00345	36
	4	0.175	3.14675	0.00119	0.00003	37
	4	0.28	4.62830	0.03534	−0.00036	38
	80	0.12	1.92126	0.02264	−0.00019	39
	80	0.16	17.06587	−0.01202	0	40
	80	0.18	9.66698	0.01292	−0.00012	41
$In_wGa_{1-w}As/InP$	4	0.53	14.37630	−0.00592	0	42
	4	0.58	23.15163	−0.00997	0	43
	4	0.72	12.73946	−0.00424	0	44
	300	0.53	28.53084	−0.00319	0	45

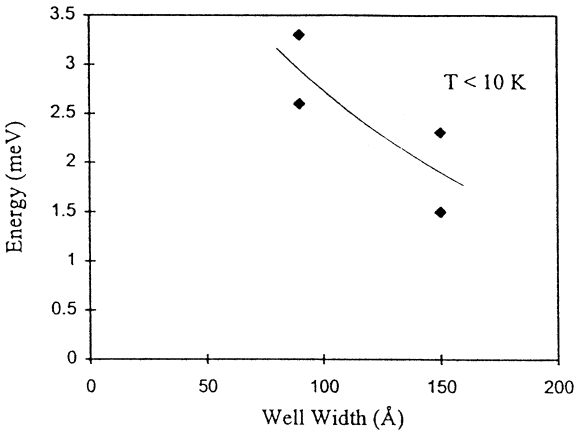

Fig. 27. Broadening line width full-width half-maximum (FWHM) energy of the AlGaAs/GaAs QW with Al concentration 0.25 at low temperature.

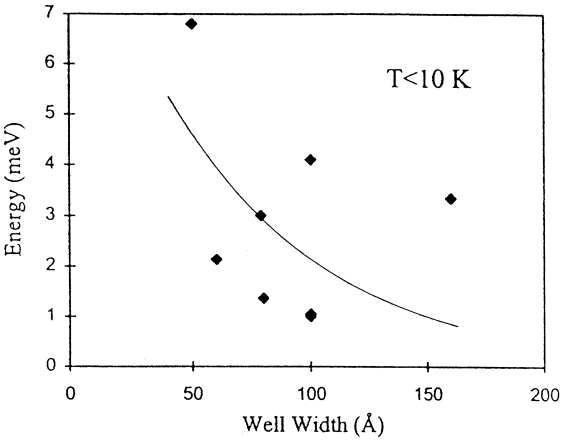

Fig. 28. Broadening line width full-width half-maximum (FWHM) energy of the AlGaAs/GaAs QW with Al concentration 0.3 at low temperature.

concentration ranges from 0.1 to 0.3. Only the multi-quantum well structure is considered.

Data for low temperature is presented in Figs. 26–30. The graph for alloy concentration 0.2 is shown in Fig. 26. The points are fitted reasonably well. A curve slowly concaving down is resulted. This indicates that broadening line width decreases as well width increases. The rate of decreasing is approximately 0.045 meV/Å. The graph for alloy concentration 0.25 is shown in Fig. 27. Only four data points are present in this case and they all have a well width

Table 15
FWHM and HWHM of $Al_wGa_{1-w}As/GaAs$

Temp. (K)	Conc.	Well width (Å)	Barrier width (Å)	FWHM	HWHM	SQW/ MQW	Ref.	Tech.
5	0.38	5	—	4.4	2.2	SQW	[169]	PL
5	0.38	5	—	7.6	3.8	SQW	[169]	PLE
8	0.38	5	—	8.3	4.15	SQW	[169]	PL
5	0.38	10	—	11.2	5.6	SQW	[169]	PL
8	0.38	10	—	5.7	2.85	SQW	[169]	PL
5	0.38	11	—	18.1	9.05	SQW	[169]	PLE
8	0.38	15	—	13.3	6.65	SQW	[169]	PL
8	0.4	15	—	13.1	6.55	MQW	[159]	PL
2	0.207	17	—	7.7	3.85	SQW	[97]	PL
5	0.38	20	—	10.9	5.45	SQW	[169]	PL
5	0.38	20	—	15.5	7.75	SQW	[169]	PLE
8	0.38	20	—	12.6	6.3	SQW	[169]	PL
8	0.4	20	—	13.0	6.5	MQW	[159]	PL
8	0.4	26	—	9.4	4.7	MQW	[159]	PL
2	0.207	30	—	5.4	2.7	SQW	[97]	PL
8	0.4	31	—	12.4	6.2	MQW	[159]	PL
8	0.4	32	—	9.5	4.75	MQW	[159]	PL
8	0.4	37	—	9.7	4.85	MQW	[159]	PL
4	0.54	40	—	13.3	6.65	SQW	[80]	PL
5	0.5	40	—	18.5	9.25	SQW	[170]	PL
5	0.5	40	40	11.7	5.85	MQW	[170]	PL
4.2	0.3	42	200	15.6	7.8	MQW	[171]	PLE
6	0.37	42	—	3.8	1.9	SQW	[172]	PL
8	0.4	43	—	7.4	3.7	MQW	[159]	PL
5	0.22	45	—	2.2	1.1	SQW	[173]	PL
5	0.38	48	—	6	3	SQW	[169]	PL
5	0.38	48	—	5.8	2.9	SQW	[169]	PLE
8	0.4	48	—	6.2	3.1	MQW	[159]	PL
8	0.4	48	—	8.7	4.35	MQW	[159]	PL
4.2	0.2	50	—	6.0	3	SQW	[174]	PL
4.2	0.3	50	—	6.8	3.4	SQW	[174]	PL
4	0.54	50	—	17.6	8.8	SQW	[80]	PL
5	0.38	53	—	6.4	3.2	SQW	[169]	PL
5	0.38	53	—	9.7	4.85	SQW	[169]	PLE
8	0.4	53	—	8.1	4.05	MQW	[159]	PL
8	0.4	53	—	8.0	4.05	MQW	[159]	PL
2	0.207	60	—	4.38	2.19	SQW	[97]	PL
5.5	0.3	60	—	2.13	1.07	MQW	[175]	Ab
8	0.4	63	—	6.4	3.2	MQW	[159]	PL
5	0.22	64	—	1.3	0.65	SQW	[173]	PL
2	0.5	64	—	19.0	9.5	SQW	[6]	PL
5	0.38	68	—	4.9	2.45	SQW	[169]	PL
5	0.38	68	—	4.9	2.45	SQW	[169]	PLE
8	0.4	68	—	4.8	2.4	MQW	[159]	PL
4	0.54	70	—	7.4	3.7	SQW	[80]	PL
8	0.35	75	—	3.9	1.95	MQW	[92]	PL
6	0.33	76	76	2.14	1.07	MQW	[176]	PLE
6	0.33	77	71	1.86	0.93	MQW	[176]	PLE
2	0.3	79	—	3	1.5	SQW	[93]	PLE
5.5	0.3	80	—	1.36	0.78	MQW	[175]	Ab

Table 15 (*continued*)

Temp. (K)	Conc.	Well width (Å)	Barrier width (Å)	FWHM	HWHM	SQW/ MQW	Ref.	Tech.
10	0.21	80	140	0.21	0.11	MQW	[99]	PL
2	0.25	90	100	3.3	1.65	MQW	[101]	Ab
2	0.25	90	25	2.6	1.3	MQW	[101]	Ab
5	0.38	93	—	2.8	1.4	SQW	[169]	PL
5	0.38	93	—	3.6	1.8	SQW	[169]	PLE
8	0.4	93	—	4.2	2.1	MQW	[159]	PL
4.2	0.2	100	—	4.6	2.3	SQW	[174]	PL
4.2	0.3	100	—	4.1	2.05	SQW	[174]	PL
2	0.3	100	—	1	0.5	MQW	[177]	PLE
5.5	0.3	100	—	1.05	0.53	MQW	[175]	Ab
5	0.27	102	207	5.5	2.75	MQW	[96]	PL
2	0.207	120	—	2.34	1.17	SQW	[97]	PL
2	0.3	120	—	0.3	0.15	SQW	[98]	PL
4.2	0.3	120	—	0.9	0.45	SQW	[98]	PL
6	0.5	144	—	1.2	0.6	SQW	[100]	PL
2	0.25	150	100	1.5	0.75	MQW	[101]	Ab
2	0.25	150	25	2.31	1.16	MQW	[101]	Ab
5	0.3	160	170	3.35	1.68	MQW	[178]	PL
1.8	0.3	188	19	1.6	0.8	MQW	[102]	PL
7	0.28	260	260	3	1.5	MQW	[107]	PL
5	0.38(1L)	5	—	8.8	4.4	SQW	[169]	PLE
5	0.38(1L)	15	—	19.5	9.75	SQW	[169]	PLE
5	0.38(1L)	20	—	23.6	11.8	SQW	[169]	PLE
4.2	0.3(1L)	42	200	12.9	6.45	MQW	[171]	PLE
5	0.38(1L)	48	—	6.6	3.3	SQW	[169]	PLE
5	0.38(1L)	53	—	7.6	3.8	SQW	[169]	PLE
5	0.38(1L)	68	—	4.8	2.4	SQW	[169]	PLE
2	0.3(1L)	79	—	3	1.5	SQW	[93]	PLE
5	0.38(1L)	93	—	3.4	1.7	SQW	[169]	PLE
80	0.4	5	—	9.3	4.65	MQW	[159]	PL
80	0.17	7	—	5.6	2.8	SQW	[169]	PL
80	0.4	10	—	21.7	10.85	MQW	[159]	PL
80	0.4	15	—	14.7	7.35	MQW	[159]	PL
80	0.4	20	—	14.3	7.15	MQW	[159]	PL
80	0.4	20	—	14.3	7.15	MQW	[159]	PL
80	0.17	23	—	10.4	5.2	SQW	[169]	PL
80	0.4	26	—	13.5	6.75	MQW	[159]	PL
80	0.4	31	—	72.2	6.1	MQW	[159]	PL
80	0.4	32	—	10.7	5.35	MQW	[159]	PL
80	0.4	32	—	11.0	5.5	MQW	[159]	PL
80	0.4	37	—	10.6	5.3	MQW	[159]	PL
80	0.4	43	—	9.7	4.85	MQW	[159]	PL
80	0.4	44	—	10.5	5.25	MQW	[159]	PL
80	0.4	48	—	7.6	3.8	MQW	[159]	PL
80	0.4	48	—	9.1	4.55	MQW	[159]	PL
80	0.4	50	—	8.7	4.35	MQW	[159]	PL
72	0.27	53	53	2	1	MQW	[179]	Ab
80	0.4	53	—	8.1	4.05	MQW	[159]	PL
80	0.4	53	—	8.7	4.35	MQW	[159]	PL
80	0.17	56	—	6.3	3.15	SQW	[169]	PL
35	0.3	60	—	3.98	1.99	MQW	[175]	Ab

Table 15 (*continued*)

Temp. (K)	Conc.	Well width (Å)	Barrier width (Å)	FWHM	HWHM	SQW/ MQW	Ref.	Tech.
77	0.3	60	—	4.69	2.35	MQW	[175]	Ab
80	0.4	63	—	8.0	4	MQW	[159]	PL
80	0.4	68	—	5.8	2.9	MQW	[159]	PL
80	0.4	70	—	5.6	2.8	MQW	[159]	PL
35	0.3	80	—	2.68	1.34	MQW	[175]	Ab
77	0.3	80	—	2.98	1.49	MQW	[175]	Ab
77	0.4	80	—	43.9	22	SQW	[180]	PL
80	0.17	83	—	5.3	2.65	SQW	[169]	PL
80	0.4	93	—	6.1	3.5	MQW	[159]	PL
35	0.3	100	—	1.54	0.77	MQW	[175]	Ab
77	0.3	100	—	1.63	0.82	MQW	[175]	Ab
80	0.4	105	—	0.8	3.4	MQW	[159]	PL
80	0.4	136	—	5.2	2.6	MQW	[159]	PL
72	0.27(1L)	53	53	3.3	1.65	MQW	[179]	Ab
300	0.26	42	200	7.9	3.95	MQW	[79]	PR
300	0.26	54	100	7.6	3.8	MQW	[79]	PR
300	0.3	98	200	9.91	4.46	MQW	[181]	Ab
300	0.17	100	150	8	4	MQW	[84]	PR
300	0.3	100	—	3.38	1.19	MQW	[175]	Ab
300	0.26	102	100	4.4	2.2	MQW	[79]	PR
300	0.1	104.5	—	6.0	3	MQW	[87]	PR
300	0.5	120	80	41.4	20.7	MQW	[86]	PL
300	0.3	144	—	6.1	3.05	MQW	[87]	PR
300	0.3	145	101	45.4	22.7	MQW	[86]	PL
300	0.15	150	100	6.6	3.3	MQW	[79]	PR
300	0.26	190	100	8.6	4.3	MQW	[79]	PR
300	0.24	210	150	6.4	3.2	MQW	[88]	PR
300	0.24	214	150	5.8	2.9	MQW	[88]	PR
300	0.26(1L)	42	200	20.7	10.35	MQW	[79]	PR
300	0.26(1L)	54	100	9.2	4.6	MQW	[79]	PR
300	0.26(2H)	54	100	12.2	6.1	MQW	[79]	PR
300	0.26(2L)	54	100	16.9	8.45	MQW	[79]	PR
300	0.17(1L)	100	150	7	3.5	MQW	[84]	PR
300	0.17(2H)	100	150	10	5	MQW	[84]	PR
300	0.17(2L)	100	150	13	6.5	MQW	[84]	PR
300	0.3(1L)	100	—	4.22	2.11	MQW	[175]	Ab
300	0.26(1L)	102	100	8.3	4.15	MQW	[79]	PR
300	0.26(2H)	102	100	16.8	8.4	MQW	[79]	PR
300	0.1(1L)	104.5	—	6.4	3.2	MQW	[87]	PR
300	0.3(1L)	144	—	7.3	3.65	MQW	[87]	PR
300	0.3(2H)	144	—	10.8	5.4	MQW	[87]	PR
300	0.3(2L)	144	—	11.6	5.08	MQW	[87]	PR
300	0.3(3H)	144	—	11.0	5.5	MQW	[87]	PR
300	0.15(1L)	150	100	8.2	4.1	MQW	[79]	PR
300	0.15(2H)	150	100	12.5	6.25	MQW	[79]	PR
300	0.15(2L)	150	100	4.1	2.05	MQW	[79]	PR
300	0.15(3H)	150	100	13.3	6.65	MQW	[79]	PR
300	0.26(1L)	190	100	7.7	3.85	MQW	[79]	PR
300	0.26(2H)	190	100	12.1	6.05	MQW	[79]	PR
300	0.26(2L)	190	100	18.1	9.05	MQW	[79]	PR
300	0.26(3H)	190	100	9.6	4.8	MQW	[79]	PR
300	0.26(4H)	190	100	12.4	6.2	MQW	[79]	PR

Table 15 (*continued*)

Temp. (K)	Conc.	Well width (Å)	Barrier width (Å)	FWHM	HWHM	SQW/ MQW	Ref.	Tech.
300	0.26(5H)	190	100	20.7	10.35	MQW	[79]	PR
300	0.26(4L)	190	100	18.5	8.25	MQW	[79]	PR
300	0.24(1L)	210	150	6.4	3.2	MQW	[88]	PR
300	0.24(2H)	210	150	8.5	4.25	MQW	[88]	PR
300	0.24(2L)	210	150	9.3	4.65	MQW	[88]	PR
300	0.24(3H)	210	150	11.7	5.85	MQW	[88]	PR
300	0.24(3L)	210	150	35	17.5	MQW	[88]	PR
300	0.24(4H)	210	150	13.1	6.65	MQW	[88]	PR
300	0.24(4L)	210	150	35	17.5	MQW	[88]	PR
300	0.24(5H)	210	150	16.9	8.45	MQW	[88]	PR
300	0.24(1L)	214	150	6.5	3.25	MQW	[88]	PR
300	0.24(2H)	214	150	9.1	4.55	MQW	[88]	PR
300	0.24(2L)	214	150	12.0	6	MQW	[88]	PR
300	0.24(3H)	214	150	10.6	5.3	MQW	[88]	PR
300	0.24(3L)	214	150	49	24.5	MQW	[88]	PR
300	0.24(4H)	214	150	12.6	6.3	MQW	[88]	PR
300	0.24(4L)	214	150	39	19.5	MQW	[88]	PR
300	0.24(5H)	214	150	13.7	6.9	MQW	[88]	PR

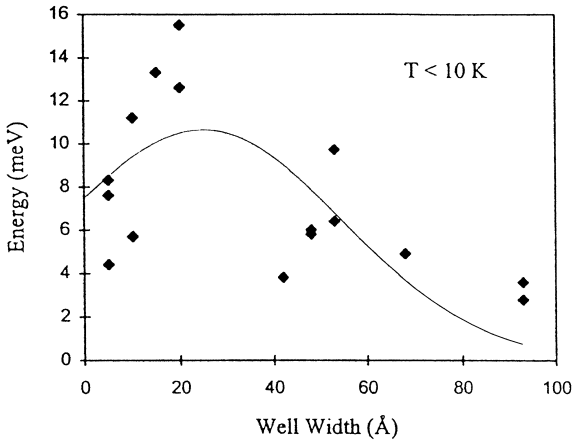

Fig. 29. Broadening line width full-width half-maximum (FWHM) energy of the AlGaAs/GaAs QW with Al concentration 0.39 at low temperature.

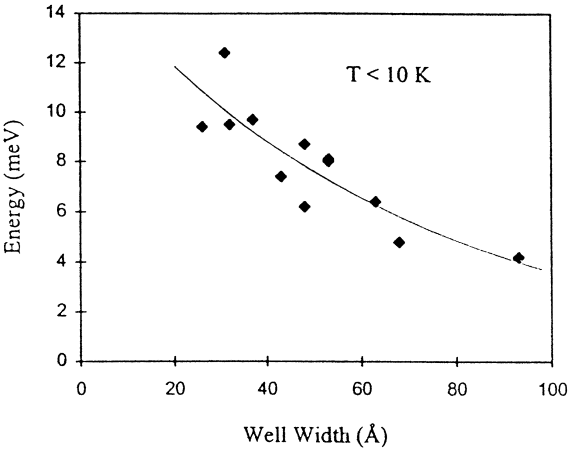

Fig. 30. Broadening line width full-width half-maximum (FWHM) energy of the AlGaAs/GaAs QW with Al concentration 0.4 at low temperature.

greater than 80 Å. The curve for alloy concentration 0.3 is presented in Fig. 28. A concave curve is fitted but the data points are located either above or below the arranged line except one point. The points all have a well width greater than 50 Å. Unlike the graphs discussed so far, it is observed in Fig. 29 (alloy concentration 0.39) that if the well width decreases, FWHM energy of broadening line width increases initially. At about 20 Å, FWHM energy starts to decrease as well width further decreases. This phenomenon is also observed by Bertolet [159]. The data are quite scattered. A concave curve is shown in Fig. 30, with alloy concentration 0.4. This curve is quite nicely fitted. The rate of decreasing is about 0.1 meV/Å. An interesting point is that Figs. 29 and 30 have alloy concentrations

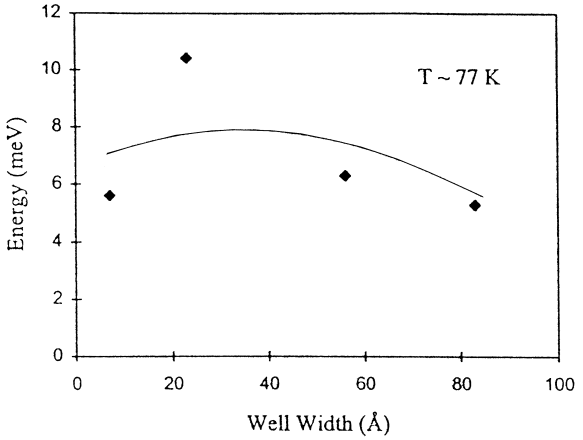

Fig. 31. Broadening line width full-width half-maximum (FWHM) energy of the AlGaAs/GaAs QW with Al concentration 0.17 at 77 K.

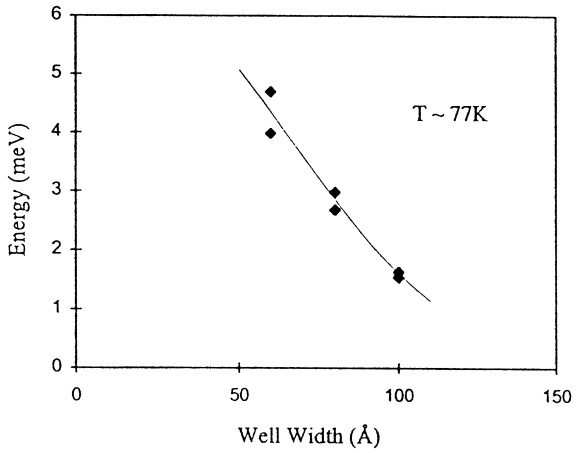

Fig. 32. Broadening line width full-width half-maximum (FWHM) energy of the AlGaAs/GaAs QW with Al concentration 0.3 at 77 K.

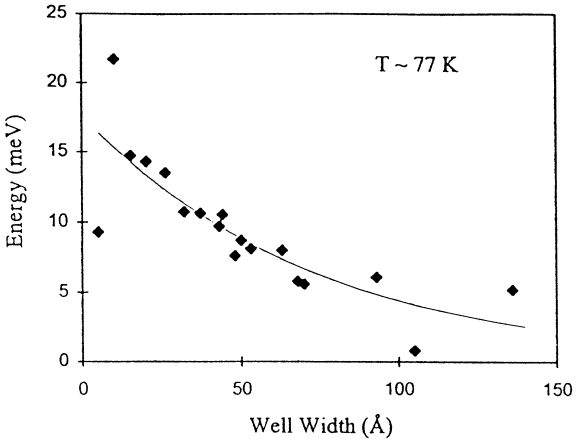

Fig. 33. Broadening line width full-width half-maximum (FWHM) energy of the AlGaAs/GaAs QW with Al concentration 0.4 at 77 K.

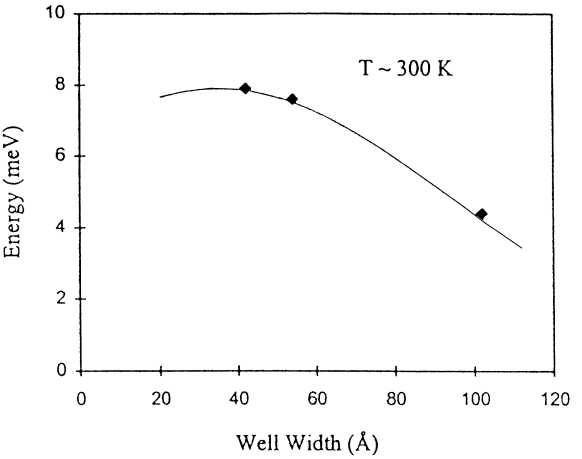

Fig. 34. Broadening line width full-width half-maximum (FWHM) energy of the AlGaAs/GaAs QW with Al concentration 0.26 at room temperature.

very close to each other (0.39 and 0.4, respectively) but their data behavior are different. One possible explanation is that in Fig. 29, a number of data points have well width narrower than 10 Å. The broadening line width for those points is comparatively low. This is critical when fitting the curve.

For 77 K, the graphs of FWHM energy against well width are shown in Figs. 31–33. The concentrations considered are 0.17, 0.3, and 0.4, respectively. In Fig. 31, the curve is convex shaped, suggesting the FWHM energy increases slowly and then decreases as well width decreases. It is to note that a data point with well width less than 10 Å is present and its broadening line width is significantly lower. This point is critical. If it is neglected, the shape of the curve will be different, suggesting a different trend. The points in Fig. 32 all have a well width greater than 60 Å. The curve is nicely fitted with broadening line width decreases as well width increases. The rate of decreasing is approximately 0.07 meV/Å. However, it contains no information for narrow well width. Data in Fig. 33

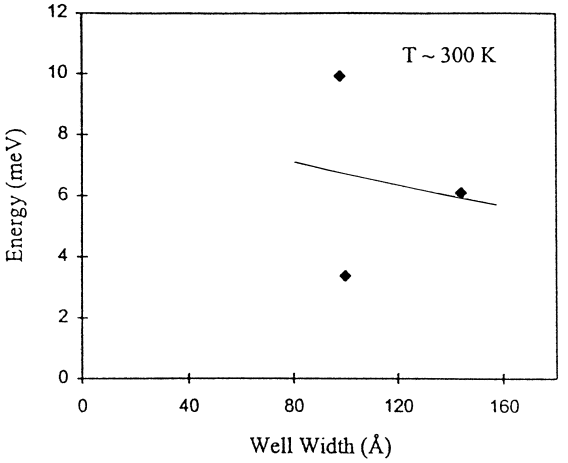

Fig. 35. Broadening line width full-width half-maximum (FWHM) energy of the AlGaAs/GaAs QW with Al concentration 0.3 at room temperature.

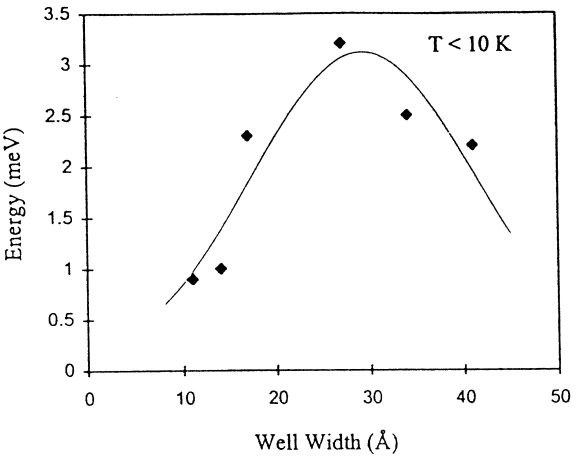

Fig. 36. Broadening line width full-width half-maximum (FWHM) energy of the InGaAs/GaAs QW with In concentration 0.12 at low temperature.

lie closely to the fitted curve. Much more points are available. In this figure, interesting data points with well width less than 10 Å show first a dramatic rise and then drop in the FWHM energy.

For room temperature, the graphs for alloy concentrations 0.26 and 0.3 are shown in Figs. 34 and 35, respectively. In both figures, data are insufficient. Although the three points in Fig. 34 are nicely fitted, the shape of the curve in the region where well width is less than 40 Å is not certain since it is not supported by any data point. However, this shape can serve as a reasonable prediction. Fig. 35 is even more uncertain since there are only three points and the FWHM energies of the two points at about 100 Å can either bring the trend up or down. Error in either point can lead to distinct results.

Most of the data discussed here indicate as well width increases, there will be a decrease in FWHM energy. A different trend is shown in a few sets. In Fig. 29, for instance, the curve more or less has a convex shape: there is a maximum at about 10 Å. If examined carefully, points with well width less than 10 Å are likely to have a drop in FWHM energy as well width decreases. In fact, they are crucial in determining the behavior of the broadening line width. Figures with a majority of data points that have a well width greater than 10 Å basically have a concave down behavior, showing when well width gets larger, broadening line width gets smaller. If data points have a well width narrower than 10 Å are present, the curve is likely to have a convex shape, in which the curve has a maximum point. This means that broadening line width increases initially and then decreases as well width narrows.

6.2. *InGaAs/GaAs*

Data for the InGaAs/GaAs QW structure is shown in Table 16.

For low temperature ranged from 2 to 15 K, well width varies between 11 and 171 Å and In alloy concentration varies from 0.063 to 0.28. The technique used is mainly PL. For the set of data for temperature around 77 K, well width ranges from 15 to 180 Å and alloy concentration varies from 0.06 to 0.23. The PL and Ab techniques are used. For the InGaAs/GaAs QW structure, both single and multi-quantum well structures are considered.

For low temperature, graphs corresponding to alloy concentrations 0.12, 0.175, and 0.28 are shown in Figs. 36–38, respectively. It is observed in Fig. 36 that the FWHM energy increases to a maximum and then decreases as the well width gets narrower. The maximum point is at about 30 Å. The same trend is observed in Fig. 38. In this case, the maximum point is at about 50 Å. From these two figures, it is noted that the FWHM energy drops when the well width gets

Table 16
FWHM and HWHM of $In_wGa_{1-w}As/GaAs$

Temp. (K)	Conc.	Well width (Å)	Barrier width (Å)	FWHM (meV)	HWHM (meV)	SQW/ MQW	Ref.	Tech.
2.2	0.12	11	—	0.9	0.45	SQW	[169]	PL
2.5	0.12	11	—	0.9	0.45	SQW	[18]	PL
4	0.12	14	100	1.0	0.5	MQW	[114]	PL
2.2	0.12	17	—	2.3	1.15	SQW	[169]	PL
15	0.28	17	—	6.8	3.4	SQW	[120]	PL
15	0.28	17	—	6	3	SQW	[18]	PL
20	0.28	17	—	10	5	SQW	[182]	PL
2.2	0.12	27	—	3.2	1.6	SQW	[169]	PL
2	0.063	28	25	0.5	0.25	MQW	[183]	PL
2.2	0.12	34	—	2.5	1.25	SQW	[169]	PL
15	0.28	38	—	10.5	5.25	SQW	[120]	PL
2	0.175	40	200	4.0	2	MQW	[184]	PL
2	0.175	40	200	3.0	1.5	MQW	[185]	PL
2.2	0.12	41	—	2.2	1.1	SQW	[169]	PL
4	0.12	48	200	4.0	2	MQW	[114]	PL
2	0.063	50	45	0.8	0.4	MQW	[183]	PL
2.2	0.12	56	—	1.8	0.9	SQW	[169]	PL
5	0.16	60	—	7.4	3.7	SQW	[186]	PL
15	0.28	68	—	37.7	18.8	SQW	[120]	PL
2	0.175	80	200	4.4	2.2	MQW	[184]	PL
2	0.175	80	200	4.1	2.05	MQW	[185]	PL
10	0.2	80	150	20.7	10.35	MQW	[187]	Ab
2	0.28	90	—	5.9	2.95	SQW	[184]	PL
15	0.28	103	—	34.4	17.2	SQW	[120]	PL
2	0.13	110	190	23.3	11.65	MQW	[188]	Ab
2	0.175	120	200	6.25	3.13	MQW	[184]	PL
2	0.175	120	200	5.6	2.8	MQW	[185]	PL
15	0.28	137	—	47.6	23.8	SQW	[120]	PL
2	0.158	150	—	4.1	2.05	SQW	[185]	PL
2	0.175	160	200	9.0	4.5	MQW	[184]	PL
2	0.175	160	200	9.1	4.55	MQW	[185]	PL
15	0.28	171	—	21.6 (×100)	10.8	SQW	[120]	PL
15	0.28	103 (1L)	—	13.5	6.75	SQW	[120]	PL
80	0.18	15	—	7.4	3.7	SQW	[169]	PL
78	0.12	17	—	2.6	1.3	SQW	[18]	PL
78	0.12	17	—	2.5	1.25	SQW	[189]	PL
77	0.2	25	—	2.9	1.45	SQW	[190]	PL
80	0.18	27	—	18.1	9.05	SQW	[169]	PL
78	0.12	28	—	3.3	1.65	SQW	[189]	PL
78	0.12	44	—	3.8	1.9	SQW	[18]	PL
77	0.06	50	80	3.5	1.75	MQW	[116]	PL
77	0.17	50	200	12.6	6.3	MQW	[191]	Ab
77	0.23	50	80	13	6.5	MQW	[116]	PL
55	0.16	60	—	8.6	4.3	SQW	[186]	PL
120	0.16	60	—	8.0	4	SQW	[186]	PL
80	0.18	61	—	11.8	5.9	SQW	[169]	PL
78	0.12	66	—	3.4	1.7	SQW	[189]	PL

Table 16 (*continued*)

Temp. (K)	Conc.	Well width (Å)	Barrier width (Å)	FWHM (meV)	HWHM (meV)	SQW/ MQW	Ref.	Tech.
78	0.12	99	—	2.8	1.4	SQW	[189]	PL
77	0.15	100	200	9.8	4.9	MQW	[191]	Ab
77	0.16	100	—	5.1	2.55	SQW	[185]	PL
77	0.15	120	200	18.9	9.45	MQW	[191]	Ab
77	0.15	130	—	3.6	1.8	SQW	[116]	PL
80	0.18	132	—	7.4	3.7	SQW	[169]	PL
77	0.165	180	—	7.6	3.8	SQW	[185]	PL
300	0.06	50	80	17.6	8.8	MQW	[116]	PL
300	0.23	50	80	19.0	9.5	MQW	[116]	PL
300	0.2	80	150	14.0	7	MQW	[187]	Ab
300	0.15	130	—	15.0	7.5	SQW	[116]	PL

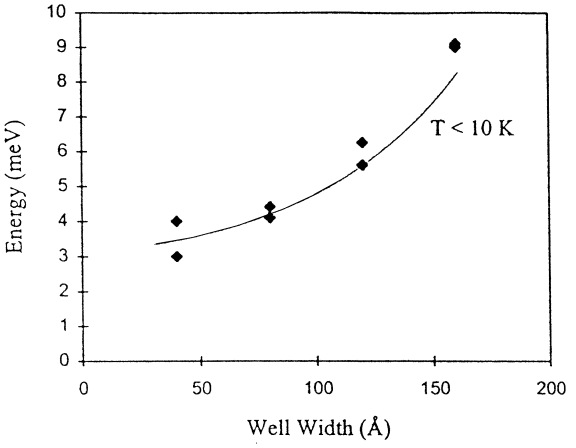

Fig. 37. Broadening line width full-width half-maximum (FWHM) energy of the InGaAs/GaAs QW with In concentration 0.175 at low temperature.

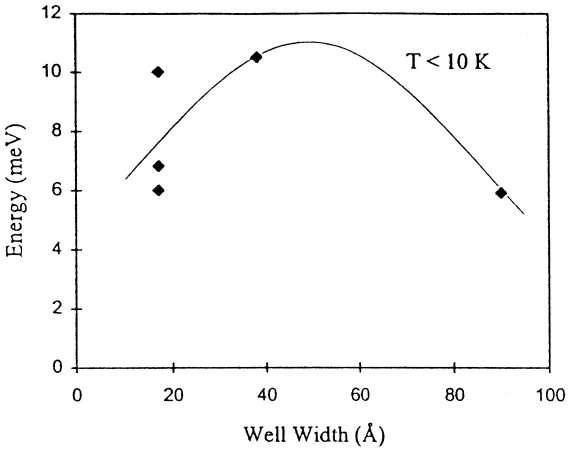

Fig. 38. Broadening line width full-width half-maximum (FWHM) energy of the InGaAs/GaAs QW with In concentration 0.28 at low temperature.

smaller than about 20 Å. Most data are fitted good. An unusual phenomenon is noticed in Fig. 37: the FWHM energy increases with the well width. As this is the only set of data showing such a trend which is not found in any literature, there is no justifiable explanation and require further investigation.

For 77 K, three graphs are plotted between 0.1 and 0.2. In concentration (Figs. 39–41). Fig. 39 is for an alloy concentration of 0.12. The curve is convex in shape and it is fitted with a small deviation. The FWHM energy increases at first as the well width decreases and then starts to drop at well width equals about 50 Å. A similar observation is made in Fig. 41, which is for alloy concentration 0.18. However, the point at well width about 20 and 30 Å are crucial. If either point is neglected, broadening line width will undergo a different behavior. Both figures give evidence that FWHM energy drops with decreasing well widths when the well width is narrower than about 20 Å. In Fig. 40 (alloy concentration 0.16), the data follow the trend that broadening line width decreases as the well width increases. The curve is nicely fitted, with a very small deviation. The rate of decreasing is around 0.06 meV/Å. Obviously, this curve can only

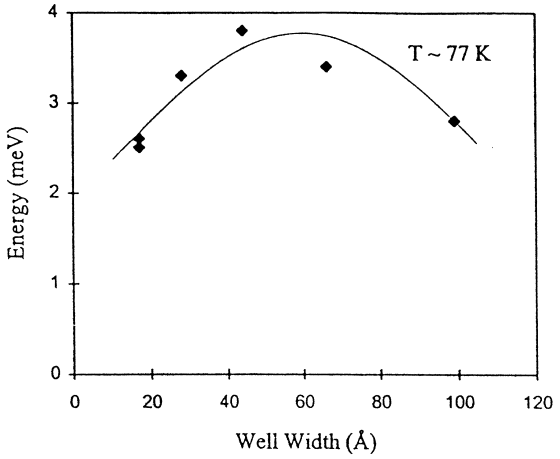

Fig. 39. Broadening line width full-width half-maximum (FWHM) energy of the InGaAs/GaAs QW with In concentration 0.12 at 77 K.

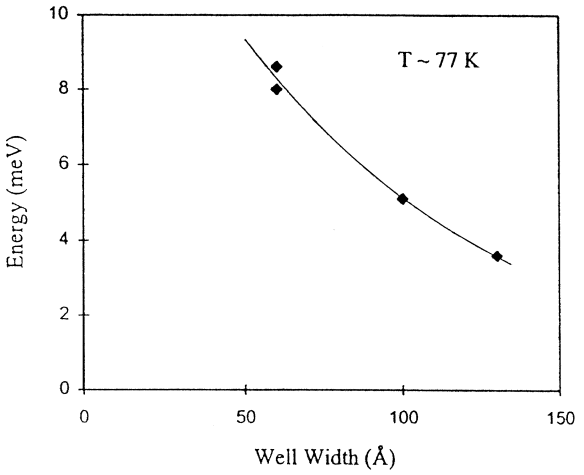

Fig. 40. Broadening line width full-width half-maximum (FWHM) energy of the InGaAs/GaAs QW with In concentration 0.16 at 77 K.

represent the range of a wider well width (> 60 Å) as no data are available for the region of narrow well width.

For the InGaAs/GaAs QW structure, most of the curves rise to a maximum and then drop as the well width continues to decrease. The FWHM energy of broadening line width is relatively low for well width narrower than about 20 Å. The curve in Fig. 40 is the only one that is concave down. There is no data point with well width less than 60 Å for this figure.

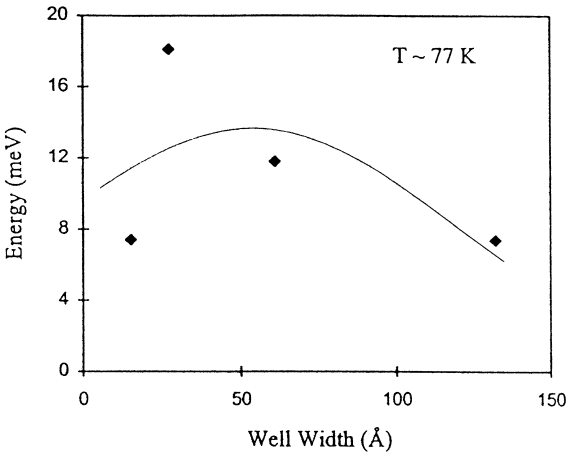

Fig. 41. Broadening line width full-width half-maximum (FWHM) energy of the InGaAs/GaAs QW with In concentration 0.18 at 77 K.

6.3. *InGaAs/InP*

Data for the InGaAs/InP QW structure is shown in Table 17.

The temperature range of the data set for low temperature is from 2 to 20 K. Three In alloy concentrations are considered: 0.53, 0.58, and 0.72. Well width ranges from 3 to 600 Å. Both single and multi-quantum well structures are considered. Various growth methods are used, including low pressure metalorganic vapor-phase epitaxy (LPMOVPE), atmospheric pressure metalorganic chemical vapor deposition (APMOCVD), organomettalic vapor phase epitaxy (OMVPE), chemical beam epitaxy (CBE), and molecular beam epitaxy (MBE). For room temperature, the set of data has well width ranging from 40 to 200 Å. The In alloy concentration of the data is mostly set at 0.53. The growth methods used are chiefly LPMOVPE, APMOCVD, and metalorganic molecular beam epitaxy (MOMBE).

The various low-temperature data below 10 K are shown in Figs. 42–44. Fig. 42 corresponds to an In alloy concentration of 0.53. Although the points are quite scatterly fitted in this figure, it is clear that they follow the trend which broadening line width decreases as well width increases. The same trend is observed in Fig. 43, which is for alloy concentration 0.58. The curve is a nice fit for the four data points.

Table 17
FWHM and HWHM of lattice-matched $In_wGa_{1-w}As_vP_{1-v}/InP$

Temp. (K)	Ab, PL	Conc. x	Well width (Å)	Barrier width (nm)	FWHM (me V)	HWHM (me V)	SQW/ MQW	Growth method	Ref.
10	PL	0.53	3	—	11	5.5	SQW	APOMVPE[a]	[192]
10	PL	0.53	5	—	10	5	SQW	APOMVPE[a]	[192]
4	PL	0.53	10	—	34.9	17.45	SQW	OMVPE[b]	[193]
2	PL	0.53	10	—	19.8	9.9	SQW	MBE[c]	[194]
2	PL	0.53	10	—	8.5	4.3	SQW	MBE[c]	[129]
10	PL	0.53	10	—	23	11.5	SQW	APOMVPE[a]	[192]
4	PL	0.53	10	—	25	12.5	SQW	APOMVPE[a]	[195]
4.2	PL	0.53	13	50	11.5	5.75	SQW	LPMOVPE[d]	[196]
2	PL	0.53	17	60	11.8	9.8	SQW	CBE[e]	[132]
4	PL	0.53	19	—	15	7.5	SQW	APOMVPE[a]	[195]
3.8	PL	0.53	20	—	11.6	5.8	SQW	MBE[c]	[194]
2	PL	0.53	20	—	7	3.5	SQW	MBE[c]	[129]
4	PL	0.53	21	—	18	9	SQW	OMVPE[b]	[193]
4.2	PL	0.72	25	—	12.5	6.25	SQW	LPMOVPE[d]	[197]
2	PL	0.53	25	60	10.6	5.3	SQW	CBE[e]	[132]
4.2	PL	0.53	25	50	8.6	4.3	SQW	LPMOVPE[d]	[196]
4.2	PL	0.53	25	—	10	5	SQW	LPMOVPE[d]	[197]
4	PL	0.53	25	—	15	7.5	SQW	APOMVPE[a]	[198]
4.2	PL	0.58	25	—	17	8.5	SQW	LPMOVPE[d]	[199]
10	PL	0.53	26	—	22	11	SQW	APOMVPE[a]	[192]
2	PL	0.53	32	—	22	11	MQW	GSMBE[f]	[126]
4	PL	0.53	35	—	9	4.5	SQW	APOMVPE[a]	[195]
2	PL	0.53	40	60	7.2	3.6	SQW	CBE[e]	[132]
2	PL	0.53	40	—	10	5	SQW	MBE[c]	[194]
2	PL	0.53	40	—	5	2.5	SQW	MBE[c]	[129]
4	PL	0.53	42	—	11.5	5.75	SQW	OMVPE[b]	[193]
4.2	PL	0.53	50	50	6.7	3.35	SQW	LPMOVPE[d]	[196]
4.2	PL	0.53	50	—	6.7	3.35	SQW	LPMOVPE[d]	[197]
4.2	PL	0.58	50	—	16.3	8.15	SQW	LPMOVPE[d]	[199]
10	PL	0.53	52	—	8	4	SQW	APOMVPE[a]	[192]
4	PL	0.53	54	—	7	3.5	SQW	APOMVPE[a]	[195]
4.2	PL	0.72	55	—	9	4.5	SQW	LPMOVPE[d]	[197]
2	PL	0.53	55	—	17	8.5	MQW	GSMBE[f]	[126]
2	PL	0.53	60	60	5.2	2.6	SQW	CBE[e]	[132]
2	PL	0.53	60	—	3.5	1.8	SQW	MBE[c]	[129]
4	PL	0.53	62	200	53	26.5	SQW	OMVPE[b]	[133]
4	PL	0.53	63	—	7.4	3.7	SQW	OMVPE[b]	[193]
2	PL	0.53	75	—	14	7	SQW	APMOCVD[g]	[200]
4.2	Ab	0.72	80	8.3	9.5	4.75	MQW	LPMOVPE[d]	[197]
2	PL	0.53	80	60	4	2	SQW	CBE[e]	[132]
4	PL	0.53	80	—	6	3	SQW	OMVPE[b]	[193]
2	PL	0.53	80	—	7.3	3.6	MQW	GSMBE[f]	[126]
2	PL	0.53	80	—	2.8	1.4	SQW	MBE[c]	[129]
4	PL	0.53	80	—	5.5	2.75	SQW	APOMVPE[a]	[198]
4.2	Ab	0.53	94	9.8	8.5	4.25	MQW	LPMOVPE[d]	[201]
4.2	PL	0.72	95	—	7.3	3.65	SQW	LPMOVPE[d]	[197]
4.2	Ab	0.53	98	9.6	6	3	MQW	LPMOVPE[d]	[201]
20	Ab	0.53	100	50	8.5	4.25	MQW	APMOCVD[g]	[121]
2	PL	0.53	100	—	7.9	3.95	SQW	APMOCVD[g]	[200]

Table 17 (*continued*)

Temp. (K)	Ab, PL	Conc. *x*	Well width (Å)	Barrier width (nm)	FWHM (meV)	HWHM (meV)	SQW/ MQW	Growth method	Ref.
4.2	PL	0.53	100	50	4.3	2.15	SQW	LPMOVPE[d]	[196]
5	PL	0.53	100	20	6	3	MQW	LPMOCVD[h]	[202]
6	PL	0.53	100	—	5	2.5	SQW	LPMOCVD[h]	[202]
4.2	PL	0.58	100	—	6.7	3.35	SQW	LPMOVPE[d]	[199]
4	PL	0.53	103	—	8	4	SQW	APOMVPE[a]	[195]
4.2	Ab	0.53	103	9.4	4.7	2.35	MQW	LPMOVPE[d]	[201]
4.2	Ab	0.53	104	9.2	6	3	MQW	LPMOVPE[d]	[197]
4.2	PL	0.53	105	—	5.3	2.65	SQW	LPMOVPE[d]	[197]
2	PL	0.53	110	—	2.8	1.4	SQW	MBE[c]	[129]
4	PL	0.53	125	200	21.5	10.75	SQW	OMVPE[b]	[133]
2	PL	0.53	130	60	3	1.5	SQW	CBE[e]	[132]
4	PL	0.53	136	—	5.6	2.8	SQW	OMVPE[b]	[193]
2	PL	0.53	150	—	2.8	1.4	SQW	MBE[c]	[129]
20	Ab	0.53	150	20	8.5	4.25	MQW	APMOCVD[g]	[121]
2	PL	0.53	150	—	19.1	9.55	SQW	APMOCVD[g]	[200]
4.2	PL	0.53	150	50	3	1.5	SQW	LPMOVPE[d]	[196]
4.2	PL	0.58	150	—	5.8	2.9	SQW	LPMOVPE[d]	[199]
4	Ab	0.53	154	16	12	6	MQW	APMOCVD[g]	[127]
4.2	PL	0.53	155	—	4	2	SQW	LPMOVPE[d]	[197]
4	PL	0.53	160	—	4.5	2.25	SQW	APOMVPE[g]	[198]
4.2	PL	0.72	175	—	7	3.5	SQW	LPMOVPE[d]	[197]
20	Ab	0.53	200	20	12.4	6.2	MQW	APMOCVD[g]	[121]
2	PL	0.53	200	50	8.3	4.15	SQW	LPMOCVD[h]	[203]
2	PL	0.53	200	—	14.4	7.2	SQW	APMOCVD[g]	[200]
4.2	PL	0.53	200	50	3.3	1.65	SQW	LPMOVPE[d]	[196]
4	PL	0.53	500	200	20	10	SQW	OMVPE[b]	[133]
6	PL	0.53	600	—	3	1.5	SQW	LPMOCVD[h]	[202]
77	PL	0.53	60	30	11.7	5.85	MQW	MOMBE[i]	[122]
77	Ab	0.58	95	10	6.3	3.15	MQW	LPMOVPE[d]	[196]
77	Ab	0.72	102	10	7.2	3.6	MQW	LPMOVPE[d]	[196]
77	Ab	0.53	103	10	4.7	2.35	MQW	LPMOVPE[d]	[196]
300	PL	0.53	40	25	58.4	29.2	SQW	MOMBE[i]	[204]
300	Ab	0.53	50	7.5	25.3	12.65	MQW	MOMBE[i]	[122]
300	PL	0.53	50	400	70	35	SQW	LPMOVPE[d]	[205]
300	Ab	0.53	50	50	38.6	19.3	MQW	APMOCVD[g]	[121]
300	PL	0.53	61	13.9	39	19.5	MQW	SSMBE[j]	[125]
300	PL	0.53	80	—	83.5	41.75	MQW	GSMBE[f]	[126]
300	Ab	0.53	80	20	15.5	7.75	MQW	CBE[e]	[206]
295	Ab	0.53	98	9.6	12	6	MQW	LPMOVPE[d]	[201]
295	Ab	0.53	99	9.8	14	7	MQW	LPMOVPE[d]	[201]
300	Ab	0.53	100	20	26.6	13.3	MQW	LPMOCVD[h]	[202]
300	Ab	0.53	100	50	13	6.5	MQW	APMOCVD[g]	[121]
295	Ab	0.53	103	9.4	11	5.5	MQW	LPMOVPE[d]	[201]
295	Ab	0.53	103	10	11	5.5	MQW	LPMOVPE[d]	[196]
300	Ab	0.53	104	9.2	11	5.5	MQW	LPMOVPE[d]	[197]
300	Ab	0.53	150	20	19.4	9.7	MQW	APMOCVD[g]	[121]
300	Ab	0.53	154	16	30.8	15.4	MQW	APMOCVD[g]	[127]
300	Ab	0.53	200	20	25.8	12.9	MQW	APMOCVD[d]	[121]
295	Ab	0.58	95	10	12.5	6.25	MQW	LPMOVPE[d]	[196]

Table 17 (*continued*)

Temp. (K)	Ab, PL	Conc. x	Well width (Å)	Barrier width (nm)	FWHM (meV)	HWHM (meV)	SQW/ MQW	Growth method	Ref.
300	Ab	0.58	100	10	14.3	7.15	SQW	LPMOVPE[d]	[199]
300	Ab	0.72	80	8.3	13	6.5	MQW	LPMOVPE[d]	[197]
295	Ab	0.72	102	10	14	7	MQW	LPMOVPE[d]	[196]

[a]APOMVPE – atmosphereic pressure organometallic vapor phase epitaxy.
[b]OMVPE – organometallic vapor-phase epitaxy.
[c]MBE – molecular beam epitaxy.
[d]LPMOVPE – low-pressure metalorganic vapor-phase epitaxy.
[e]CBE – chemical beam epitaxy.
[f]GSMBE – gas source molecular beam epitaxy.
[g]APMOCVD – atmospheric pressure metalorganic chemical vapor deposition.
[h]LPMOCVD – low-pressure metalorganic chemical vapor deposition.
[i]MOMBE – metalorganic molecular beam epitaxy.
[j]SSMBE – solid source molecular beam epitaxy.

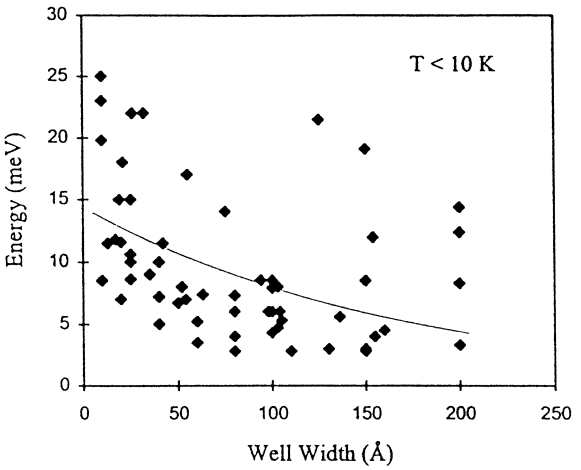

Fig. 42. Broadening line width full-width half-maximum (FWHM) energy of the InGaAs/GaAs QW with In concentration 0.53 at low temperature.

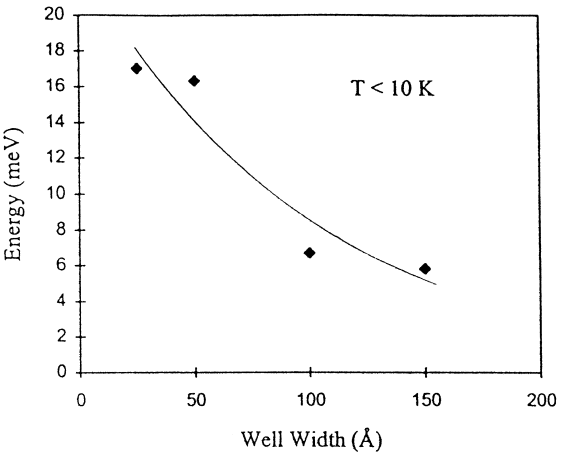

Fig. 43. Broadening line width full-width half-maximum (FWHM) energy of the InGaAs/InP QW with In concentration 0.58 at low temperature.

The rate of decrease is approximately 0.09 meV/Å. Fig. 44 (alloy concentration 0.72) also has a curve slowly concaving down. The trend is the same as the two previous curves. The rate of decreasing is approximately 0.03 meV/Å.

Since not enough data are collected for 77 K, no discussion is made. For room temperature, only one graph, Fig. 45, is presented, with alloy concentration 0.53. The data are quite scattered and a general observation is that FWHM energy decreases as well width increases. The fit for the curve is not as good as the other ones, but still, the trend is quite apparent.

In summary, there seems to be two possible trends for the effect of well width on line width of absorption peak. One is that the FWHM energy of broadening line width decreases as the well width of the QW structures increase. The other is that the FWHM energy of broadening line width increases to a maximum point and then decreases as the well width of the QW structures decreases. In fact, for the AlGaAs/GaAs

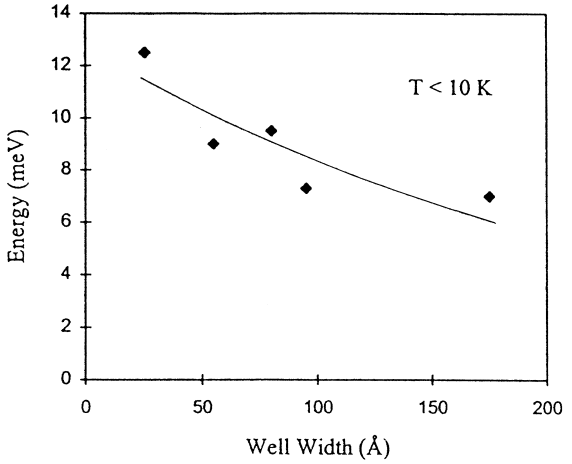

Fig. 44. Broadening line width full-width half-maximum (FWHM) energy of the InGaAs/InP QW with In concentration 0.72 at low temperature.

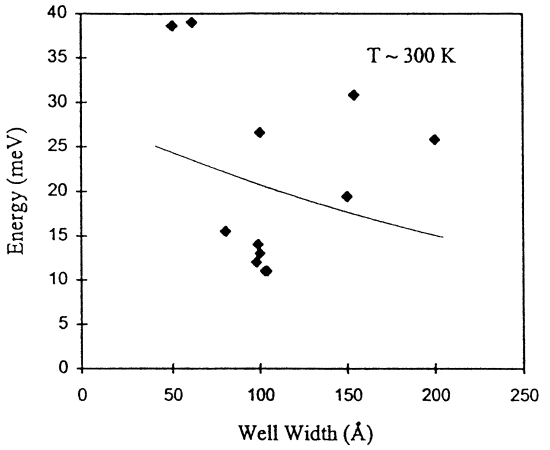

Fig. 45. Broadening line width full-width half-maximum (FWHM) energy of the InGaAs/InP QW with In concentration 0.53 at room temperature.

and InGaAs/GaAs QW structures, there is just one trend. It is found that if the well is narrower than a particular width, broadening line width will drop. In the case of the AlGaAs/GaAs QW structure, that particular well width is about 10 Å. For figures with abundant data points having a well width less than 10 Å, broadening line width undergoes a convex behavior. The result of the concave behavior can be explained by the lack of data points with well width less than 10 Å. The same interpretation can be applied to the InGaAs/GaAs QW structure. In this case, the particular well width which marks the maximum of the convex curve is about 20 Å. There is only one exception: for $In_{0.175}Ga_{0.825}As/GaAs$ fabricated by MBE, measured by PL at 10 K, line width increases with well width. For the InGaAs/InP QW structure, all the curves are concave down. The FWHM energy of broadening line width monotonically gets smaller as the well width increases and there is no sign of reduction in line width as well width gets as narrow as 10 Å.

7. Conclusion

In conclusion, QW structures, AlGaAs/GaAs, InGaAs/GaAs, InGaAs/InP, InGaAs/AlGaAs, and InGaAs/InAlAs grown on (1 0 0) substrates are investigated. We have presented five sets of material parameters of binary alloys (GaAs, InAs, InP, GaP and AlAs), AlGaAs, InAlAs, InGaAsP and InAlGaAs alloy from a systematic point of view at both low temperature and room temperature. By using our chosen sets, we calculate the band-gap energy and higher state transition energy by a proper model. Proper band offset ratio is also carefully chosen. Experimental values, which are collected from available literatures, are listed. The experimental values are measured by different measurement techniques: PL, PLE, Ab, PC, PR, ER, TR, and PMT. A detailed comparison between theoretical calculated values and the existing experimental results of the band-gap energy and higher state transition energy is carried out. Good agreement between the calculated and experimental results over a wide range of well width and alloy concentration is achieved in the QW structures. Therefore, it is believed that our assignment of the different sets of parameters are correct. As a result, a reliable source of material parameters in predicting the electronic and optical properties of QW structures is provided.

For the effect of well width on line width of absorption peak, two possible trends are observed for the AlGaAs/GaAs, InGaAs/GaAs, and InGaAs/InP QW structures. In one case, the FWHM energy of broadening line width decreases as the well width of the QW structures increases. For the other case, FWHM en-

ergy of broadening line width increases to a maximum point and then decreases as the well width of the QW structures decreases. There is only one exceptional case (for the $In_{0.175}Ga_{0.825}As/GaAs$ QW structure at 10 K) in which line width increases with well width. Further investigation is recommended in order to acquire an explanation for that particular phenomenon.

Acknowledgements

The author is supported by the RGC Research Grants of Hong Kong and the CRCG Grants of the University of Hong Kong. The author would also like to acknowledge the technical support of Vincent Leung of IBM (Hong Kong), Jeanny Chan of Proactive Technology, Hong Kong, and Donna Tang of Queen's University, Canada. He also appreciates the hospitality provided by Professor Eric Mazur during his substantial leave.

References

[1] M.J. Kelly, Low-Dimensional Semiconductors, Oxford University Press, Oxford, 1995.
[2] See for example D. Gershoni, H. Temkin, J. Lumin. 44 (1989) 381.
[3] E.M. Koteles, Mater. Res. Soc. Symp. Proc. 240 (1992) 99.
[4] J.P. Praseuth, M.C. Joncour, J.M. Gerard, P. Henoc, M. Quille, Appl. Phys. Lett. 63 (1988) 400.
[5] W.T. Tsang, R.C. Miller, Appl. Phys. Lett. 48 (1986) 1288.
[6] K. Fujiwara, K. Ploog, Appl. Phys. Lett. 45 (1984) 1222.
[7] Landolt-Börnstein, Numerical Data and Functional Relationships in Science and Technology, New Series, Springer, Berlin, 1981, 1986.
[8] B.L. Weiss, Series Advisor, Electronic Materials Information Service Datareviews Series, INSPEC, IEE, London, 1988–1995.
[9] S. Adachi, GaAs and Related Materials: Bulk semiconductor and Superlattice Properties, World Scientific, Singapore, 1994.
[10] S. Adachi, Physical Properties of III–IV Semiconductor Compounds: InP, lnAs, GaAs, GaP, InGaAs, and InGaAsP, Wiley, USA, 1992.
[11] T.P. Pearsall, GaInAsP Alloy Semiconductor, Wiley, New York, 1982.
[12] S. Adachi, J. Appl. Phys. 58 (1985) R1.
[13] S. Adachi (Ed.), Properties of Indium Phosphide, INSPEC, The Institution of Electrical Engineers, London, 1993.
[14] J.S. Blakemore, J. Appl. Phys. 53 (1982) R123.
[15] P.K. Bhattacharya, U. Das, F.Y. Juang, Y. Nashimoto, S. Dhar, Solid State Electron. 29 (1986) 261.
[16] S. Adachi, Properties of Aluminium Gallium Arsenide, INSPEC, The Institution of Electrical Engineers, London, 1993.
[17] G. Ji, D. Huang, U.K. Reddy, T.S. Henderson, R. Houdre, H. Morkoc, J. Appl. Phys. 62 (1987) 3366.
[18] X. Marie, J. Barrau, B. Brousseau, Th. Amand, M. Brousseau, E.V.K. Rao, F. Alexandre, J. Appl. Phys. 69 (1991) 812.
[19] T.Y. Wang, G.B. Stringfellow, J. Appl. Phys. 67 (1990) 344.
[20] D. Gershoni, H. Temkin, J. Lumin. 44 (1989) 381.
[21] D. Gershoni, H. Tekin, M.B. Panish, Phys. Rev. B 38 (1988) 7870.
[22] R.E. Nahorny, M.A. Pollack, W.D. Johnston, Appl. Phys. Lett. 33 (1978) 659.
[23] S. Adachi, J. Appl. Phys. 53 (1982) 8775.
[24] I. Ishikawa, J.E. Bowers, IEEE J. Quantum Elect. 30 (1994) 562.
[25] D. Olego, T.Y. Chang, E. Silberg, E.A. Caridi, A. Pinczuk, Appl. Phys. Lett. 41 (1982) 476.
[26] D.J. BenDaniel, C.B. Duke, Phys. Rev. 152 (1966) 683.
[27] G. Bastard, J.A. Brum, R. Ferreira, Electronic states in semiconductor heterostructures, in: H. Ehrenreich, D. Turnbull (Eds.), Solid State Physics — Advances in Research and Applications, Academic Press, New York, 1991, pp. 229–415.
[28] T.P. Pearsall (Ed.), GaInAsP Alloy Semiconductors, Wiley, New York, 1982, pp. 295.
[29] E.H. Li, B.L. Weiss, Proc. SPIE 1675 (1992) 98.
[30] D.D. Sell, H.C. Casey, J. Appl. Phys. 45 (1974) 800.
[31] P. Varshni, Physica 34 (1967) 149.
[32] D.D. Sell, Phys. Rev. B 6 (1972) 3750.
[33] P. Lawaetz, Phys. Rev. B 4 (1971) 3460.
[34] M.P.C.M. Krijn, Semicond. Sci. Technol. 6 (1991) 27.
[35] M. Yim, J. Appl. Phys. 42 (1971) 2854.
[36] Onton, Proceedings of the 10th International Conference of Physics of Semiconductors, Cambridge, MA, USAFC, New York, p. 107.
[37] M. Cadorna, K.L. Shaklee, F.H. Pollak, Phys. Rev. Lett. 16 (1966) 696.
[38] Casey, M.B. Panish, Heterostructure Lasers, Part A, Academic Press, New York, 1978.
[39] B.R. Bennett, R.A. Soref, IEEE J. Quantum Electron. QE-23 (1987) 2159.
[40] P. Rochon, E. Fortin, Phys. Rev. B 12 (1975) 5803.
[41] K. Ekardt, K. Losch, D. Bimberg, Phys. Rev. B 20 (1976) 3303.
[42] A.V. Varfolomeev, R.P. Seisyan, R.N. Yakimova, Sov. Phys. Semicond. (English version) 9 (1975) 530; Fiz. Tekh. Poluprovodn 9 (1975) 804.
[43] S.E. Stokowski, D.D. Sell, Phys. Rev. B 5 (1972) 1636.
[44] F. Luke, Phys. Status Solidi B 84 (1977) K113.
[45] D.F. Nelson, L.F. Johnson, M. Gershenzon, Phys. Rev. 135 (1964) A1399.
[46] G.E. Stillman, D.M. Larsen, C.M. Wolfe, R.C. Brandt, Solid State Commun. 9 (1971) 2245.
[47] M. Cadorna, Phys. Rev. 121 (1961) 752.

[48] S. Adachi, Phys. Rev. B 35 (1987) 7454.
[49] Suzuki, N. Miura, Solid State Commun. 18 (1976) 233.
[50] E.D. Palik, B.D. Henvis, J.R. Stevenson, S. Isawa, Solid State Commun. 6 (1968) 721.
[51] R.C. Miller, D.A. Kleinman, A.C. Gossard, Phys. Rev. B. 29 (1984) 7085.
[52] M. Cardona, J. Appl. Phys. 32 (1961) 2151.
[53] M. Chamberlain, P.E. Simmonds, R.A. Stardling, C.C. Bradley, Proceedings of the 11th International Conference of Physics Semiconductors Polish Scientific Publishers, Warsaw, 1972, p. 1016.
[54] Fiedler, A. Schylachetzki, Solid State Electron. 30 (1987) 73.
[55] A.B. Chen, A. Sher, Semiconductors Alloys, Plenum Press, New York, 1995, p. 245.
[56] A.K. Walton, W.K. Mishra, J. Phys. C1 (1968) 533.
[57] Perlin, W. Trezeciakowski, E.L. Staszewska, J. Muszalski, M. Micovic, Semicond. Sci. Technol. 9 (1994) 2239.
[58] E.O. Kane, J. Phys. Chem. Solids 1 (1957) 249.
[59] S. Adachi, J. Phys. Soc. Japan 24 (1968) 1178.
[60] C.C. Bradley, P.E. Simmonds, J.R. Stockton, R.A. Stradling, Solid State Commun. 12 (1973) 413.
[61] O. Berolo, J.C. Woolley, Can. J. Phys. 49 (1971) 1335.
[62] S. Monemar, K.K. Shih, G.D. Petit, J. Appl. Phys. 47 (1976) 2604.
[63] R. Dingle, R.A. Logan, J.R. Arthur Jr., in: C. Hilsum (Ed.), Gallium Arsenide and Related Compounds, IOP Conference Ser. No. 33a, IOP, Bristol, 1997, p. 210.
[64] N.C. Miller, S. Zemon, G.P. Werber, W. Powazinik, J. Appl. Phys. 57 (1985) 512.
[65] G. Oelgart, R. Schwabe, M. Heider, B. Jacobs, Semicond. Sci. Technol. 2 (1987) 468.
[66] B. Lambert, J. Caulet, A. Regreny, M. Baudet, B. Deveaud, A. Chomette, Semicond. Sci. Technol. 2 (1987) 491.
[67] T.F. Kuech, D.J. Wolford, R. Potemski, J.A. Bradley, K.H. Kelleher, D. Yan, J.P. Farrell, P.M.S. Lesser, F.H. Pollak, Appl. Phys. Lett. 51 (1987) 505.
[68] C. Bosio, J.L. Staehli, M. Guzzi, G. Burri, R.A. Logan, Phys. Rev. B 38 (1988) 3263.
[69] D.E. Aspnes, S.M. Kelso, R.A. Logan, R. Bhat, J. Appl. Phys. 60 (1986) 754.
[70] M.D. Camras, N. Holonyak Jr., K. Hess, J.J. Coleman, Appl. Phys. Lett. 41 (1982) 317.
[71] M.L. Cohen, T.K. Bergstresser, Phys. Rev. 141 (1966) 789.
[72] H. Hrivnak, Appl. Phys. Lett. 56 (1990) 2425.
[73] L. Moon, G.A. Antypas, L.W. James, J. Elect. Mater. 3 (1974) 635.
[74] A. Hamoudi, A. Ougazzaden, Ph. Krauz, E.V.K. Rao, M. Juhel, H. Thibierge, Appl. Phys. Lett. 66 (1995) 718, see Ref. [9].
[75] D. Olego, T.Y. Chang, E. Silberg, E.A. Caridi, A. Pinczuk, Ints. Phys. Conference Ser. No. 65 International Symposium GaAs and Related Compounds, Albuquerque 195.
[76] Y. Hirayama, W.Y. Choi, L.H. Peng, C.G. Fonstad, J. Appl. Phys. 74 (1993) 570.
[77] C.A. Wang, J.N. Walpole, L.J. Missaggia, J.P. Donnelly, H.K. Choi, Appl. Phys. Lett. 58 (1991) 2208.
[78] H. Nagai, S. Adachi, T. Fukui, III–V Mixed Crystals, Corona Publishing, Tokyo, 1988, p. 35.
[79] U.K. Reddy, G. Ji, T. Henderson, H. Morkkoc, J.N. Schulman, J. Appl. Phys. 62 (1987) 145.
[80] M. Erman, J.B. Theeten, P. Frijlink, S. Gaillard, Fan Jia Hia C. Ailbert, J. Appl. Phys. 56 (1984) 3241.
[81] J. Sonek, J.M. Ballantyne, Y.J. Chen, G.M. Carter, S.W. Brown, E.S. Koteles, J.P. Salerno, IEEE J. Quantum Electron 22 (1986) 1015.
[82] J.P. Pocholle, M. Razeghi, J.P. Hirtz, J.P. Schnell, J. Raffy, B. Guyon, M. Papuchon, C. Puech, P. Dandrin, H. Wanderstichel, Adv. Optoelectron. Tech. (1987) 864.
[83] A. Fox Mark, D.A.B. Miller, G. Livescu, J.E. Cunni, W.Y. Jan, IEEE J. Quantum Electron. 27 (1991) 2281.
[84] H. Shen, P. Parayanthal, F.H. Pollak, A.L. Smirl, J.N. Schulman, R.A. McFarlane, I. D'Haenens, Solid State Commun. 59 (1986) 557.
[85] I.J. Fritz, T.M. Brennan, D.S. Ginley, Solid State Commun. 75 (1990) 289.
[86] E.V.K. Rao, H. Thibierge, F. Brillouet, F. Alexandre, R. Azoulay, Appl. Phys. Lett. 46 (1985) 867.
[87] R. Enderlein, D. Jiang, Y. Tang, Phys. Stat. Sol. 145 (1988) 167.
[88] P. Paraythanal, H. Shen, F.H. Pollak, O.J. Glembocki, B.V. Shanabrook, W.T. Beard, Appl. Phys. Lett. 48 (1986) 1261.
[89] H. Mathieu, P. Lefebvre, J. Allegre, B. Gil, Phys. Rev. B 36 (1987) 6581.
[90] E.S. Koteles, B. Elman, J. Lee, S. Charbonneau, M.W.L. Thewalt, Quantum-Well Superlattice Phys. III 1283 (1990) 143.
[91] H. Chu, Y.C. Chang, Phys. Rev. B 39 (1989) 10 861.
[92] P. Dawson, K.J. Moore, G. Duggan, H.I. Ralph, C.T.B. Foxon, Phys. Rev. B 34 (1986) 6007.
[93] B. Gil, Y. El Khalifi, H. Mathieu, C. de Paris, J. Massies, G. Neu, T. Fukunaga, Nakashima, Phys. Rev. B 41 (1990) 2885.
[94] D. Gershoni, I. Brener, G.A. Baraff, S.N.G. Chu, L.N. Pfeiffer, K. West, Inernational Symposium on GaAs and Related Compounds, Vol. XXX, 1991.
[95] O. Brandt, K. Kanamoto, Y. Tokuda, N. Tsukada, Phys. Rev. B 48 (1993) 17 599.
[96] R.C. Miller, A.C. Gossard, G.D. Sanders, Y.C. Chang, J.N. Schulman, Phys. Rev. B 32 (1985) 8452.
[97] Y. El Khilifi, B. Gil, H. Mathieu, T. Fukunaga, H. Nakashima, Phys. Rev. B 39 (1989) 13 533.
[98] F.Y. Juang, Y. Nashimoto, P.K. Bhattacharya, J. Appl. Phys. 58 (1985) 1986.
[99] E.O. Gobel, H. Jung, J. Kuhl, K. Ploog, Phys. Rev. Lett. 51 (1983) 1588.
[100] W.T. Tsang, R.C. Miller, Appl. Phys. Lett. 48 (1986) 1288.
[101] W.T. Masselink, P.J. Pearah, J. Klem, C.K. Peng, H. Morkoc, G.D. Sanders, Y.C. Chang, Phys. Rev. B 32 (1985) 8027.
[102] C. Weisbuch, R.C. Miller, R. Dingle, A.C. Gossard, W. Wiegmann, Solid State Commun. 37 (1981) 219.
[103] P.W. Yu, G.D. Sanders, D.C. Reynolds, K.K. Bajaj, C.W. Litton, J. Klem, D. Huang, H. Morkoc, Phys. Rev. B 35 (1987) 9250.

[104] F.H. Pollak, H. Shen, J. Crystal Growth 98 (1989) 53.
[105] J. Dalfors, T. Lundstrom, P.O. Holtz, B. Monemar, J. Wallin, G. Landgren, Superlattices Microstruct. 17 (1995) 407.
[106] D.A. Kleinman, R.C. Miller, Phys. Rev. B 32 (1985) 2266.
[107] R.C. Miller, D.A. Kleinman, W.A. Nordland Jr., A.C. Gossard, Phys. Rev. B 22 (1980) 863.
[108] Y.S. Tang, Semicond. Sci. Technol. 4 (1989) 871.
[109] U.K. Reddy, G. Ji, T. Henderson, D. Huang, R. Houdre, H. Morkoc, J. Vac. Sci. Technol. B 7 (1989) 1106.
[110] D.J. Arent, K. Deneffe, C. Van Hoof, J. De Boeck, G. Borghs, J. Appl. Phys. 66 (1989) 1739.
[111] G. Ji, W. Dobbelaere, D. Huang, H. Morkoc, Phys. Rev. B 39 (1989) 3216.
[112] A. Salokatve, M. Hovinen, M. Pessa, Appl. Phys. Lett. 58 (1991) 1878.
[113] T.E. Van Eck, P. Chu, W.S.C. Chang, H.H. Wieder, Appl. Phys. Lett. 49 (1986) 135.
[114] K.J. Moore, G. Duggan, K. Woodbridge, C. Roberts, Phys. Rev. B 41 (1990) 1095.
[115] D. Gershoni, H. Temkin, J. Lumin. 44 (1989) 381.
[116] F. Martelli, M.G. Proietti, J. Appl. Phys. 71 (1992) 539.
[117] G. Ji, D. Huang, U.K. Reddy, T.S. Henderson, R. Houdre, H. Morkoc, J. Appl. Phys. 62 (1987) 3366.
[118] J.P. Reithmaier, R. Hoger, H. Riechert, P. Hiergeist, G. Abstreiter, Appl. Phys. Lett. 57 (1990) 957.
[119] Y.S. Huang, H. Qiang, F.H. Pollak, G.D. Pettit, P.D. Kirchner, J.M. Woodall, H. Stragier, L.B. Sorensen, J. Appl. Phys. 70 (1991) 7537.
[120] R.M. Kolbas, N.G. Anderson, W.D. Laidig, Y.K. Sin, Y.V. Lo, K.Y. Hsieh, Y.J. Yang, IEEE J. Quantum Electron. 24 (1988) 1605.
[121] M.S. Skolnick, L.L. Taylor, S.J. Bass, A.D. Pitt, D.J. Mowbray, A.G. Cullis, N.G. Chew, Appl. Phys. Lett. 51 (1987) 24.
[122] Y. Kawaguchi, H. Asahi, Appl. Phys. Lett. 50 (1987) 1243.
[123] D. Gershoni, H. Temkin, M.B. Panish, Appl. Phys. Lett. 53 (1988) 1294.
[124] A.J. Moseley, M.D. Scott, P.J. Williams, R.H. Wallis, J.J. Davies, J.R. Riffat, Electron. Lett. 23 (1987) 516.
[125] I.J. Pape, Wa.P. Li Kam, J.P.R. David, P.A. Claxton, P.N. Robson, Electron. Lett. 24 (1988) 1218.
[126] H. Temkin, M.B. Panish, P.M. Petroff, R.A. Hamm, J.M. Vandenberg, S. Sumski, Appl. Phys. Lett. 47 (1985) 394.
[127] M.D. Scott, Westland, A.M. Fox, A.C. Maciel, J.F. Ryan, Appl. Phys. Lett. 50 (1987) 839.
[128] M.S. Skolnick, P.R. Tapster, S.J. Bass, N. Apsley, A.D. Pitt, N.G. Chew, G. Cullis, S.P. Aldred, C.A. Warwick, Appl. Phys. Lett. 48 (1986) 21.
[129] W.T. Tsang, E.F. Schubert, Appl. Phys. Lett. 49 (1986) 220.
[130] L. Hrivnak, J. Appl. Phys. 71 (1992) 4370.
[131] T.Y. Wang, G.B. Stringfellow, J. Appl. Phys. 67 (1990) 344.
[132] R. Sauer, T.D. Harris, W.T. Tsang, Phys. Rev. B 34 (1986) 9023.
[133] C.P. Kuo, K.L. Fry, G.B. Stringfellow, Appl. Phys. Lett. 47 (1985) 855.
[134] J. Oiknine-Schlesinger, E. Ehrenfreund, D. Gershoni, D. Ritter, M.B. Panish, R.A. Hamm, Appl. Phys. Lett. 59 (1991) 970.
[135] M. Razghi, J. Nagle, P. Maurel, F. Omnes, J.P. Pocholle, Appl. Phys. Lett. 49 (1986) 1110.
[136] K. Wakita, L. Kotaka, A. Kozen, Electron. Lett. 30 (1994) 1711.
[137] K. Wakita, Y. Kawamura, Y. Yoshikuni, H. Asahi, Electron. Lett. 21 (1985) 574.
[138] H. Uenohara, Y. Kawamura, H. Iwamura, IEEE J. Quantum. Electron. 31 (1995) 2142.
[139] I.J. Fritz, J.F. Klem, M.J. Hafich, A.J. Howard, H.P. Hjalmarson, IEEE. Photon. Technol. Lett. 7 (1995) 1270.
[140] R. Takahashi, Y. Kawamura, T. Kagawa, H. Iwamura, Appl. Phys. Lett. 65 (1994) 1790.
[141] M.K. Chin, J. Appl. Phys. 76 (1994) 518.
[142] K. Alavi, Y.P. Persall, S.R. Forrest, A.Y. Cho, Electron. Lett. 19 (1983) 227.
[143] H.W. Wan, T.C. Chong, S.J. Chua, IEEE Photon. Technol. Lett. 3 (1991) 730.
[144] S. Moneger, Y. Baltagi, T. Benyattou, A. Tabata, B. Ragot, G. Guillot, J. Appl. Phys. 74 (1993) 1437.
[145] D.F. Welch, G.W. Wicks, L.F. Eastman, Appl. Phys. Lett. 43 (1983) 762.
[146] W. Stolz, J.C. Maan, M. Altarelli, Phys. Rev. B 36 (1987) 4310.
[147] F.S. Turco, M.C. Tamargo, D.M. Hwang, R.E. Nahory, J. Werner, K. Kash, Appl. Phys. Lett. 56 (1990) 72.
[148] R.G. Waters, R.J. Dalby, J.A. Baumann, J.L. De Sanctis, A.H. Shepard, IEEE Photon. Technol. Lett. 3 (1991) 409.
[149] D. Ahn, S.C. Choi, J. Appl. Phys. 75 (1994) 7648.
[150] M.H. Moloney, J. Hegarty, Appl. Phys. Lett. 64 (1994) 997.
[151] M.H. Moloney, J. Hegarty, Appl. Phys. Lett. 62 (1993) 3327.
[152] K. Fujiwara, K. Kawashima, K. Kobayashi, Appl. Phys. Lett. 57 (1990) 2234.
[153] L. Buydens, P. Demeester, Z. Yu, P.V. Daele, J. Appl. Phys. 71 (1992) 3249.
[154] M. Kunzer, G. Hendofer, U. Kaufmann, K. Kohler, Phys. Rev. B 45 (1992) 11 151.
[155] S.F. Yoon, K. Radhakrishnan, H.M. Li, Supperlattice Microstruct. 14 (1993) 79.
[156] Mendez, G. Basterd, L.L. Chang, L. Esaki, Phys. Rev. B 26 (1982) 7101.
[157] Chemla, T.C. Damen, D.A.B. Miller, A.C. Gossard, W. Wiegmann, Appl. Phys. Lett. 42 (1983) 864.
[158] E. Kash, E. Mendez, H. Morkoc, Appl. Phys. Lett. 46 (1985) 173.
[159] D.C. Bertolet, J.K. Hsu, K.M. Lau, J. Appl. Phys. 62 (1987) 120.
[160] A. Qteish, R.J. Needs, Phys. Rev. B 45 (1992) 1317.
[161] D.E. Apsnes, S.M. Kelso, R.A. Logan, R. Bhat, J. Appl. Phys. 60 (1986) 754.
[162] P. Voisin, Quantum Wells & Superlattices in Optoelect. Devices & Integrated Optics 88, SPIE Vol. 861, 1987.
[163] S. Kamiyama, IEEE Photon. Technol. Lett. 4 (4) (1993) 439.

[164] S.W. Corzine, Appl. Phys. Lett. 57 (26) (1990) 2835.
[165] J.S. Blaskemore, J. Appl. Phys. 53 (10) (1982).
[166] S. Adachi, Properties of Aluminum Gallium Arsenide, EMIS Data Review Series, INSPEC, The Institute of Electrical Engineers, London, New York, 1986, pp. 62–72.
[167] J. Singh, Properties of Lattice Matched and Strained Indium Gallium Arsenide, EMIS Data Series, INSPEC, The Institute of Electrical Engineers, London, 1993, pp. 66–72.
[168] J.C. Brice, Properties of Gallium Arsenide, EMIS Data Review Series, INSPEC, The Institute of Electrical Engineers, London, New York, Section 1.5, 1986.
[169] D.C. Bertolet, J.K. Hsu, K.M. Lau, E.S. Koteles, D. Owens, J. Appl. Phys. 64 (1988) 6562.
[170] R.C. Miller, W.T. Tsang, Appl. Phys. Lett. 39 (1981) 334.
[171] T. Hayakawa, K. Takahashi, M. Kondo, S. Yamamoto, T. Hijikata, Phys. Rev. B 38 (1988) 1526.
[172] R.C. Miller, D.A. Kleinman, A.C. Gossard, W.T. Tsang, Phys. Rev. B 24 (1981) 1134.
[173] E.S. Koteles, J.Y. Chi, Phys. Rev. B 37 (1988) 6332.
[174] P.J. Hughes, T.J.V. Thosea, B.L. Weiss, Semicond. Sci. Technol. 10 (1995) 1339.
[175] J. Singh, S. Shong, P.K. Mhattacharya, Ri. Saha, C. Lastufka, H.R. Sobel, J. Lightwave Technol. 6 (1988) 818.
[176] L.W. Molenkamp, G.E.W. Bauer, R. Eppenga, C.T. Foxon, Phys. Rev. B 38 (1988) 6147.
[177] D.A. Broido, E.S. Koteles, C. Jagannath, J.Y. Chi, Phys. Rev. B 37 (1988) 2725.
[178] R.C. Miller, A.C. Gossard, W.T. Tsang, O. Munteanu, Phys. Rev. B 25 (1982) 3871.
[179] S. Selci, A. Cricentri, M. Righini, C. Petrillo, F. Sacchetti, F. Alexandre, G. Chiarotti, Solid State Commun. 79 (1991) 561.
[180] J.Y. Tang, K. Hess, N. Holonyak Jr., J.J. Coleman, Dapkus, J. Appl. Phys. 53 (1982) 6043.
[181] T. Hayakawa, K. Takahashi, M. Kondo, T. Suyama, S. Yamamoto, T. Hijikata, Phys. Rev. Lett. 60 (1988) 349.
[182] N.G. Anderson, W.D. Laidig, R.M. Kolbas, T.C. Lo, J. Appl. Phys. 60 (1986) 2361.
[183] M. Sato, Y. Horikoshi, Appl. Phys. Lett. 52 (1988) 123.
[184] T.G. Anderson, Z.G. Chen, V.D. Kulakovkil, A. Uddin, J.T. Valin, Appl. Phys. Lett. 51 (1987) 752.
[185] T.G. Anderson, Z.G. Chen, V.D. Kulakovskii, A. Uddin, J.T. Valin, Phys. Rev. B 37 (1988) 4032.
[186] R.F. Schnabel, R. Zimmermann, D. Bimberg, H. Nickel, R. Losch, W. Schlapp, Phys. Rev. B 46 (1992) 9873.
[187] K.F. Huang, K. Tai, J.L. Jewell, R.J. Fischer, S.L. McCall, A.Y. Cho, Appl. Phys. Lett. 54 (1988) 2192.
[188] J.Y. Matinz, E.V.K. Rao, Appl. Phys. Lett. 43 (1983) 560.
[189] D.C. Bertolet, J.K. Hsu, S.H. Jones, K.M. Lau, Appl. Phys. Lett. 52 (1988) 293.
[190] S.M. Wang, J.V. Thordson, T.G. Anderson, S. Jiang, L.X.T. Yang, S.C. Shen, Appl. Phys. Lett. 65 (1994) 336.
[191] J.Y. Martinz, M.N. Charasse, B. Sermage, Phys. Rev. B 31 (1985) 8298.
[192] T.Y. Wang, K.L. Fry, A. Persson, E.H. Reihlen, G.B. Stringfellow, Appl. Phys. Lett. 52 (1988) 290.
[193] B.I. Miller, E.F. Schubert, U. Koren, A. Aourmazd, A.H. Dayem, R.J. Capik, Appl. Phys. Lett. 49 (1986) 1384.
[194] J.H. Marsh, J.S. Roberts, P.A. Calxton, Appl. Phys. Lett. 46 (1985) 1161.
[195] K.W. Carey, R. Hull, J.E. Fouquet, F.G. Kellert, G.R. Trott, Appl. Phys. Lett. 51 (1987) 910.
[196] M. Sugaware, T. Fujii, S. Yamazaki, K. Nakajima, Phys. Rev. B 44 (1991) 1782.
[197] M. Sugaware, T. Fujii, M. Kondo, K. Kato, K. Domen, S. Yamazaki, K. Nakajima, Appl. Phys. Lett. 53 (1988) 2290.
[198] D. Moroni, J.P. Andre, E.P. Menu, Ph. Gentric, J.N. Patillon, J. Appl. Phys. 62 (1987) 2003.
[199] M. Sugaware, T. Fujii, S. Yamazaki, K. Nakajima, Appl. Phys. Lett. 53 (1989) 1353.
[200] M.S. Skolnick, P.R. Tapster, S.J. Bass, N. Apsley, A.D. Pitt, N.G. Chew, A.G. Cullis, S.P. Aldred, C.A. Warwick, Appl. Phys. Lett. 48 (1986) 1455.
[201] M. Sugaware, T. Fujii, S. Yamazaki, K. Nakajima, Phys. Rev. B 42 (1990) 9587.
[202] M. Razeghi, J. Nagle, P. Maurel, F. Omnes, J.P. Pocholle, Appl. Phys. Lett. 49 (1986) 1110.
[203] M. Razeghi, J.P. Hirtz, Appl. Phys. Lett. 43 (1983) 585.
[204] M.A. Cotta, R.A. Hamm, S.N.G. Chu, L.R. Harriott, J. Appl. Phys. 75 (1994) 630.
[205] J. Oshinowo, A. Forchel, Appl. Phys. Lett. 60 (1992) 2660.
[206] K. Tai, J. Hegarty, W.T. Tsang, Appl. Phys. Lett. 51 (1987) 152.